# THE EFFECT OF CHAIN EXTENDER ON THE MOLECULAR WEIGHT AND HYDROLYTIC DEGRADATION OF POLY(LACTIC ACID)

By

Wanwarang Limsukon

A THESIS

Submitted to
Michigan State University
in partial fulfillment of the requirements
for the degree of

Packaging—Master of Science

2019

## ABSTRACT

THE EFFECT OF CHAIN EXTENDER ON THE MOLECULAR WEIGHT AND HYDROLYTIC DEGRADATION OF POLY(LACTIC ACID)

By

Wanwarang Limsukon

The effect of chain extender (Cex) on the molecular weight properties and hydrolytic degradation of modified PLA films (PLA–Cex) was determined and compared with PLA without Cex (PLA–Con). Effects of the Cex content and the residence time on the molecular weight were reviewed using melt blending and compression molding. A response surface methodology was applied to design the experiments and estimate the optimal conditions for obtaining the maximum weight average and number average molecular weight achieved at 1.5 wt% Cex and residence time of 17 minutes.

The hydrolytic degradation experiments were run in water from 40 to 95 °C and in 50% ethanol from 40 to 85 °C. The rate of hydrolytic degradation of PLA–Cex film was estimated using mathematical models, and it was considerably lower than that of PLA–Con in all conditions. The activation energy for hydrolysis above $T_g$ was determined using the Arrhenius equation, showing no significant difference between PLA–Cex and PLA–Con. The Vogel-Tammann-Fulcher (VTF) and the Williams-Landel-Ferry (WLF) models were used for studying the hydrolytic degradation of polymers over a broad range of temperature crossing $T_g$. A master curve was constructed using the time-temperature superposition principle. The experimental data at 85 °C were used to predict the degradation behavior at 40 °C. It was found that PLA–Cex would take approximately 72 percent more time than PLA–Con to degrade to soluble oligomer chains.

This thesis is dedicated to my beloved family

## ACKNOWLEDGEMENTS

I would like to pay special thankfulness and appreciation to the persons below who have contributed to this thesis and support me to pass all the steps.

First of all, I would like to express my sincere thanks to my advisor, Dr. Rafael Auras for the great experience and opportunities as a member of his RAA research group. I appreciate his contributions of time for my research and writing processes. His patience guidance, encouragement, and valuable advice help me to reach this stage in my life. I would like to present my special thanks to my committee members, Dr. Susan Selke (School of Packaging) and Dr. Yan Liu (Biosystems and Agricultural Engineering) for their expertise and valuable suggestions. I would like to extend my gratitude to Dr. Kirk Dolan (Department of Food Science and Human Nutrition) for his precious class, BE835, and also his great help and valuable guidance on the model estimation.

I am highly grateful to my current and former friends from RAA research group for sharing their knowledge, experience and helping me in my research. Many thanks go to my fellow students, Xinyi, Yuzhu, Judy, Sonal, Gauri, Vijay, Zhao, Kexin, Pooja, and P'Pom, who always provide friendship and support.

I would like to thank the Royal Thai Government and Rajamangala University of Technology Tawan-ok for the scholarship and financial support during my studies at the School of Packaging.

Finally, nobody has been more important to me than my family. I would like to thank for their unconditional love and support. Thank you for always encouraging me to pursue my dreams.

## TABLE OF CONTENTS

## LIST OF TABLES

## LIST OF FIGURES

## KEY TO ABBREVIATIONS

| | |
|---|---|
| $\%wt_{filler}$ | Weight percentage of the chain extender |
| $\rho_{Crystal}$ | Density of crystalline PLA |
| $\rho_{PLA}$ | Density of amorphous PLA |
| ANOVA | Analysis of variance |
| CCD | Central composite designs |
| $C_E$ | Number of ester units of all the long chain per unit volume |
| $C_{E0}$ | Initial number of ester units of all the chain per unit volume |
| Cex | Chain extender |
| $C_{ol}$ | Number of ester units of all the short chain per unit volume |
| CRF | Crystalline fraction |
| DMA | Dynamic mechanical analysis |
| DSC | Differential scanning calorimeter |
| $E_a$ | Activation energy |
| $E_{VTF}$ | Pseudo activation energy |
| FCCCD | Face-centered central composite design |
| GPC | Gel permeation chromatography |
| HDPE | High-density polyethylene |
| $k_0$ | Pre-exponential factor |
| $k_{1st}$ | first-order rate constant |
| $K_a$ | Acid dissociation |
| $k_C$ | Kinetic rate constant of Avrami model |

| | |
|---|---|
| $k_{deg}$ | Degradation model rate constant |
| $k_{ref}$ | Rate constant at $T_{ref}$ |
| $m$ | Average degree of polymerization of oligomers |
| MAF | Mobile amorphous fraction |
| $M_n$ | Number average molecular weight |
| $\bar{M}_n$ | Normalized number average molecular weight |
| $M_{n0}$ | Initial number average molecular weight |
| $M_w$ | Weight average molecular weight |
| MWD | Molecular weight distribution |
| $N_{chain0}$ | Number of polymer chains per unit volume |
| PET | Polyethylene terephthalate |
| PLA | Poly(lactic acid) |
| PS | Polystyrene |
| RAF | Rigid amorphous fraction |
| $R_S$ | Total number of chain scissions per unit volume |
| RSM | Response surface methodology |
| SEC | Size exclusion chromatography |
| SSC | Scaled sensitivity coefficient |
| $T$ | Experimental temperature |
| $t$ | Time |
| $\bar{t}$ | Mean of residence time |
| $T_c$ | Cold crystallization temperature |
| $T_g$ | Glass transition temperature |

| | |
|---|---|
| TGA | Thermal gravimetric analysis |
| THF | Tetrahydrofuran |
| $T_i$ | Temperature of interest |
| $T_m$ | Melting temperature |
| $T_{ref}$ | Reference temperature |
| $T_s$ | Vogel Temperature |
| VTF | Vogel-Fulcher-Temmann |
| WLF | William-Landel-Ferry |
| $X_C$ | Degree of crystallinity |
| $X_{C_0}$ | Initial degree of crystallinity |
| $\alpha$ and $\beta$ | Dimensionless constants |
| $\alpha_T$ | Shift factor |
| $\Delta H_c$ | Cold crystallization enthalpy |
| $\Delta H_m$ | Heat of fusion |
| $\Delta H_m^0$ | Heat of fusion for 100% crystalline PLA |
| $\omega$ | Number of ester units of the crystalline phase per unit volume |

# CHAPTER 1

## Introduction

### 1.1 Background and motivation

The production and use of fossil-based plastics for packaging materials have rapidly been increasing over the past two decades due to the benefits of broad availability, reasonable price, and tailorable properties. However, non-degradable fossil plastic takes hundreds of years to disintegrate or never breaks down. According to the U.S. Environmental Protection Agency's report in 2015, plastics was one of the major portions of the municipal solid stream (MSW). Approximately, 34,500 thousand tons or 13 percent of the total MSW generated were plastic. The report also shows that only about nine percent of plastic waste was recycled and composted [1].

Biodegradable plastics introduced around 1980 have attracted widespread interest, mainly due to increased environmental awareness and education to conserve fossil fuel resource and reduce the accumulation of plastic waste from daily single use applications. Biodegradable refers to materials that can be broken down into natural elements, carbon dioxide and water by the enzymatic action of microorganism [2].

Poly(lactic acid) (PLA) is the most common biodegradable plastic from biobased resources generally derived from the fermentation of sugars obtained from agricultural byproducts [3,4]. PLA has been approved for use in food packaging, and it has been used as a partial substitute for PS, HDPE, and PET in different forms, for example, rigid thermoforms, oriented films, and beverage bottles. So, several studies have focused on developing the stability, processability, biodegradability, and recyclability of PLA to serve specific requirements suitable for a wide range of industrial applications [5]. However,

one of the major drawbacks of PLA is that it can undergo hydrolytic degradation leading to a significant deterioration of its performance. Several techniques have been developed to improve the hydrolytic stability of PLA. For example, Rodriguez et al. [6] and Huang et al. [7] investigated the effect of PLA blended with PMMA and a natural rubber, respectively. Another approach proposed by Li et al. [8] was adding different types of nucleating agent particles (i.e., titanium dioxide, carbon nanotubes, and graphene nanoplatelets). Unfortunately, none of the methods have resulted in a significant effect on the hydrolysis kinetics, and molecular weight reduction of PLA.

Modifying PLA's structure by using chain extenders is a method that has been widely used during melt processing to connect or reconnect the backbone chains and finally obtain a modified structure of PLA with higher molecular weight, which depends on the chemical structure of chain extender and the mechanism of the chain extension reaction. One of the commercial chain extenders used in several research studies has been a multi-functional epoxy-based chain extender [10–19]. According to the research findings, it can improve mechanical, rheological, physical properties, and maintain optical properties [11,18,19]. However, the effect of thermal and hydrolytic stability of modified PLA with chain extender is still unclear and scarcely reportedly. Therefore, detailed understanding is required to evaluate the influence of the chain extender on the hydrolytic degradation of PLA.

The effect of temperature on hydrolytic degradation is very crucial. Thus, the service time of materials depends on the temperature conditions. If hydrolysis experiments are conducted at low temperature, it may take more than three years for PLA to be entirely degraded [16]. So, the time-temperature superposition principle can be

applied to use to determine the hydrolytic degradation behavior of PLA over a broad range of temperature. The mathematical models were used in the experimental analysis and allowed using the experimental data under accelerated condition (i.e., higher temperatures) to predict values at the lower temperature of interest [20–22].

## 1.2 Overall goal and objectives

The overall goal of this thesis is to determine the hydrolytic degradation of modified PLA films with chain extender in water and 50% ethanol over a wide range of temperature and compare with regular PLA films. To achieve this goal, this project aims to accomplish the following objectives.

1) To determine the factors affecting the chain extension reaction of the modified PLA on the molecular weight variation.

2) To understand the effect of the modified PLA with chain extender on the hydrolytic degradation at different temperatures.

3) To describe the kinetic effects of hydrolytic degradation of the modified PLA using the experimental data in mathematical models.

4) To construct a master curve to predict the hydrolytic degradation process of modified PLA at lower temperature.

## REFERENCES

## REFERENCES


[1] EPA. Advancing Sustainable Materials Management : 2015 Tables and Figures 2018.https://www.epa.gov/sites/production/files/2018-07/documents/2015_smm_msw_factsheet_07242018_fnl_508_002.pdf (accessed February 20, 2019).

[2] Trinetta V, Trinetta V, State K. Biodegradable Packaging. Elsevier; 2016.

[3] Garlotta D. A Literature Review of Poly ( Lactic Acid ) 2002;9:63–4.

[4] Jabeen N, Majid I, Nayik GA. Bioplastics and food packaging : A review. Cogent Food Agric 2015;42:1–6.

[5] Farah S, Anderson DG, Langer R. Physical and mechanical properties of PLA, and their functions in widespread applications — A comprehensive review. Adv Drug Deliv Rev 2016;107:367–92.

[6] Rodriguez E, Shahbikian S, Marcos B, Huneault MA. Hydrolytic stability of polylactide and poly ( methyl methacrylate ) blends 2018;45991:1–14.

[7] Huang Y, Zhang C, Pan Y, Zhou Y, Jiang L, Dan Y. Effect of NR on the hydrolytic degradation of PLA. Polym Degrad Stab 2013;98:943–50.

[8] Li M, Kim S, Choi S, Goda K, Lee W. Effect of reinforcing particles on hydrolytic degradation behavior of poly (lactic acid) composites. Compos2016;96:248–54.

[9] Iñiguez-Franco F, Auras R, Ahmed J, Selke S, Rubino M, Dolan K, et al. Control of hydrolytic degradation of Poly(lactic acid) by incorporation of chain extender: From bulk to surface erosion. Polym Test 2018;67:190–6.

[10] Baimark Y, Cheerarot O. Effect of chain extension on thermal stability behaviors of polylactide bioplastics. Orient J Chem 2015;31:635–41.

[11] Frenz V, Scherzer D, Ag B, Germany L, Villalobos M, Awojulu AA, et al. Multifunctional Polymers as Chain Extenders and Compatibilizers for Polycondensates and Biopolymers . Chain Extension vs Solid State Polymerization 2008:1682–6.

[12] Sudanese I, View PM, Elhassan ASM, Saeed HAM, Eltahir YA, Xia YM, et al. Modification of PLA with Chain Extender. Appl Mech Mater 2014;716–717:44–7.

[13] Najafi N, Heuzey MC, Carreau PJ. Polylactide (PLA)-clay nanocomposites prepared by melt compounding in the presence of a chain extender. Compos Sci Technol 2012;72:608–15.

[14] Cailloux J, Santana OO, Franco-Urquiza E, Bou JJ, Carrasco F, Gámez-Pérez J, et al. Sheets of branched poly(lactic acid) obtained by one step reactive extrusion calendering process: Melt rheology analysis. Express Polym Lett 2012;7:304–18.

[15] Simmons H, Kontopoulou M. Hydrolytic degradation of branched PLA produced by reactive extrusion. Polym Degrad Stab 2018;158:228–37.

[16] Rathi S, Coughlin E, Hsu S, Golub C, Ling G, Tzivanis M. Maintaining Structural Stability of Poly(lactic acid): Effects of Multifunctional Epoxy based Reactive Oligomers. Polymers (Basel) 2014;6:1232–50.

[17] Jaszkiewicz A, Bledzki AK, Duda A, Galeski A, Franciszczak P. Investigation of processability of chain-extended polylactides during melt processing - Compounding conditions and polymer molecular structure. Macromol Mater Eng 2014;299:307–18.

[18] Arruda LC, Magaton M, Bretas RES, Ueki MM. Influence of chain extender on mechanical, thermal and morphological properties of blown films of PLA/PBAT blends. Polym Test 2015;43:27–37.

[19] Dong W, Zou B, Yan Y, Ma P, Chen M. Effect of chain-extenders on the properties and hydrolytic degradation behavior of the poly(lactide)/ poly(butylene adipate-co-terephthalate) blends. Int J Mol Sci 2013;14:20189–203.

[20] Lyu SP, Schley J, Loy B, Lind D, Hobot C, Sparer R, et al. Kinetics and time-temperature equivalence of polymer degradation. Biomacromolecules 2007; 8:2301–10.

[21] Shangguan Y, Chen F, Jia E, Lin Y, Hu J, Zheng Q. New insight into Time-Temperature correlation for polymer relaxations ranging from secondary relaxation to terminal flow: Application of a Universal and developed WLF equation. Polymers (Basel) 2017;9.

[22] Peleg M. Temperature–viscosity models reassessed. Crit Rev Food Sci Nutr 2017;0:1–9.

# CHAPTER 2

## Literature Review

### 2.1 Poly(lactic acid) - PLA

The development of biodegradable materials has recently attracted attention as an environmentally friendly alternative to traditional petrochemical-based plastics. Poly(lactic acid) (PLA) is a biodegradable polymer synthesized from bio-derived monomers, which is compostable under industrial conditions. Lactic acid (2-hydroxy propionic acid) is the basic building block for PLA preferentially produced by bacterial fermentation of carbohydrate sources. Lactic acid (LA) has a chiral carbon so that it exists in two optically active configurations, L-lactic acid (LLA) or (s)-lactic acid and its mirror image, D-lactic acid (LLD) or (r)-lactic acid showing opposite polarized light rotation. LLA can be used to produce a lactide which is an intermediate for polymerization of PLA with greater yields and higher molecular weight. The production of pure LLA can be prepared by the homofermentation using species of *Lactobacillus* genus such as *Lactobacillus delbrueckii*, *L. amylophilus*, *L. bulgaricus,* and *L, leichmanii* under conditions of pH values, temperature, and oxygen content [1,2]. Polycondensation of the hydroxyl and the carboxylic acid functional groups of LA molecules can be used to produce an oligomer of PLA and generates water as a byproduct. Since this reaction is reversible, a water removal process is needed. When LA is converted into a higher molecular weight polymer, the reaction mixture becomes more viscous, so that the removal of water becomes critical. Therefore, direct condensation is generally limited to yield a low molecular weight PLA which is glassy, brittle, and weak in mechanical properties [3,4]. Although condensation polymerization is the cheapest reaction process, to obtain high

molar mass PLA, several catalysts, chain coupling agents and additional methods are required, increasing cost and complexity. Ring-opening polymerization (ROP) is the commercial method used to achieve high molecular weight PLA [3,5–7]. ROP requires several steps starting with a direct polycondensation reaction of lactic acid to produce low molar mass prepolymer (around 1-5 kDa [8]). The second step is a catalytic depolymerization reaction to synthesize lactide, a cyclic LA dimer, under high temperature and low pressure. Since LA has two optical configurations, lactide exists in three diastereomeric structures: L-lactide, D-lactide, and DL-lactide or meso-lactide. The terminal step is the ROP reaction of the lactide and final polymerization. The pathway for the synthesis of PLA polymers is illustrated in **Figure 2.1**. The different fractions of the lactide monomer affect the three produced stereoisomers, poly(L-lactide) (PLLA), poly(D-lactide) (PDLA), and poly(DL-lactide) (PDLLA). The stereochemical purity of PLA produces polymers with different characteristics such as crystallinity, melting point, and mechanical properties [9,10].

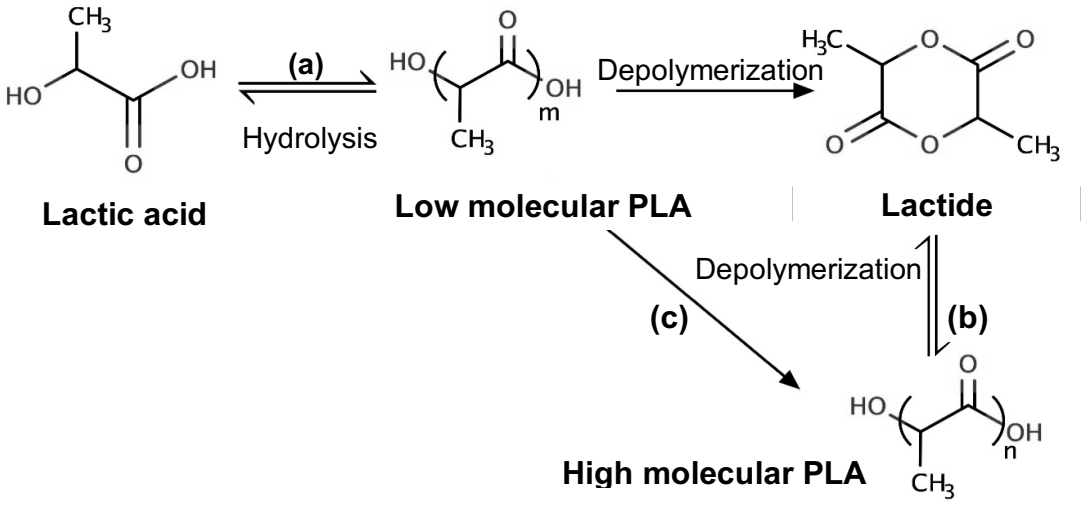


**Figure 2.1** The pathway for the synthesis of PLA: (a) direct polymerization, (b) ROP of lactide, and (c) polycondensation with additional methods. Figure adapted from Ren [8].

## 2.2 Packaging Applications of PLA

Current commercial PLA production has enabled high-volume packaging applications with desirable functionalities, not only because of its biodegradability but also due to its good processability and acceptable properties [10–12]. PLA can be processed for extrusion, injection molding, thermoforming, foaming, blending, casting and blown film [14]. PLA properties are comparable to other petroleum-based materials especially polystyrene, due to its excellent clarity, high strength, and moderate barrier properties [15]. Currently, PLA has been used on short shelf life products such as dairy containers, drinking cups, lids and laminating films. However, it has some significant drawbacks which limit its uses in packaging applications; for instance, it has poor toughness, high brittleness, low melt strength, and low thermal stability [8]. In addition to the mentioned properties, PLA is subject to hydrolytic degradation, which is one of the most critical drawbacks to PLA restricting the expansion of the PLA market for longer shelf life and higher temperature requirements.

## 2.3 Hydrolytic Degradation of PLA

The degradation of PLA is dominated by the hydrolytic degradation process occurring in the presence of water that penetrates the amorphous region of the polymer matrix and then hydrolyzes the ester bonds. During the degradation process, PLA consists of mainly three components: long molecular chains, water-soluble oligomers able to diffuse out of the matrix, and LA monomers as illustrated in **Figure 2.2**. The cleavage of the molecular chains by water molecules causes PLA to break into smaller segments and generate shorter chains. The reduction of the chain length results in decreased molecular weight leading to the deterioration of PLA properties [10,16–18].

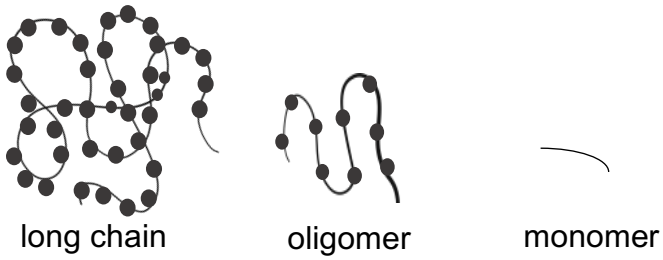


**Figure 2.2** The major components of the hydrolyzed PLA: long molecular chain, oligomer, and monomer. Dots illustrate ester linkages. Figure adapted from Pan [19].

As the degradation proceeds, PLA undergoes structural changes due to the mass loss. This phenomenon is called an erosion process, due to oligomers and monomers diffusing out of the polymer [20]. **Figure 2.3** shows a schematic illustration of surface erosion and bulk erosion mechanisms. If the degradation rate on the surface is faster than the diffusion of water molecules into the matrix, surface erosion occurs. The surface erosion occurs mainly on the surface of the PLA at constant velocity during degradation. On the other hand, if the water diffusion rate is much higher than the hydrolysis, PLA tends to under the homogenous degradation and subsequently bulk erosion which occurs throughout the entire materials. Several studies reported that the hydrolytic degradation of PLA thin film mainly takes place through the bulk erosion pathway [10,21–24]. Burkersroda et al. [24] found that the hydrolytic degradation mechanism of PLA changes from the bulk to surface erosion when its thickness is more significant than 7.4 cm, which is called the critical thickness ($L_{critical}$).

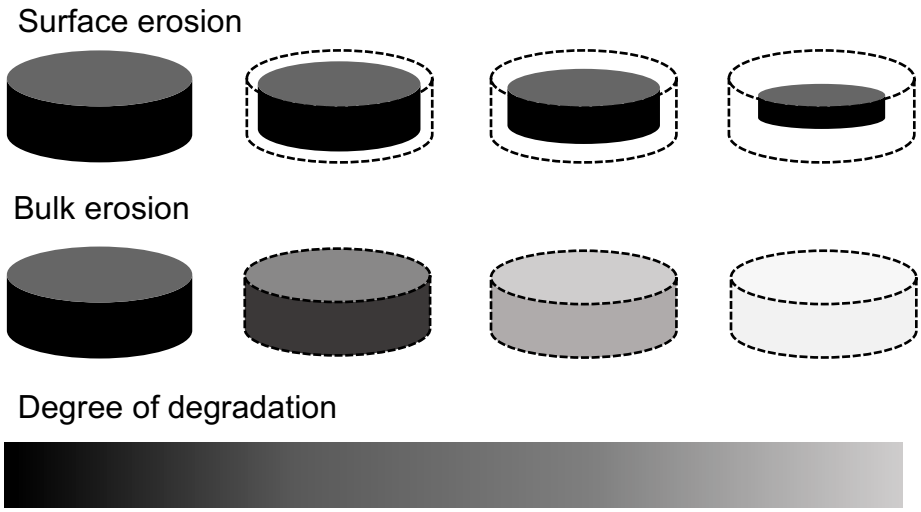


**Figure 2.3** Schematic illustration of surface erosion and bulk erosion mechanism. The black to white gradient represents the degree of degradation. Figure adapted from Burkersroda et al. [24].

### 2.3.1 The kinetics of PLA hydrolysis

The hydrolytic degradation of PLA is a complex process affected by various factors. Initially, when PLA is exposed to high humidity, a water molecule randomly reacts with an ester linkage in the PLA chain to cleave it and produce two shorter chains with carboxyl and hydroxyl ends. The reaction of the chain scission of PLA is given by:

$$R\text{–}C(CH_3)COO\text{–}R' + H_2O \rightarrow R\text{–}C(CH_3)COOH + HO\text{–}R' \qquad (2.1)$$

in which R and R' denote the repeating units of the initial PLA chains. (R – $C(CH_3)$ – COOH) and (R' – OH) represent the hydrolyzed PLA with carboxylic acid and hydroxyl ends. In general, the hydrolysis rate depends on the concentration of the ester bonds, and acidic products, while water molecules are abundant and remain constant [25].

**Table 2.1** shows a list of the simple kinetic models used in research studies to estimate the rate of hydrolysis by tracking the change in molecular weight, which is

considered to be a sensitive parameter for modeling degradation. In order to determine the rate of reaction, the hydrolysis can be described by two main mechanisms, non-catalytic and autocatalytic reactions. The non-catalytic reaction generally occurs in the beginning of the degradation when no catalyst is required. The rate of non-catalytic degradation can be determined as a function of the concentration of ester bonds expressed using molecular weight as shown in Equation A1 **(Table 2.1)**. Several studies have reported that the major reaction in the hydrolytic degradation of PLA is preferentially autocatalytic hydrolysis by generating carboxylic acid end groups which have a high rate of dissociation.

The rate equation is expressed as:

$$d[COOH]/dt = k'[COOH][H_2O][E] \qquad (2.2)$$

where *[COOH], [E]* and *$[H_2O]$* are the concentration of carboxylic acid end groups, esters and water molecules, respectively. *k'* is the rate of degradation. *$[H_2O]$* and *[E]* can be assumed constant throughout the hydrolytic degradation, while *[COOH]* is equal to $1/M_n$. The first order reaction can be expressed as:

$$[COOH] = [COOH]_0 \exp(kt) \qquad (2.3)$$

$$M_n = M_{n_0} \exp(-kt) \qquad (2.4)$$

in which $M_{n_0}$ and $M_n$ are the initial and time-dependent molecular weight of PLA. *t* is time. Equations A2–A7 show the applications of the first order reaction in the hydrolysis studies. In certain cases, the change in the concentration of water and ester bonds is considered, and the second and third order reaction can be applied as shown in Equation A8.

**Table 2.1** The studies using mathematical models for hydrolytic degradation

| Eq. | Hydrolysis system | Model | Mechanism | Ref |
|---|---|---|---|---|
| A1 | Polyester elastomer in high humidity | $\frac{1}{M_{n,t}} - \frac{1}{M_{n,0}} = kt$ | Non-catalytic | [26] |
| A2 | PLLA in PBS solution | 1nd order: $M_{n,t} = M_{n,0}exp(-kt)$ | Autocatalytic | [26-29] |
| A3 | PLA in water and ethanol solution | 1nd order: $M_n = M_{n_0}exp(-kt)$ | Autocatalytic | [31–33] |
| A4 | PLGA in PBS solution | 1nd order: $M_w = M_{w0}exp[k_d(t - t_{lag})]$ | Autocatalytic | [34] |
| A5 | PLGA in PBS Solution | 1nd order: $M_w = M_{w0}exp(-k_{deg}t)$ | Autocatalytic | [33-34] |
| A6 | Polyglyconate in PBS | 1nd order: $M_n = M_{n0}exp(-kt)$ | Autocatalytic | [37] |
| A7 | PLA – PCL in PBS solution | 1nd order: $M_n = M_{n0}exp(-u_m t)$ | Autocatalytic | [38] |
| A8 | PLA in aqueous solutions: HCl, PBS, and NaOH | 2nd order: $\frac{1}{M_n} = \frac{1}{M_{n0}} + \frac{1}{M_0} k_2 c_S t$<br>3rd order: $log(M_n) = log(M_{n_0}) - k_3 c_B c_S t$ | Autocatalytic | [39] |
| A9 | PLA, PCL, and PLGA in PBS solution | $M_n = \left(\frac{[A]_0}{\rho} \cdot \frac{exp(c_1 t) - 1}{1 + c_2 exp(c_1 t)} + \frac{1}{M_{n,0}}\right)^{-1}$<br>$c_1 = ([E]_0 + [A]_0)k,\ c_2 = \frac{[A]_0}{[E]_0}$ | Autocatalytic | [40] |
| A10 | Hydrolytic degradation of biodegradable polymer for medical device | $\frac{dR_s}{dt} = k_1 C_E + k_2 C_E \left(C_m + \frac{C_{ol}}{m}\right)^n$<br>$C_E = C_{E_0} - C_{ol}$<br>$M_n = \frac{C_E M_0}{N_{chain0} + R_s - \left(\frac{C_{ol}}{m}\right)}$ | Non-catalytic<br>Autocatalytic | [39–45] |
| A11 | Hydrolytic degradation of biodegradable polymer for medical device | $\frac{dR_{rs}}{dt} = k_{r1} C_E + k_{r2} \left(C_m + \frac{C_{ol}}{m}\right)^n$<br>$\frac{dR_{es}}{dt} = k_{e1} C_{end} + k_{e2} C_{end} \left(C_m + \frac{C_{ol}}{m}\right)^n$<br>$C_E = C_{E_0} - (C_{ol} + C_m)$<br>$M_n = \frac{C_E M_0}{N_{chain0} + R_{rs} - \left(\frac{C_{ol}}{m}\right)}$ | Non-catalytic<br>Autocatalytic (random and end scission) | [46-47] |

Referring to Equation A10 (**Table 2.1**), the model has been proposed by Pan [19]. It was developed for modeling degradation of biodegradable medical devices. The model can be capable of depicting the hydrolytic process which describes the changes of the physical and chemical compositions. Variations of this model can be found in many studies [39-47], which provided a better understanding by taking into account more variables affecting the hydrolysis behavior; for example, the diffusion of small oligomers, the initial molecular weight, and monomer residues.

The rate of chain scission reaction can be written as:

$$\frac{dR_s}{dt} = k_1 C_E + k'_2 C_E C_{H^+} \qquad (2.5)$$

in which $R_s$ is the total number of chain scissions per unit volume, $k_1$ and $k'_2$ are the rate constant of the non-catalytic and auto-catalytic reaction, respectively, and $C_{H^+}$ is the concentration of the catalyst $H^+$. During the hydrolytic degradation of a PLA chain, the scission of one ester bond produces two shorter polymer chains. As the total number of ester units of all the long chains per unit volume ($C_E$) decreases due to chain cleavage reactions, the total number of ester units of all the short chains ($C_{ol}$) gradually increases, which can be expressed as:

$$C_E = C_{E_0} - C_{ol} \qquad (2.6)$$

where $C_{E_0}$ is the initial $C_E$. $C_{E_0}$ can be calculated from the molecular weight of the repeating unit and the initial density of PLA. Moreover, the concentration of the carboxylic end groups increases and accumulates inside the sample. Since the hydrolytic degradation of PLA is predominantly autocatalytic, the reaction is catalyzed by hydrogen ions from the dissociation of carboxylic end groups [28,48,50].

The production of $H^+$ can be represented as:

$$R\text{–}C(CH_3)COOH \rightleftharpoons R\text{–}COO^- + H^+ \qquad (2.7)$$

The acid dissociation constant ($k_a$) can be written as:

$$k_a = \frac{C_{H^+} C_{COO^-}}{C_{COOH}} \qquad (2.8)$$

in which $C_{H^+}$ and $C_{COO^-}$ are the concentration of the catalyst $H^+$ and $COO^-$ .

At equilibrium:

$$k_a C_{COOH} = C_{H^+} C_{COO^-} = C_{H^+}{}^2 \qquad (2.9)$$

$$C_{H^+} = [\, k_a C_{COOH}]^{0.5} \qquad (2.10)$$

Substituting Eq. (2.10) into Eq. (2.5), the rate of chain scission can be expressed as:

$$\frac{dR_s}{dt} = k_1 C_E + k'_2 C_E [k_a C_{COOH}]^{0.5} \qquad (2.11)$$

Due to the limited mobility of the molecular chains, only the carboxylic end groups of the oligomers can catalyze the hydrolytic degradation. The concentration of *–COOH* end groups can be determined as:

$$C_{COOH} = \frac{C_{ol}}{m} \qquad (2.12)$$

where *m* is the average degree of polymerization of oligomers.

$$\frac{dR_s}{dt} = k_1 C_E + k'_2 C_E \left[k_a \frac{C_{ol}}{m}\right]^{0.5} \qquad (2.13)$$

$$\frac{dR_s}{dt} = k_1 C_E + k_2 C_E [C_{ol}]^{0.5} \qquad (2.14)$$

in which $k_2 = k'_2 \left[\frac{k_a}{m}\right]^{0.5}$

Generally, the hydrolytic degradation process experiences a combination of random and end-chain scission. A schematic illustration of chain scission is presented in **Figure 2.4**. In random scission, the ester bonds are randomly cleaved along the PLA chains. Then, shorter chains and oligomers are produced. Alternatively, the end-chain scission occurs only at the ester bonds next to the chain ends generating monomers. Hence, random scission is the main factor for a reduction in the average molecular weight. Nevertheless, it has been reported that the end-chain ester groups are more susceptible to cleavage. It can occur up to 100 times more than random scission [51].

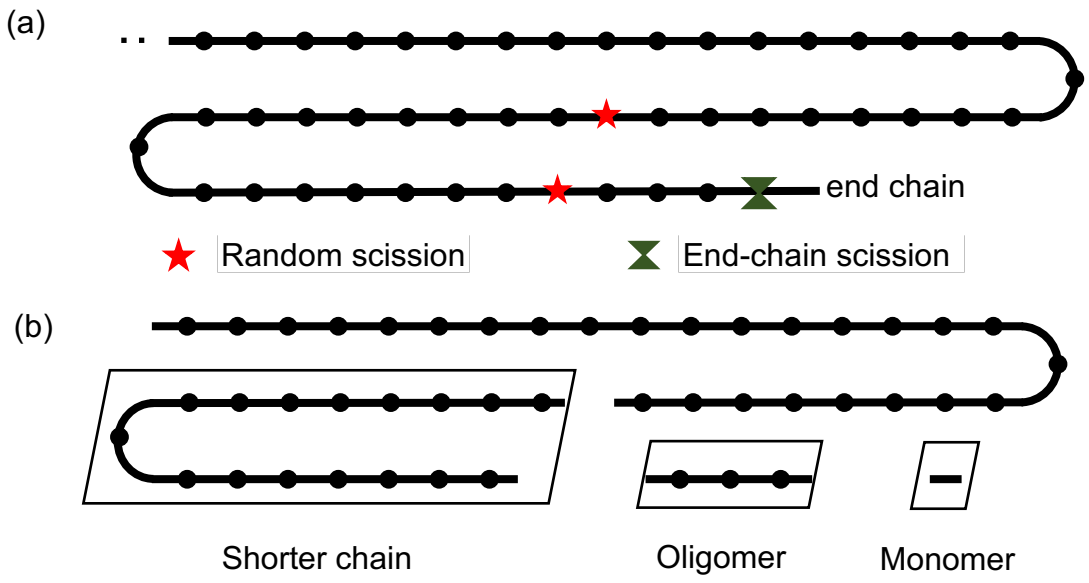


**Figure 2.4** Schematic illustration of random and end-chain scission: (a) example of the locations of chain scission, (b) the products obtained from chain scission

By using statistical analysis, the relationship between the production of the short chains and the chain scission can be determined as [49]:

$$\frac{C_{ol}}{C_{E0}} = \alpha \cdot \left(\frac{R_s}{C_{E0}}\right)^{\beta} \qquad (2.15)$$

where $\alpha$ and $\beta$ are dimensionless constants used to describe the relationship between $C_{ol}$

and $R_s$. The set of both factors represents the nature of the chain scission. The $\alpha$ and $\beta$ can be determined by fitting the equation with experiments with Monte Carlo simulation. The relationship of $\alpha$ and $\beta$ was reported for two extreme cases [19,52]. In the case of end-chain scission, one monomer was produced by one chain scission; therefore, the $\alpha$ and $\beta$ were equal to 1. On the other hand, for random chain scission, the values of $\alpha$ and $\beta$ were estimated as $\alpha$ = 36 and $\beta$ = 2. The values of $\alpha$ and $\beta$ have a significant effect on the hydrolytic degradation mechanism, particularly the auto-catalytic reaction. Han et al. [44] and Sevim and Pan [46] studied the hydrolysis kinetics by simulating using existing data for PLA degradation. The values of $\alpha$ and $\beta$ were set as 0.4 and 1, which expressed the combination of random and end scission so that one oligomer was achieved after ten chain scissions occur which m (in Eq. (2.14)) was assumed as 4. It was found that this set of values can be used to fit the experimental data of the hydrolysis of PLA of Lyu et al. [50], Weir et al. [53], and Grizzi et al. [54].

Substituting Eq. (2.6) and (2.15) into Eq. (2.14) gives:

$$\frac{dR_s}{dt} = C_{E_0}\left[1-\left(\alpha\left(\frac{R_s}{C_{E_0}}\right)^{\beta}\right)\right]\left\{k_1+k_2\left[C_{E_0}\cdot\alpha\left(\frac{R_s}{C_{E_0}}\right)^{\beta}\right]^{0.5}\right\} \qquad (2.16)$$

During hydrolysis experiments, the degree of crystallinity of PLA drastically increases. The polymer crystals form and grow due to an increase of the new potential nucleation entities and the chain mobility of the short chains to crystallize [10,17,42,47,55]. Therefore, the reduction in $C_E$ during the degradation is calculated by subtracting the concentration of the crystallinity. Eq. (2.6) can be adjusted as:

$$C_E = C_{E_0} - C_{ol} - \omega\left(X_C - X_{C_0}\right) \qquad (2.17)$$

in which $\omega$ is the number of ester units per unit volume of the crystalline phase which can

be calculated from the molecular weight of the repeating unit of PLA and the initial density of the polymer crystal. $X_{C_0}$ and $X_C$ are the initial and time-dependent degree of crystallinity. As aforementioned, the chain cleavage dominantly occurs in amorphous regions, while the crystallites are much harder to hydrolyze and remained as crystal residues after the degradation process.

So, $R_s$ has to consider only the amorphous phase, which can be rewritten as:

$$\frac{dR_s}{dt} = C_{E_0}\left[1 - \left(\alpha\left(\frac{R_s}{C_{E_0}}\right)^{\beta} - \frac{\omega(X_C - X_{C_0})}{C_{E_0}}\right)\right]\left\{k_1 + k_2\left[\alpha\left(\frac{R_s}{C_{E_0}}\right)^{\beta}\cdot\left(\frac{1}{1\text{-}X_C}\right)\right]^{0.5}\right\} \qquad (2.18)$$

Eq. (2.18) can be written into a normalized form as:

$$\frac{d\bar{R}_S}{dt} = \left[1 - \left(\alpha(\bar{R}_S)^{\beta} - \bar{\omega}(X_C - X_{C_0})\right)\right]\left\{k_1 + k_2\left[C_{E_0}\cdot\alpha(\bar{R}_S)^{\beta}\cdot\left(\frac{1}{1\text{-}X_C}\right)\right]^{0.5}\right\} \qquad (2.19)$$

where $\bar{R}_S$, $\overline{\omega}$, and $\overline{M_n}$ are the normalized forms can be expressed as: $\frac{R_s}{C_{E_0}}$, $\frac{\omega}{C_{E_0}}$, *and* $\frac{M_n}{M_{n0}}$

The average molecular weight of the degraded polymer can be assessed by quantifying the weight of all chains in the amorphous and crystalline regions. The number average molecular weight can be calculated as:

$$M_n = \left(\frac{(C_{E_0} + \omega X_{C_0})\, M_0}{N_{chain0} + R_s}\right) \qquad (2.20)$$

where $M_0$ is the molecular weight of the repeating unit of PLA and $N_{chain0}$ is the number of the polymer chains in the unit volume, which can be assessed from the initial density of the polymer and initial molecular weight. The short chains, the small oligomers and monomers, are assumed to be soluble in the hydrolysis media. They can migrate out of the matrix and cannot be detected by the measurements of molecular weights of the hydrolyzed sample [44].

Eq.(2.20) can be adjusted by discounting the short chains as follows:

$$M_n = \left( \frac{(C_{E_0} + \omega X_{C_0} - C_{ol}) M_0}{N_{chain_0} + R_s - \left(\frac{C_{ol}}{m}\right)} \right) = \left( \frac{\left(C_{E_0} + \omega X_{C_0} - \alpha \cdot C_{E_0} \cdot \left(\frac{R_s}{C_{E_0}}\right)^{\beta}\right) M_0}{N_{chain_0} + R_s - \left(\frac{\alpha}{m} \cdot C_{E_0} \cdot \left(\frac{R_s}{C_{E_0}}\right)^{\beta}\right)} \right) \qquad (2.21)$$

Now, the normalized $M_n$ can be expressed as:

$$\overline{M_n} = \frac{M_n}{M_{n0}} = \left( \frac{1 + \bar{\omega} X c_0 - \alpha \left(\overline{R_s}\right)^{\beta}}{(1 + \bar{\omega} X c_0) \left[1 + \frac{C_{E_0}}{N_{chain0}} \left(\overline{R_s} - \frac{\alpha}{m} \left(\overline{R_s}\right)^{\beta}\right)\right]} \right) \qquad (2.22)$$

### 2.3.2 Parameters affecting hydrolytic degradation

The hydrolytic degradation of polymeric biodegradable materials is diverse and complex. There are a lot of parameters affecting its rate and the behavior of degradation associated with the surrounding media and the characteristics of the material. The major factors listed below are crucial to take into account when studying and controlling the hydrolysis of PLA.

#### 2.3.2.1 pH

The chain scission reaction that occurs during hydrolytic degradation of PLA can be catalyzed by the presence of a high concentration of hydroxide ($OH^-$) and hydronium ($H3O^+$) ions in the alkaline and acidic media, respectively. **Figure 2.5** illustrates a suggestion for the mechanism of hydrolysis in alkaline and acidic environments proposed by de Jong et al. [56]. It has been reported that the hydrolysis of PLA under acidic conditions undergoes chain-end scission faster than intramolecular scission when the molecular weight of PLA is less than 100 kDa [10,57]. Sailema-Palate [58] explained that the differences in the pH of media have a significant effect on the hydrophobicity. In alkaline solution, the hydroxyl ions are entrapped on the outer surface, which can reduce

the diffusion into the inner structure of the material [59]. As a result, surface erosion mechanism can occur. Jung et al.[60] evaluated the hydrolytic degradability of PLA in acidic and basic aqueous solutions by varying pH. A higher degradation rate constant was discovered under strongly basic conditions compared to ones in strong acid, while the lowest rate constant occurred at intermediate conditions. Thus it was confirmed that the hydrolysis of PLA can be accelerated by acidic or alkaline conditions.

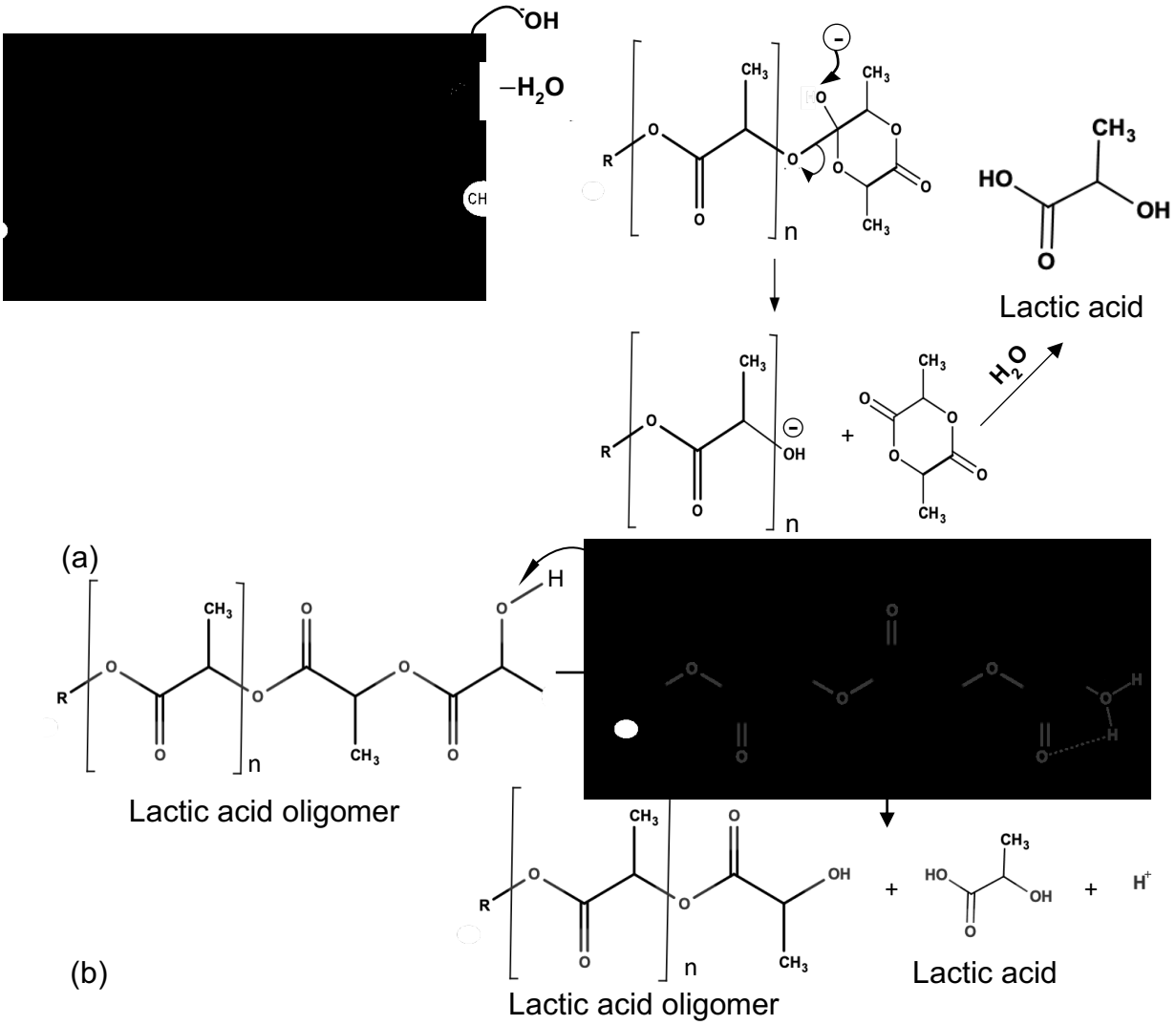


**Figure 2.5** Suggestions for the mechanism of hydrolytic chain scission of PLA: (a) in alkaline and (b) in acidic media, adapted from de Jong et al. [56].

#### 2.3.2.2 Temperature

The rate constant of the kinetic reaction of hydrolysis of PLA is highly affected by the temperature of the media. Hydrolysis proceeds slowly at low temperatures, while the reaction takes less time at higher temperatures. It has been widely accepted that as the temperature increases, the rate of reaction increases without changing the mechanism [44]. Weir et al. [53] reported that the hydrolysis mechanism of PLA at 50 °C and 70 °C proceeds via bulk degradation similarly to that tested at 37 °C. Many hydrolysis studies have been carried at elevated temperatures in order to accelerate the reaction and extrapolate the result to others at lower temperatures [61].

The activation energy ($E_a$) which is the minimum energy required to initiate the chemical reaction of the material can be determine using the Arrhenius model as below:

$$k = k_0 \exp\left(\frac{-E_a}{RT}\right) \qquad (2.23)$$

where $k$ is the rate constant, $k_0$ is the pre-exponential factor, $E_a$ is the activation energy of the reaction, $R$ is the gas constant (8.314 kg $m^2/s^2$ $K^{-1}$ $mol^{-1}$), and $T$ is the experimental temperature in Kelvin. The $E_a$ is obtained from the slope of the plot of log $k$ versus $T^{-1}$.

Generally, the experimental temperature used for the hydrolytic degradation can be separated into two ranges by the glass transition temperature ($T_g$) which is the boundary temperature between the glassy rigid and rubbery flexible states of polymer. Many studies have reported that the $E_a$ values for hydrolytic degradation conducted at a temperatures below and above $T_g$ were distinctly different [9,39,44,62]. When the hydrolysis temperatures are above $T_g$, the molecular chains have high segmental mobility and free volume, which is defined as the space between molecules. As a result, water

molecules can penetrate into amorphous and attack the ester bonds causing chain scission reaction. In contrast, if the degradation temperature is less than $T_g$, the molecules has less mobility and lack of space among the molecular chains as shown in **Figure 2.6**. The change in the slope of Arrhenius plot below and above $T_g$, can be illustrated by **Figure 2.7**. It demonstrates that $E_a$ values of the two ranges are different. Therefore, the hydrolytic degradation above $T_g$ cannot be used for predicting the result of hydrolysis below $T_g$.

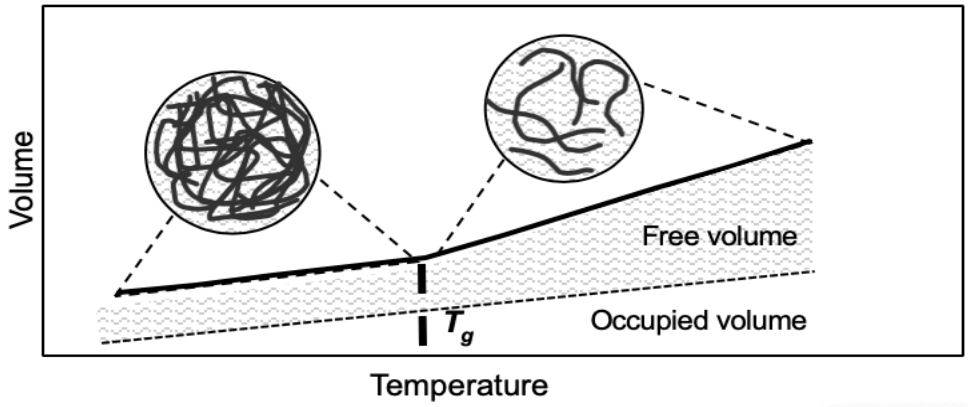


**Figure 2.6** Free volume diagram of polymer chains at the temperature below and above $T_g$. Figure adapted from Danner [63].

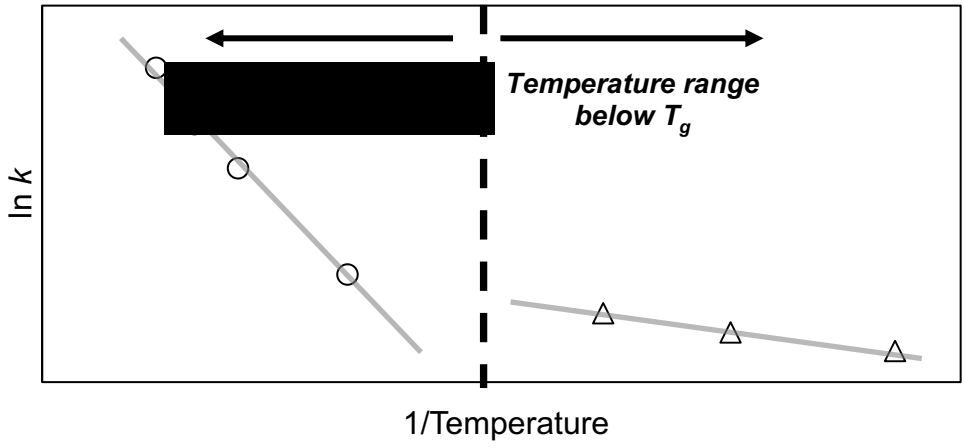


**Figure 2.7** Arrhenius plot of rate constant at the temperature below and above $T_g$

The effect of temperature on the rate of hydrolysis over at below and above $T_g$ has been investigated using the Vogel-Fulcher-Tammann (VTF) equation.

The VTF equation is expressed in the following form:

$$k = k_0 \exp\left(\frac{-E_{VTF}}{R(T - T_s)}\right) \qquad (2.24)$$

whereas $T_s$ is called "Vogel Temperature" which is a temperature that the movement of the polymer chains is totally zero. For viscoelastic polymer, $T_s$ has been found to be approximately 50 K below its $T_g$ [39]. $T$ is the experimental temperature and $E_{VTF}$ is the activation energy of VTF equation.

William-Landel-Ferry (WLF), an mathematical equivalent model of the VTF equation, can be expressed as follows [64–66] :

$$\alpha_T = \frac{k_T}{k_{T_i}} = \left(\frac{exp\left(\frac{-E_{VTF}}{R\,(T - T_s)}\right)}{exp\left(\frac{-E_{VTF}}{R\,(T_i - T_s)}\right)}\right) = exp\left(\frac{-E_{VTF}}{R\,(T - T_s)} - \frac{-E_{VTF}}{R\,(T_i - T_s)}\right) \qquad (2.25)$$

$$\log(\alpha_T) = \left(\frac{\frac{E_{VTF}/R}{2.303\,(T_i - T_s)}(T - T_i)}{(T_i - T_s) + (T - T_i)}\right) \qquad (2.26)$$

$$\log(\alpha_T) = \left(\frac{-C_1(T - T_i)}{C_2 + (T - T_i)}\right) \qquad (2.27)$$

$$C_1 = \frac{E_{VTF}/R}{2.303\,(T_i - T_s)} \text{ and } C_2 = (T_i - T_s) \qquad (2.28)$$

where $\alpha_T$ is the shift factor as ratio of hydrolysis rate at an experimental temperature ($T$) to one at a temperature of interest ($T_i$) The shift factor can be calculated using the $E_{VTF}$ estimated from the experiments at the range of temperatures of interest and used to construct the master curve at $T_i$ [64,65]. Lyu et al.[39] studied the accelerated hydrolysis

testing of PLA and proposed the master curve of the degradation at 37°C by shifting the experimental data at elevated temperature.

#### 2.3.2.3 Crystallinity

In hydrolytic degradation, the morphology of semi-crystalline polymer can be explained by a two-phase structural model, amorphous and crystalline regions. As previously mentioned, the hydrolytic degradation of polymers dominantly occurs in the amorphous regions because the water molecules can penetrate faster compared to in the restricted crystal area. It can be observed that the hydrolytic chain scission provides extra mobility which encourages the molecular chains to form crystal structures in both initially amorphous and semi-crystalline polymers [17,18,47,67,68]. The Avrami model as shown in Eq.(2.29) is one of the classical theories used for predicting chain cleavage-induced crystallization [69] :

$$X_t = 1 - exp[-(k_c t)^n] \tag{2.29}$$

where $k_c$ is a kinetic rate constant, $t$ is crystallization time, and $n$ is the Avrami exponent.

Studies of the properties of the semi-crystalline polymer are much more complicated than ones of amorphous polymers. On the other hand, there are some phenomena relating to several properties, for instance, mechanical properties, oxygen permeation, and complex behaviors, that cannot be explained by the two-phase model. A three-phase model has been purposed to provide a complete understanding of the properties of semi-crystalline materials. The different regions can be considered as the crystalline fraction (CRF), the mobile amorphous fraction (MAF), and the rigid amorphous fraction (RAF) [70–78]. **Figure 2.8** shows a schematic illustration of a spherulite with oriented lamellar stacks growing from a nucleation point and the three different regions:

CAF, MAF, and RAF of semi-crystalline PLA. The RAF relates to an intermediate phase between the CRF and MAF which has high density and restricted mobility due to the fixation of the RAF chains to the crystalline lamellar stack.

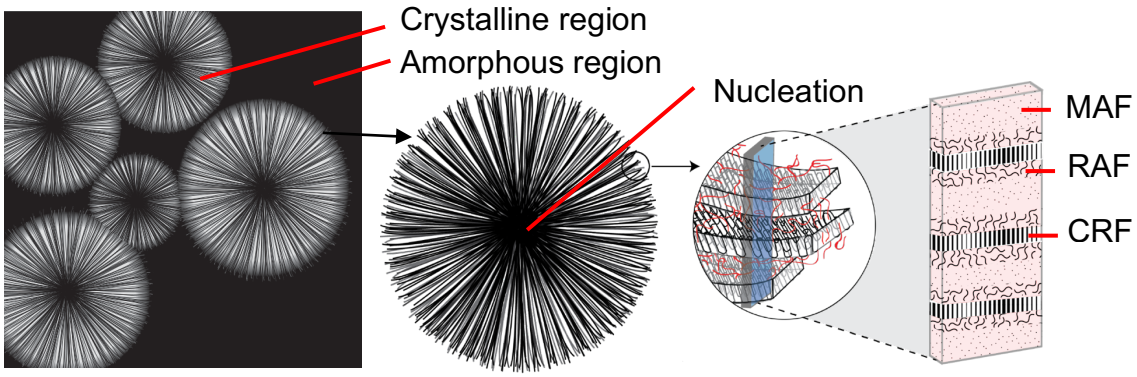


**Figure 2.8** Schematic illustration of a spherulite with oriented lamellar stacks growing from a nucleation point and the three different regions, adapted from Martin et al. [72]

Many research studies have investigated the complex characteristics of the RAF of a three-phase model. Generally, the fraction of non-crystalline phase contributes to the $T_g$ of the polymer, which can be observed as a change in heat capacity over the glass transition. The RAF naturally mobilizes at a broad range of temperature between the $T_g$ and $T_m$ depending on the various degrees of coupling between the crystals and the amorphous phase [25]. Moreover, the RAF formation is dependent on the crystal perfection [76,79]. One of the important properties affecting the hydrolytic degradation of PLA is the water diffusion. Drieskens et al.[80] evaluated the change in morphology of PLA during cold crystallization at a different temperature. They reported that the permeability decreased with the crystallinity increasing; however, it did not represent a linear relationship with the decrease in the amorphous fraction. They also concluded that the RAF could be one of the morphological factors affecting the diffusivity and permeability. Rio et al. [78] studied the effect of the CRF and RAF on the free volume of

PLLA using positron annihilation lifetime spectroscopy (PALS) and found that the RAF increased with the increase of CRF during annealing time. The formation of RAF can increase the free volume due to the occluded areas in the inter-spherulite boundaries and the de-densification of the amorphous fraction. As a result, the diffusivity of the molecules was found to be increased and decreased through the RAF and CRF, respectively. Due to the balance of the two phases, the overall diffusivity was assumed to be constant. Sangroniz et al. [77] observed a different result for PDLA-PLLA 50:50 which naturally has a small amount of RAF compared to PLLA. They reported that the crystallinity increased with the annealing time, while the RAF decreased due to the more compact nature of the crystalline phase and more mobility of the chains in the amorphous regions of the stereocomplex PLA. Contrarily to the PLLA properties, the diffusivity of PDLA-PLLA was decreased compared to PLLA owing to the smaller effect of RAF. The existence of the RAF have been confirmed in many studies [67–77]; however, the properties of the RAF have not been fully investigated.

#### 2.3.2.4 Molecular weight

The effect of molecular weight on the hydrolytic degradation of PLA-based materials has been examined in many studies. It was reported that the hydrolysis of PLA with molecular weight less than $4x10^4$ g/mol was accelerated as molecular weight decreased because PLA matrix with shorter molecular chains has higher chain mobility, hydrophilicity, and concentration of catalytic end groups, while the effect was not significant in higher molecular weight polymer [54,81–84]. Gleadall et al. [49] studied the effect of initial molecular weight on the degradation of bioresorbable polyesters by considering the type of hydrolysis, namely noncatalytic random scission, autocatalytic

random scission, noncatalytic end scission, and autocatalytic end scission. They found that by considering the reaction in one-unit volume of polymer, a lower initial molecular weight of polymer had a greater number of chains. They have a higher chance to produce of oligomers and monomers. Moreover, the concentration of carboxyl ends of PLA chains, especially the short chains, had a significant impact on both autocatalytic end and random scissions.

#### 2.3.2.5 Molecular branching

Nowadays, branched PLA has been developed using various methods during ROP and post-polymerization modification to achieve desired properties and stabilities. The branched PLA can be produced with many topologies, for example, star-shaped, comb-shaped, hyperbranched, H-shaped, long-chain branched, and dumbbell-shaped PLA which have different characteristics [85,86]. Simmons and Kontopoulou [87] studied the hydrolytic degradation of long chain branched PLA at 60 °C and found that the branched chain structure had a significant effect on the degradation behavior and elevated the rate of hydrolysis. However, Numata et al. [88] investigated the effect of the number of molecular branches of PLA on the alkaline hydrolysis. They concluded that PLA with fewer branches had no effect on the hydrolytic degradation since the effect of branched PLA is dependent on the number of catalytic terminal groups and hydrophilic ends. According to Corneillie and Smet [86], the special structures of modified branched PLA, for example, dumbbell-shaped PLA, exhibited decrease of hydrophobicity, and degradation. Tsuji and Hayashi [89] studied the hydrolytic degradation of a linear aliphatic, and star-shaped polyester which had two and four hydroxyl ends, respectively. They found that the rate of degradation decreased with increasing branching structure

because it had higher mobility and a greater number of hydrophilic hydroxyl groups which affected the diffusion rate and the concentration of water molecules.

## 2.4 Controlling the hydrolytic degradation by using chain extender

The chain extension reaction is a conventional method developed to modify the molecular chains of aliphatic polyesters. The higher molecular weight polymers can be obtained by adding chain extenders during melt processing to connect the reactive ends of two polymeric chains. A variety of chain extenders have been developed to serve different types of mechanism. Chain extenders can be divided into two categories, activating-type, and addition-type. The activation-type chain extenders, for example, diphenyl carbonate, diphenyl terephthalate, and diphenyl oxalate, act as intermediates for linking two polymer chains. After the reaction ends, they are not part of the final product. Therefore, the chain extenders coming as byproducts can be contaminated and need to be removed from the polymer system. In contrast, the reaction of addition-type chain extender does not produce a byproduct. This type of chain extender, generally including epoxides, anhydrides, and cyanates, can connect the polymer molecules through a ring opening reaction [90]. The addition-type chain extender tends to provide branching structure. The degree of branching and its characteristics that occur in the reaction depend on the amount of reactive functionality, the concentration of chain extender, and condition of the reaction [90–92]. Najafi et al. [43] studied the properties of PLA nanocomposites with epoxy-based chain extender. They found that the epoxy groups of the chain extender favorably react with carboxylic ends and negligibly react with the hydroxyl group. **Figure 2.9** represents a schematic of the basic chain extension reaction. Nowadays, multifunctional epoxy-based chain extenders have been

commercially used for many purposes such as enhancing the molecular weight of PLA in the production and recycling process, increasing the thermal stability, and improving properties [93–97].

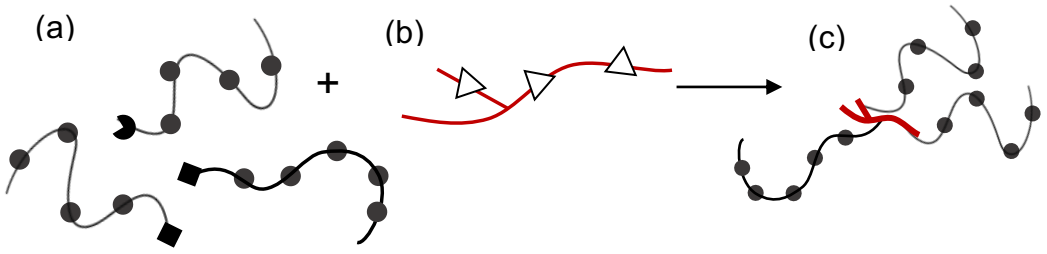


**Figure 2.9** Schematic of the basics of chain extension: (a) PLA chains, (b) chain extender, and (c) chain – extended PLA. ● represents ester linkages, ◕ ◆ represent the end groups of PLA, and △ represents the reactive functional groups of the chain extender.

## 2.5 Response Surface Methodology

Response surface methodology (RSM) is a statistical and mathematical technique commonly used in chemical and biochemical research to study the relationship between the yield of a chemical experiment and a set of independent variables affecting the yield of the experiment and/or reaction. Nowadays, RSM has been successfully applied to various fields of study such as agricultural and biological research, and chemical engineering [98–100]. It is a very useful tool for setting up and designing a set of experiments, which provides appropriate and sufficient measurements to obtain reliable response values. Moreover, it can be used to evaluate the best fit model to the experimental data from the design used. RSM can also be used for process optimization by finding the best set of factor levels to achieve the optimum yield. [101,102].

The RSM procedures can be summarized in four steps. The initial step is the determination of independent variables of the experimental system. The next step is the

selection of the experimental design, which provides the appropriate design points to fit with the experimental responses. The third step is the parameter estimation of the response value. The final step is the construction of the response surface plot and determining optimum conditions. Details of each step are explained below.

In a general study, several parameters may affect the interested outcome response of the experiment. Due to many limitations, it is almost impossible to identify and study the effect of all parameters. A screening experiment can be used to select the independent parameters which have a significant effect or the desirable outcomes. Moreover, the levels of each parameter have to be investigated to focus on the region of interest and delimiting the experimental boundary conditions. To properly analyze a response value obtained from a set of the input variable, it is assumed to be continuous within the range of the selected region. The functional relationship between the response and the independent variables can be presented by a mathematical model as followed:

$$y = f(x_1, x_2, \ldots, x_k) + \varepsilon \qquad (2.30)$$

where $y$ is the continuous scale of response value, $x_1, x_2, \ldots, x_k$ *are* the input variables and $\varepsilon$ is the error term. In the case that the experiments are conducted in a small range of the independent variables close to the initial conditions and far from a curvature effect, the response values can be fitted with a first-order model [98] such as:

$$y = \beta_0 + \sum_{i=1}^{k} \beta_i x_i + \varepsilon \qquad (2.31)$$

This model is a multiple linear regression model where the parameter $\beta_0$ represents the intercept of the plane, and $\beta_1, \beta_2, \ldots, \beta_k$ are the partial regression coefficients. When the curvature of the response surface is large, the optimum solution, which is the most

desirable response value, is expected to appear in this location. A second-order polynomial (or higher-order polynomial) is required for fitting the response surface by adding additional terms of the interactions. Therefore, if the model appropriately represents the experimental process, the optimum conditions can be identified [103,104]. The second-order polynomial model is expressed as:

$$y = \beta_0 + \sum_{i=1}^{k} \beta_i x_i + \sum_{i=1}^{k} \beta_{ii} x_i^2 + \sum \sum_{i<j}^{k} \beta_{ij} x_i x_j + \varepsilon \qquad (2.32)$$

where $\beta_{ii}$ and $\beta_{ij}$represent the quadratic and interaction main effects.

To estimate the parameters in the model, a design of experiment has to be selected to provide the appropriate prediction. The most common designs for fitting first-degree models are $2^k$ factorial, Plackett-Burman, and simplex design, while the second-order designs frequently used are the $3^k$ factorial, Box-Behnken, and central composite designs (CCDs) [103]. The most popular for second-order designs is the CCD. This design consists of the following parts: (1) F factorial points, where the factor levels are coded as -1 and 1; (2) axial points consisting of 2k located on the axis at a distance of $\alpha$ from the design center; and (3) $n_0$ center points. The selection of the axial distance is very crucial depending on the nature of the region of interest and region of operability [102,103]. An example of experimental CCD for three variables is shown in **Figure 2.10** and described in **Table 2.2.**

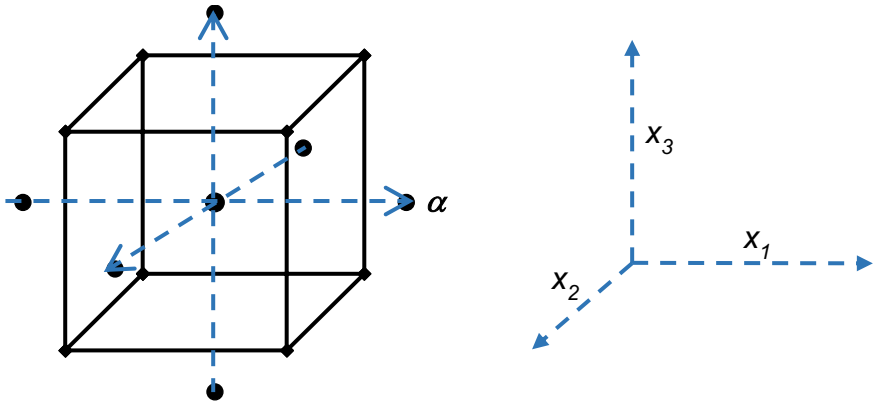


**Figure 2.10** Center composite design for three variables (k = 3)

The experimental data resulting from the combined effect of the variables is used for fitting a mathematical model. The application of analysis of variation (ANOVA) is generally used to determine a set of models that can be fit to experimental data and provide statistical analysis for an existing fitted model [105]. The optimal conditions of the experiments are evaluated from the predicted model [103,106]. The visualization of the predicted model can be presented graphically by the contour and response surface plots of the responses as a function of the independent parameters as shown in **Figure 2.11**.

**Table 2.2** Experimental center composite design for three variables (k = 3)

| | $x_1$ | $x_2$ | $x_3$ |
|---|---|---|---|
| Factorial points ($2^3$) | -1 | -1 | -1 |
| | 1 | -1 | -1 |
| | -1 | 1 | -1 |
| | -1 | -1 | 1 |
| | 1 | 1 | -1 |
| | 1 | -1 | 1 |
| | -1 | 1 | 1 |
| | 1 | 1 | 1 |
| Axial points (2x3) | $-\alpha$ | 0 | 0 |
| | $\alpha$ | 0 | 0 |
| | 0 | $-\alpha$ | 0 |
| | 0 | $\alpha$ | 0 |
| | 0 | 0 | $-\alpha$ |
| | 0 | 0 | $\alpha$ |
| Central point | 0 | 0 | 0 |

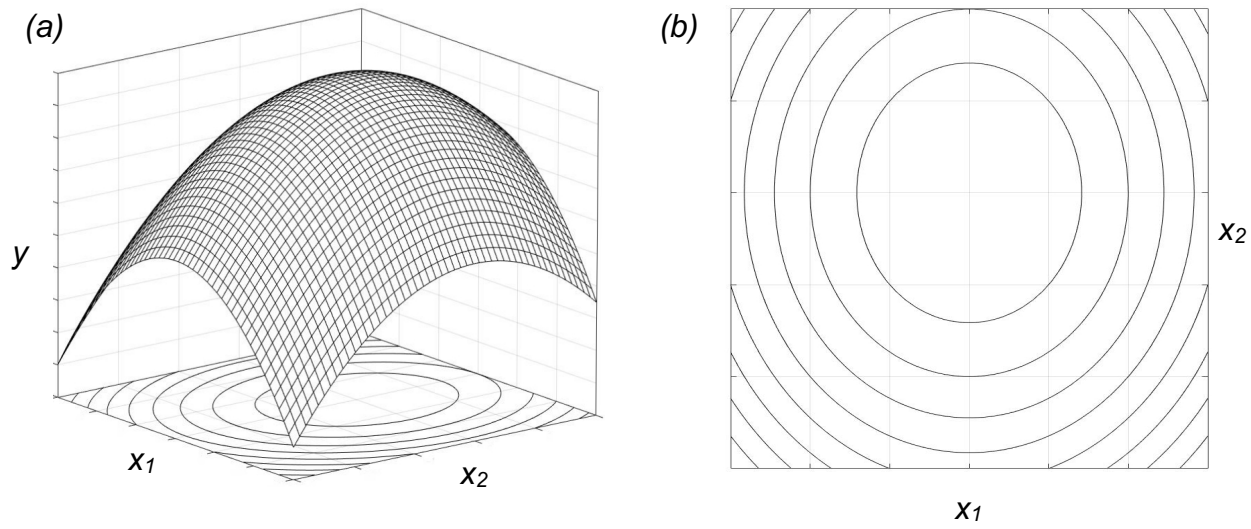


**Figure 2.11** (a) Three-dimensional response surface plot for the second-order model, and (b) two-dimensional contour plot

# REFERENCES

## REFERENCES


[1] Jamshidian M, Tehrany EA, Imran M, Jacquot M, Desobry S. Poly-Lactic Acid: Production, Applications, Nanocomposites, and Release Studies. Compr Rev Food Sci Food Saf 2010;9:552–71.

[2] Castro-Aguirre E, Iñiguez-Franco F, Samsudin H, Fang X, Auras R. Poly(lactic acid)—Mass production, processing, industrial applications, and end of life. Adv Drug Deliv Rev 2016;107:333–66.

[3] Garlotta D. A Literature Review of Poly ( Lactic Acid ) 2002;9:63–4.

[4] Elsawy MA, Kim K, Park J, Deep A. Hydrolytic degradation of polylactic acid ( PLA ) and its composites. Renew Sustain Energy Rev 2017;79:1346–52.

[5] Madhavan Nampoothiri K, Nair NR, John RP. An overview of the recent developments in polylactide(PLA)research. Bioresour Technol 2010;101:8493–501.

[6] Sin LT, Rahmat AR, Rahman WAWA. Polylactic Acid. 1st ed. Elsevier; 2013.

[7] Södergård A, Stolt M. Industrial Production of High Molecular Weight Poly(Lactic Acid). Poly(Lactic Acid),Hoboken, NJ, USA: John Wiley & Sons, Inc.;2010,p.27–41.

[8] Ren J. Biodegradable Poly(Lactic Acid): Synthesis, Modification, Processing and Applications. Berlin, Heidelberg: Springer Berlin Heidelberg; 2011.

[9] Auras R, Lim L-T, Selke SEM, Tsuji H. Poly(Lactic Acid). Hoboken, NJ, USA: John Wiley & Sons, Inc.; 2010.

[10] Laura M, Lorenzo D. Synthesis, Structure and Properties of Poly(lactic acid). vol. 279. Cham: Springer International Publishing; 2018.

[11] Song JH, Murphy RJ, Narayan R, Davies GBH. Biodegradable and compostable alternatives to conventional plastics. Philos Trans R Soc B Biol Sci 2009;364:2127–39.

[12] Hamad K, Kaseem M, Ayyoob M, Joo J, Deri F. Polylactic acid blends: The future of green, light and tough. Prog Polym Sci 2018;85:83–127.

[13] Sikorska W, Musioł M, Rydz J, Zięba M, Rychter P, Lewicka K, et al. Prediction studies of environment-friendly biodegradable polymeric packaging based on PLA. Influence of specimens' thickness on the hydrolytic degradation profile. Waste Manag 2018;78:938–47.

[14] Lim L-T, Auras R, Rubino M. Processing technologies for poly ( lactic acid )

2008;33:820–52.

[15] Kruse M, Wagner MH. Rheological and molecular characterization of long-chain branched poly(ethylene terephthalate). Rheol Acta 2017;56:887–904.

[16] Porfyris A, Vasilakos S, Zotiadis C, Papaspyrides C, Moser K, Van der Schueren L, et al. Accelerated ageing and hydrolytic stabilization of poly(lactic acid) (PLA) under humidity and temperature conditioning. Polym Test 2018;68:315–32.

[17] Iñiguez-Franco F, Auras R, Burgess G, Holmes D, Fang X, Rubino M, et al. Concurrent solvent induced crystallization and hydrolytic degradation of PLA by water-ethanol solutions. Polym (United Kingdom) 2016;99:315–23.

[18] Tsuji H. Hydrolytic Degradation. Poly(Lactic Acid), Hoboken, NJ, USA: John Wiley & Sons, Inc.; 2010, p. 343–81.

[19] Pan J. Modelling Degradation of Bioresorbable Polymeric Medical Devices. Elsevier Science; 2014.

[20] He W, Feng Y, Ma Z, Ramakrishna S. Polymers for Tissue Engineering. ACS Symp. Ser., vol. 977, 2008, p. 310–35.

[21] Lee JW, Gardella JA. In vitro hydrolytic surface degradation of poly(glycolic acid): Role of the surface segregated amorphous region in the induction period of bulk erosion. Macromolecules 2001;34:3928–37.

[22] Göpferich A. Polymer bulk erosion. Macromolecules 1997;30:2598–604.

[23] Chen Y, Zhou S, Li Q. Mathematical modeling of degradation for bulk-erosive polymers: Applications in tissue engineering scaffolds and drug delivery systems. Acta Biomater 2011;7:1140–9.

[24] Burkersroda F von, Schedl L, Göpferich A. Why degradable polymers undergo surface erosion or bulk erosion. Biomaterials 2002;23:4221–31.

[25] Di Lorenzo ML, Gazzano M, Righetti MC. The role of the rigid amorphous fraction on cold crystallization of poly(3-hydroxybutyrate). Macromolecules 2012;45:5684–91.

[26] Yamamoto K, Watanabe H. A Kinetic Study of Hydrolysis of Polyester Elastomer in Magnetic Tape 1994:4–11.

[27] Tsuji H, Mizuno A, Ikada Y. Properties and morphology of poly(L-lactide). III. Effects of initial crystallinity on long-term in vitro hydrolysis of high molecular weight poly(L-lactide) film in phosphate-buffered solution. J Appl Polym Sci 2000;77:1452–64.

[28] Tsuji H. Autocatalytic hydrolysis of amorphous-made polylactides: Effects of L-lactide content, tacticity, and enantiomeric polymer blending. Polymer (Guildf)

2002;43:1789–96.

[29] Tsuji H, Del Carpio CA. In vitro hydrolysis of blends from enantiomeric poly(lactide)s. 3. Homocrystallized and amorphous blend films. Biomacromolecules 2003;4:7–11.

[30] Tsuji H. In vitro hydrolysis of blends from enantiomeric poly(lactide)s. Part 4: well-homo-crystallized blend and nonblended films. Biomaterials 2003;24:537–47.

[31] Iñiguez-Franco F, Auras R, Dolan K, Selke S, Holmes D, Rubino M, et al. Chemical recycling of poly(lactic acid) by water-ethanol solutions. Polym Degrad Stab 2018;149:28–38.

[32] Iñiguez-Franco F, Auras R, Ahmed J, Selke S, Rubino M, Dolan K, et al. Control of hydrolytic degradation of Poly(lactic acid) by incorporation of chain extender: From bulk to surface erosion. Polym Test 2018;67:190–6.

[33] Rodriguez EJ, Marcos B, Huneault MA. Hydrolysis of polylactide in aqueous media. J Appl Polym Sci 2016;133:1–11.

[34] Raman C, Berkland C, Kim K, Pack DW. Modeling small-molecule release from PLG microspheres: Effects of polymer degradation and nonuniform drug distribution. J Control Release 2005;103:149–58.

[35] Berchane NS, Carson KH, Rice-Ficht AC, Andrews MJ. Effect of mean diameter and polydispersity of PLG microspheres on drug release: Experiment and theory. Int J Pharm 2007;337:118–26.

[36] Siepmann J, Elkharraz K, Siepmann F, Klose D. How autocatalysis accelerates drug release from PLGA-based microparticles: A quantitative treatment. Biomacromolecules 2005;6:2312–9.

[37] Farrar DF, Gillson RK. Hydrolytic degradation of polyglyconate B: The relationship between degradation time, strength and molecular weight. Biomaterials 2002;23:3905–12.

[38] Vieira AC, Vieira JC, Ferra JM, Magalhães FD, Guedes RM, Marques AT. Mechanical study of PLA-PCL fibers during in vitro degradation. J Mech Behav Biomed Mater 2011;4:451–60.

[39] Lyu S, Schley J, Loy B, Lind D, Hobot C, Sparer R, et al. Kinetics and Time - Temperature Equivalence of Polymer Degradation 2007:2301–10.

[40] H. Antheunis, J.-C van der Meer, M. de Geus, A. Heise, C.E. Koning. Autocatalytic equation describing yje chnagen in molecular weight during hydrolytic of aliphatic polyesters. Biomacromolecules 2010;11:1118–24.

[41] Wang Y, Pan J, Han X, Sinka C, Ding L. A phenomenological model for the

degradation of biodegradable polymers. Biomaterials 2008;29:3393–401.

[42] Han X, Pan J. A model for simultaneous crystallisation and biodegradation of biodegradable polymers. Biomaterials 2009;30:423–30.

[43] Han X, Pan J. Polymer chain scission, oligomer production and diffusion: A two-scale model for degradation of bioresorbable polyesters. Acta Biomater 2011;7:538–47.

[44] Han X, Pan J, Buchanan F, Weir N, Farrar D. Analysis of degradation data of poly(l-lactide-co-l,d-lactide) and poly(l-lactide) obtained at elevated and physiological temperatures using mathematical models. Acta Biomater 2010;6:3882–9.

[45] Samami H, Pan J. A constitutive law for degrading bioresorbable polymers. J Mech Behav Biomed Mater 2016;59:430–45.

[46] Sevim K, Pan J. A model for hydrolytic degradation and erosion of biodegradable polymers. Acta Biomater 2018;66:192–9.

[47] Gleadall A, Pan J, Atkinson H. A simplified theory of crystallisation induced by polymer chain scissions for biodegradable polyesters. Polym Degrad Stab 2012;97:1616–20.

[48] Gleadall A, Pan J, Kruft M-A, Kellomäki M. Degradation mechanisms of bioresorbable polyesters. Part 1. Effects of random scission, end scission and autocatalysis. Acta Biomater 2014;10:2223–32.

[49] Gleadall A, Pan J, Kruft M-A, Kellomäki M. Degradation mechanisms of bioresorbable polyesters. Part 2. Effects of initial molecular weight and residual monomer. Acta Biomater 2014;10:2233–40.

[50] Lyu SP, Schley J, Loy B, Lind D, Hobot C, Sparer R, et al. Kinetics and time-temperature equivalence of polymer degradation. Biomacromolecules 2007;8:2301–10.

[51] Gleadall A. Computer Simulation of Polymer Chain Scission in Biodegradable Polymers. J Biotechnol Biomater 2013;03:1–5.

[52] Zhang XC. Science and Principles of Biodegradable and Bioresorbable Medical Polymers: Materials and Properties. Elsevier Science; 2016.

[53] Weir NA, Buchanan FJ, Orr JF, Farrar DF, Dickson GR. Degradation of poly-L-lactide. Part 2: Increased temperature accelerated degradation. Proc Inst Mech Eng Part H J Eng Med 2004;218:321–30.

[54] Grizzi I, Garreau H, Li S, Vert M. Hydrolytic degradation of devices based on poly[m-lactic acid) size- dependence 1995;16:305–11.

[55] Zong XH, Wang ZG, Hsiao BS, Chu B, Zhou JJ, Jamiolkowski DD, et al. Structure and morphology changes in absorbable poly(glycolide) and poly(glycolide-co-lactide) during in vitro degradation. Macromolecules 1999;32:8107–14.

[56] De Jong SJ, Arias ER, Rijkers DTS, Van Nostrum CF, Kettenes-Van Den Bosch JJ, Hennink WE. New insights into the hydrolytic degradation of poly(lactic acid): Participation of the alcohol terminus. Polymer (Guildf) 2001;42:2795–802.

[57] Shih C. controlled release Chain-end scission in acid catalyzed hydrolysis of poly ( D , L- lactide ) in solution 1995;34:9–15.

[58] Sailema-Palate GP, Vidaurre A, Campillo-Fernández AJ, Castilla-Cortázar I. A comparative study on Poly(ε-caprolactone) film degradation at extreme pH values. Polym Degrad Stab 2016;130:118–25.

[59] Yuan X, Mak AFT, Yao K. Surface degradation of poly(L-lactic acid) fibres in a concentrated alkaline solution. Polym Degrad Stab 2003;79:45–52.

[60] Jung JH, Ree M, Kim H. Acid- and base-catalyzed hydrolyses of aliphatic polycarbonates and polyesters. Catal Today 2006;115:283–7.

[61] Buchholz B. Accelerated Degradation Test on Resorbable Polymers. Degrad. Phenom. Polym. Biomater., Berlin, Heidelberg: Springer Berlin Heidelberg; 1992, p. 67–76.

[62] Agrawal CM, Huang D, Schmitz JP, Athanasiou KA. Elevated Temperature Degradation of a 50:50 Copolymer of PLA-PGA. Tissue Eng 1997;3:345–52.

[63] Danner RP. Measuring and correlating diffusivity in polymer-solvent systems using free-volume theory. Fluid Phase Equilib 2014;362:19–27.

[64] Shangguan Y, Chen F, Jia E, Lin Y, Hu J, Zheng Q. New insight into Time-Temperature correlation for polymer relaxations ranging from secondary relaxation to terminal flow: Application of a Universal and developed WLF equation. Polymers (Basel) 2017;9.

[65] Billen J. Williams-Landel-Ferry and Vogel Fulcher Tamman equations 2012:1–11.

[66] Amiri A, Hosseini N, Ulven CA. Long-Term Creep Behavior of Flax/Vinyl Ester Composites Using Time-Temperature Superposition Principle. J Renew Mater 2015;3:224–33.

[67] Pan J. Modelling degradation of semi-crystalline biodegradable polyesters. Model. Degrad. Bioresorbable Polym. Med. Devices, Woodhead Publishing Limited; 2014, p. 53–69.

[68] Albuerne J, Marquez L, Müller AJ, Raquez JM, Degée P, Dubois P. Hydrolytic degradation of double crystalline PPDX-b-PCL diblock copolymers. Macromol Chem Phys 2005;206:903–14.

[69] Saeidlou S, Huneault MA, Li H, Park CB. Poly(lactic acid) crystallization. Prog Polym Sci 2012;37:1657–77.

[70] Zuza E, Ugartemendia JM, Lopez A, Meaurio E, Lejardi A, Sarasua JR. Glass transition behavior and dynamic fragility in polylactides containing mobile and rigid amorphous fractions. Polymer (Guildf) 2008;49:4427–32.

[71] Magoń A, Pyda M. Study of crystalline and amorphous phases of biodegradable poly(lactic acid) by advanced thermal analysis. Polymer (Guildf) 2009;50:3967–73.

[72] Martin J, Stingelin N, Cangialosi D. Direct Calorimetric Observation of the Rigid Amorphous Fraction in a Semiconducting Polymer.J PhysChem Lett 2018;9:990-5.

[73] Rastogi R, Vellinca WP, Rastogi S, Schick C, Meijer HEH. The three-phase structure and mechanical properties of poly(ethylene terephthalate). J Polym Sci Part B Polym Phys 2004;42:2092–106.

[74] Badia JD, Strömberg E, Karlsson S, Ribes-Greus A. The role of crystalline, mobile amorphous and rigid amorphous fractions in the performance of recycled poly (ethylene terephthalate) (PET). Polym Degrad Stab 2012;97:98–107.

[75] Schick C, Wurm A, Mohammed A. Formation and disappearance of the rigid amorphous fraction in semicrystalline polymers revealed from frequency dependent heat capacity. Thermochim Acta 2003;396:119–32.

[76] Nassar SF, Domenek S, Guinault A, Stoclet G, Delpouve N, Sollogoub C. Structural and Dynamic Heterogeneity in the Amorphous Phase of Poly(l, l -lactide) Confined at the Nanoscale by the Coextrusion Process. Macromolecules 2018;51:128–36.

[77] Sangroniz A, Chaos A, Iriarte M, Del Río J, Sarasua JR, Etxeberria A. Influence of the Rigid Amorphous Fraction and Crystallinity on Polylactide Transport Properties. Macromolecules 2018;51:3923–31.

[78] Del Río J, Etxeberria A, López-Rodríguez N, Lizundia E, Sarasua JR. A PALS contribution to the supramolecular structure of poly(l -lactide). Macromolecules 2010;43:4698–707.

[79] Lee JH. Solubility of Physical Blowing Agents in Semi-Crystalline Polymers: Consideration of Rigid Amorphous Fraction. University of Toronto, 2014.

[80] Drieskens M, Peeters R, Mullens J, Franco D, Lemstra PJ, Hristova-Bogaerds DG. Structure versus properties relationship of poly(lactic acid). I. Effect of crystallinity

on barrier properties. J Polym Sci Part B Polym Phys 2009;47:2247–58.

[81] Gorrasi G, Pantani R. Hydrolysis and Biodegradation of Poly(lactic acid) BT - Synthesis, Structure and Properties of Poly(lactic acid). In: Di Lorenzo ML, Androsch R, editors., Cham: Springer International Publishing; 2018, p. 119–51.

[82] Celikkaya E, Denkbas EB, Piskin E. Poly( DL-ladide)/Poly(ethylene glycol) Copolymer Particles. I. Preparation and Characterization 1996:1439–46.

[83] Deplaine H. Scaffold design and characterisation for osteochondral tissue regeneration. Universitat Politècnica de València, 2012.

[84] Huttunen M. Analysis of the factors affecting the inherent viscosity of oriented polylactides during hydrolytic degradation 2013:1131–44.

[85] Gu L, Xu Y, Fahnhorst GW, Macosko CW. Star vs long chain branching of poly (lactic acid) with multifunctional aziridine 2017;785.

[86] Corneillie S, Smet M. Polymer Chemistry PLA architectures : the role of branching 2015:850–67.

[87] Simmons H, Kontopoulou M. Hydrolytic degradation of branched PLA produced by reactive extrusion. Polym Degrad Stab 2018;158:228–37.

[88] Numata K, Srivastava RK, Finne-wistrand A, Albertsson A, Doi Y, Abe H. Branched Poly ( lactide ) Synthesized by Enzymatic Polymerization : Effects of Molecular Branches and Stereochemistry on Enzymatic Degradation and Alkaline Hydrolysis 2007:3115–25.

[89] Tsuji H, Hayashi T. Hydrolytic degradation and crystallization behavior of linear 2-armed and star-shaped 4-armed poly(l -lactide)s: Effects of branching architecture and crystallinity. J Appl Polym Sci 2015;132:1–13.

[90] Inata H, Matsumura S. Chain Extenders for Polyesters. I. Addition-Type Chain Extenders Reactive with Carboxyl End Groups of Polyesters. Szycher's Handb Polyurethanes, Second Ed 1985;30:3325–37.

[91] Bousfield G. Effect of Chain Extension on Rheology and Tensile Properties of PHB and PHB-PLA Blends 2014:93.

[92] Arruda LC, Magaton M, Bretas RES, Ueki MM. Influence of chain extender on mechanical, thermal and morphological properties of blown films of PLA/PBAT blends. Polym Test 2015;43:27–37.

[93] Najafi N, Heuzey MC, Carreau PJ. Polylactide (PLA)-clay nanocomposites prepared by melt compounding in the presence of a chain extender. Compos Sci Technol 2012;72:608–15.

[94] Rathi S, Coughlin E, Hsu S, Golub C, Ling G, Tzivanis M. Maintaining Structural Stability of Poly(lactic acid): Effects of Multifunctional Epoxy based Reactive Oligomers. Polymers (Basel) 2014;6:1232–50.

[95] Dong W, Zou B, Yan Y, Ma P, Chen M. Effect of chain-extenders on the properties and hydrolytic degradation behavior of the poly(lactide)/ poly(butylene adipate-co-terephthalate) blends. Int J Mol Sci 2013;14:20189–203.

[96] Frenz V, Scherzer D, Ag B, Germany L, Villalobos M, Awojulu AA, et al. Multifunctional Polymers as Chain Extenders and Compatibilizers for Polycondensates and Biopolymers . Chain Extension vs . Solid State Polymerization 2008:1682–6.

[97] Ghalia MA, Dahman Y. Investigating the effect of multi-functional chain extenders on PLA/PEG copolymer properties. Int J Biol Macromol 2017;95:494–504.

[98] Raymond H. Myers, Montgomery DC. Response Surface Methodology: Process and Product in Optimization Using Designed Experiments. 1st ed. New York: John Wiley & Sons, Inc.; 1995.

[99] Ba D, Boyaci IH. Modeling and optimization i: Usability of response surface methodology. J Food Eng 2007;78:836–45.

[100] Garcia-Diaz A, Phillips DT. Principles of Experimental Design and Analysis. Springer; 1995.

[101] Khuri I, Mukhopadhyay S. Response surface methodology 2010.

[102] Myers RH, Montgomery DC, Anderson-Cook CM. Response Surface Methodology: Process and Product Optimization Using Designed Experiments. Wiley; 2016.

[103] Khuri AI, Cornell JA. Response Surfaces: Designs and Analyses: Second Edition. Taylor & Francis; 1996.

[104] Kunnan Singh J, Ching Y, Abdullah L, Ching K, Razali S, Gan S. Optimization of Mechanical Properties for Polyoxymethylene/Glass Fiber/Polytetrafluoroethylene Composites Using Response Surface Methodology. Polymers (Basel) 2018;10:338.

[105] Gelman A. Analysis of variance—why it is more important than ever. Ann Stat 2005;33:1–53.

[106] Bezerra MA, Santelli RE, Oliveira EP, Villar LS, Escaleira LA. Response surface methodology (RSM) as a tool for optimization in analytical chemistry. Talanta 2008;76:965–77.

# CHAPTER 3

## Experimental

### 3.1 Materials

Poly(lactic acid) resin (PLA 4032D with a D-lactide content of 3.8-4.2%) was supplied by NatureWorks LLC (Minnetonka, MN, USA). Joncryl® ADR4300F, a styrene-acrylic multi-functional epoxide oligomeric agent with Epoxy Equivalent Weight (EEW) of 445 g/mol, provided from BASF (Sturtevant, WI, USA) was used as a chain extender. The general structure of Joncryl® can be seen in **Figure 3.1**. Ethanol (200 proof, HPLC/spectrophotometric grade) and water (certified for HPLC grade) were purchased from Sigma-Aldrich (St. Louis, MO, USA) and VWR (Radnor, PA, USA), respectively. Tetrahydrofuran (THF) obtained from Pharmco-AAPEP (North East, CA, USA) was used as the mobile phase solvent in size exclusion chromatography (SEC) experiments.

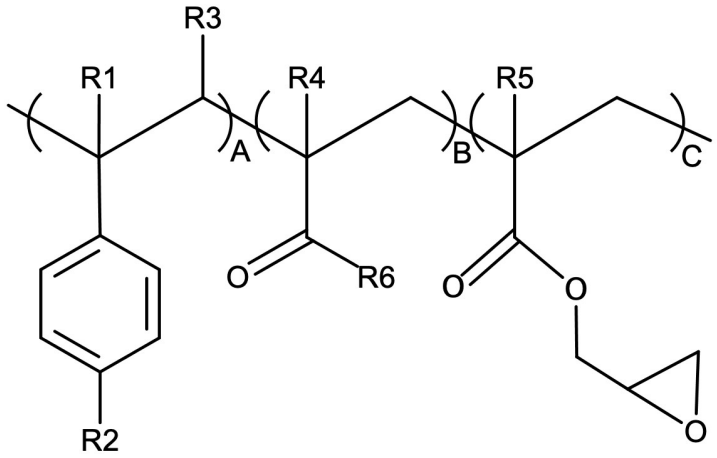


**Figure 3.1** General structure of Joncryl®: $R_1$–$R_5$ are H, $CH_3$, a higher alkyl group, $R_6$ is an alkyl group, A and B are each between 1 and 20, and C is between 1 and 12, adapted from Cailloux et al. [1].

## 3.2 Methods

### 3.2.1 Experimental design

A response surface methodology (RSM) study was conducted aiming to optimize the molecular weight of PLA after the chain extension reaction using a software program, JMP® software version 14.2.0, 2018 created by SAS Institute Inc., (Cary, NC). The two design factors were the content of chain extender (Cex) *($x_1$*, wt% on PLA basis) and the residence time in the melt blending process ($x_2$, minutes) with the range of $x_1$ and $x_2$ between 0-2 wt% and 5-15 minutes, respectively. For this process, the most appropriate design of RSM was faced-centered central composite design (FCCCD), where the axial points occur at the center of the faces (boundaries) since the experiment was designed to study inside the range of *x* as seen in **Figure 3.2a**. JMP® provided a design table where the experimental runs were randomly generated as shown in **Table 3.1**. The combination of the two factors was studied and optimized to obtain the maximum average molecular weight of the modified PLA. The experimental design contained eleven experimental points, four full factorial, three center, and four axial factorial points, where the distance from the center of the design space to axial points ($\alpha$) was ±1. The analysis was conducted with JMP® following the designed experiments.

**Table 3.1** The experimental design condition for the two factors faced-centered central composite design (FCCCD)

| Run | Type | Coded levels | | Actual levels | |
|---|---|---|---|---|---|
| | | $x_1$ | $x_2$ | $x_1$ (wt%) | $x_2$ (minute) |
| 1 | F | -1 | -1 | 0 | 5 |
| 2 | F | -1 | +1 | 0 | 15 |
| 3 | F | +1 | -1 | 2 | 5 |
| 4 | F | +1 | +1 | 2 | 15 |
| 5 | C | 0 | 0 | 1 | 10 |
| 6 | C | 0 | 0 | 1 | 10 |
| 7 | C | 0 | 0 | 1 | 10 |
| 8 | A | 0 | -1 | 1 | 5 |
| 9 | A | -1 | 0 | 0 | 10 |
| 10 | A | +1 | 0 | 2 | 10 |
| 11 | A | 0 | +1 | 1 | 15 |

Note: F = Full factorial, C = Center-full factorial, and A = Axial factorial point

**Table 3.2** Experimental design for the additional runs to extend the residence time

| Run | Coded levels | | Actual levels | |
|---|---|---|---|---|
| | $x_1$ | $x_2$ | $x_1$ (wt%) | $x_2$ (minute) |
| 1 | -1 | +1 | 0 | 15 |
| 2 | -1 | +2 | 0 | 20 |
| 3 | -1 | +3 | 0 | 25 |
| 4 | +0.5 | +1 | 1.5 | 15 |
| 5 | +0.5 | +2 | 1.5 | 20 |
| 6 | +0.5 | +3 | 1.5 | 25 |

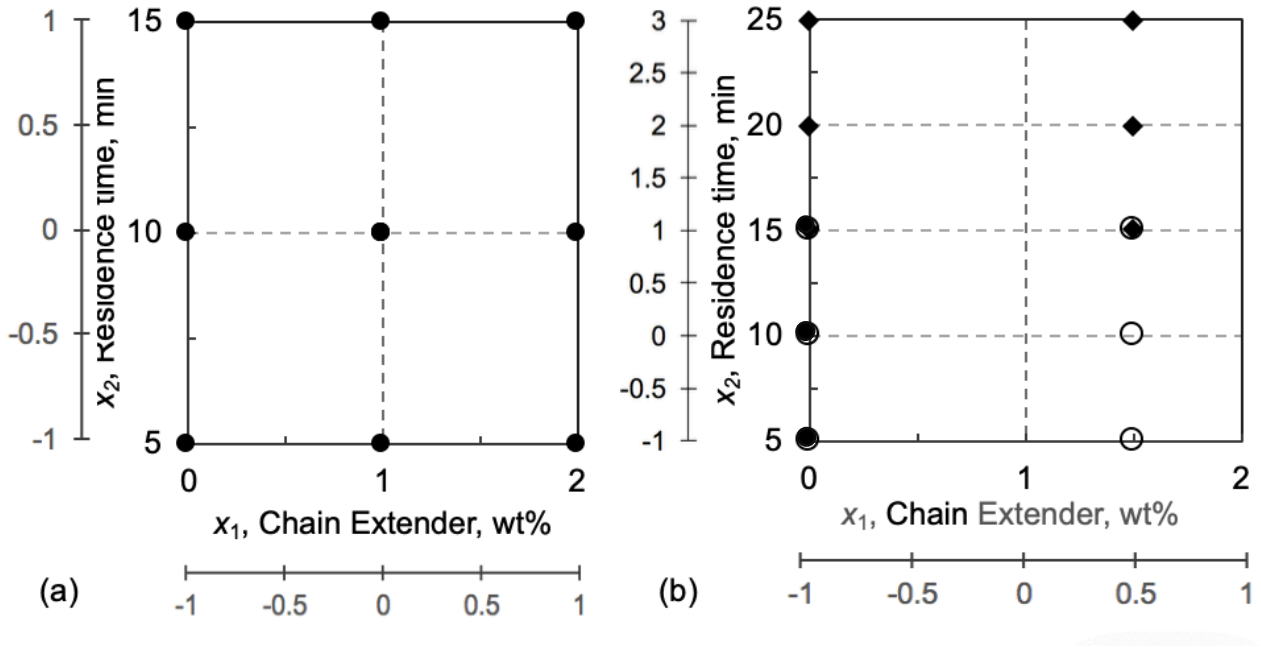


**Figure 3.2** (a) Face central composite design and (b) the experimental design condition for the additional runs. (●, o, and ♦) symbols represent the initial experimental runs, the predicted data of the initial runs and the additional experimental points, respectively.

The result obtained from the eleven runs was then analyzed by JMP® to solve the optimization using the desirability function following methods described in **section 3.2.3**. According to the results, the optimum residence time was initially estimated as 15 minutes, which was on the upper boundary of the experimental conditions. Therefore, the initial design was expanded by using the optimal condition of chain extender content of 1.5 wt%, and extended residence time to 15, 20, and 25 minutes as shown **Table 3.2** and **Figure 3.2b**. The data set of the average molecular weight of the PLA with 1.5 wt% chain extender at the residence time of 5, 10, and 15 minutes was estimated from the initial experiment. Afterward, both the prediction and the experimental data were used to optimize the residence time for processing PLA with 1.5 wt% chain extender.

### 3.2.2 Model development using RSM and statistical analysis

In order to evaluate the optimization, the response values, the molecular weight properties ($M_n$ and $M_w$), were fitted to a second-order polynomial model that can be expressed as:

$$E\{Y\} = \beta_0 + \beta_1 x_1 + \beta_2 x_2 + \beta_{11} x_1^2 + \beta_{22} x_2^2 + \beta_{12} x_1 x_2 \qquad (3.1)$$

where $E\{Y\}$ = Estimate of interested parameter

$x_1$ = The content of chain extender (wt% on PLA basis)

$x_2$ = The residence time (minutes)

$\beta_0$ = Intercept

$\beta_1$ = Linear main effect of the content of chain extender

$\beta_2$ = Linear main effect of the residence time

$\beta_{11}$ = Quadratic main effect of the content of chain extender

$\beta_{22}$ = Quadratic main effect of the residence time

$\beta_{12}$ = Interaction effect

The model equations were fitted by the least square methodology in an attempt to obtain good model parameter estimates. Statistical analysis was performed using the JMP® program. Analysis of variance (ANOVA) was performed to determine if the parameters were statistically significant. Moreover, the coefficient of determination ($R^2$) was used to assess the level of fit of the RSM model.

### 3.2.3 Optimization of molecular weight properties using the desirability method

The desirability function was developed by Derringer and Suichin [2] in order to optimize multiple responses simultaneously. The D global index which is the overall desirability determined from the different criteria combination of the responses is obtained using the following equation [3]:

$$D = \left(d_1(y_1) \times d_2(y_2) \times d_3(y_3) \times \ldots. \times d_n(y_n)\right)^{1/n} \qquad (3.2)$$

where $y_1, y_2, y_{3,\ldots,} y_n$ are the responses, $d_1, d_2, d_{3,\ldots,} d_n$ are the individual desirability functions of each response indicating the level of the desire condition and $n$ is the number of variables. The optimization of the process conditions is achieved when the value of $D$ global index is maximized (close to 1).

### 3.2.4 Sheet production

PLA resins and chain extruder were dried at 50°C in a vacuum oven for 12 hours, premixed with chain extender, and fed into the counter-rotating conical twin-screw extruder with a length to diameter (L/D) ratio of 13:1 (C.W. Brabender Instruments, Inc., South Hackensack, NJ), at a rotation speed of 40 rpm. The temperature profile was set at 180 °C. The chain extender content and the residence time for melt blending were set following the experimental design mentioned in **section 3.2.1.** The extrudates were cooled and compressed to a sheet form by using a compression molding machine (Model 12-10HC) (Carver Hydraulic Laboratory Press Menomonee Falls, Wisconsin, USA) set at 176.5°C (350 °F). For the pre-heating step, the pressure was set at zero for 7 minutes and then increased to 20 ton for 10 minutes at the heating step. Three replicates of each sample were collected after melt blending and compression molding.

### 3.2.5 Cast film production

Chain extender in the clear flake form was ground into powder by a hand grinder. The PLA resin and the chain extender were dried at 50°C in a vacuum oven for 12 hours. After drying, PLA pellets were premixed with 1.5 wt% of chain extender and then extruded in a Microextruder model RCP-0625 (Randcastle Extrusion Systems, Inc., Cedar Grove, NJ) with a screw of 1.5875 cm diameter, 24/1 LD ratio extruder. The temperature profile of the extruder was 335-380-390-385-385-385-385°F (168-193-199-196-196-196-196 °C) for zone 1, zone 2, zone 3, transfer tube, adapter, feed block, and die, respectively. Samples were processed using three different screw speeds: 10, 20, and 40 rpm, which affected the mean residence time ($\bar{t}$) which can be increased by reducing the screw speed. Neat PLA and PLA with chain extender were processed at the same conditions and referred to as PLA–Con and PLA–Cex, respectively. The thickness of the film was measured using a digital micrometer (Testing Machines Inc., Ronkonkoma, NY, USA).

### 3.2.6 Molecular weight determination

A sample of around 0.0100 g was weighed and dissolved in THF at a concentration of 2 mg/mL. A gel permeation chromatography (GPC) unit from Waters (Milford MA, USA) equipped with an isocratic pump (Waters 1515), an autosampler (Waters 717), a refractive index detector (Waters 2414) was used with THF running with a flow rate of 1 mL/min. A series of HR Styragel® HR4, HR3, HR2 (300 mm x 7.8 mm (I.D)) columns with a controlled temperature of 35 °C was used. The molecular weight distribution (MWD) curve for each sample was determined by analyzing the raw data provided using Breeze™ 2 Software (Waters, Milford MA, USA).

The deconvolution of the MWDs which is a method to determine subpopulations of molecular chains of PLA was analyzed using Fityk 1.3.0 developed under the terms of the GNU General Public License for nonlinear fitting of a LogNormal function to experimental MWD [4]. The main peaks with the highest peak area representing the majority of the chain length were used to represent the average molecular weight of samples. The number average molecular weight ($M_n$) and the weight average molecular weight ($M_w$) of each sample were analyzed using the following equations:

$$M_n = \frac{\sum N_i - M_i}{\sum N_i} \tag{3.3}$$

$$M_w = \frac{\sum N_i - M_i^2}{\sum N_i M_i} \tag{3.4}$$

$$PDI = \frac{M_n}{M_w} \tag{3.5}$$

where $i$ = 1 to $I = \infty$, $N_i$ is the number of molecules with the molecular weight $M_i$ and PDI is the polydispersity index which is used to indicate the broadness of a molecular weight distribution.

### 3.2.7 Characterizations of PLA–Con and PLA–Cex films

The tensile properties, tensile strength, elongation at break, and modulus of elasticity, were measured using a Universal Testing Machine 5560 series (Intron, Inc., Norwood, MA) following ASTM D882–12 [5]. Rate of grip separation was set at 2 in/min and initial grip separation of 4 in. Ten samples for each specimen were tested in the machine direction.

Thermal gravimetric analysis (TGA) was investigated using a TGA Q50 (TA instruments, New Castle, DE, USA) to study the effect of temperature on weight loss of the materials as a function of temperature. The samples were weighed on a platinum pan and heated from 23 to 600 °C with a constant heating rate of 10 °C·min$^{-1}$ under a nitrogen atmosphere.

Differential scanning calorimeter (DSC) (Q100, TA Instrument), was used to determine the degree of crystallinity ($\%X_C$), crystallization temperature ($T_c$), glass transition temperature ($T_g$), and melting temperature ($T_m$) for the initial condition of samples using the DSC thermogram of the second heating scan. While, the variation of the crystallinity during the hydrolytic degradation was tracked by the first heating cycle. Approximately 5–10 mg of samples was placed in a sealed aluminum pan, and then the samples were cooled to 5 °C at the constant rate of 10 °C/min, equilibrated for 3 min, and then heated to 210 °C at a ramping rate of 10 °C/min. The degree of crystallinity was calculated as following equation [6]:

$$\%X_c = \left( \frac{\Delta H_m - \Delta H_c}{\Delta H_m^0 \left(1 - \frac{\%\ wt_{\ filler}}{100}\right)} \right) \times 100 \qquad (3.6)$$

where $\Delta H_m$ is the heat of fusion, $\Delta H_c$ is cold crystallization enthalpy, $\Delta H_m^0$ is the heat of fusion for 100% crystalline PLA = 93.0 J·g$^{-1}$ and $\%\ wt_{\ filler}$ is the weight percentage of the chain extender = 1.5%.

The Avrami theory was used to study the crystallinity process of the hydrolysis experiment as following equation:

$$X_t = 1 - exp[-(k_c t)^n] \quad (3.7)$$

whereas $X_t$ is the time-dependent of crystallinity fraction,$k_c$ is a kinetic rate constant, $t$ is crystallization time, and $n$ is Avrami exponent.

Dynamic mechanical analysis (DMA) was evaluated using a TA RSA-G2 Solids Analyzer Immersion System (TA Instruments, New Castle, DE, USA) equipped with a tension geometry and set of frequency value at 1 Hz. The samples were tested under the two conditions, dry and wet conditions, which indicate the properties of materials before and after immersion in the media. For the dry condition, the samples were heated from 25 °C to 90 °C at a constant rate of 5 °C/min. For the wet condition, the immersion cell was installed, and the test solution was pre-cooled to approximately 0 °C with liquid nitrogen. After solution preparation, the solution was filled in the immersion cell which contained the mounted sample. The solution was heated to approximately 60 °C. The $T_g$ of PLA was determined from the temperature at which the tan delta peak was located.

### 3.2.8 Hydrolytic degradation

The hydrolysis test method was adapted from ASTM D4754 – 18 [7] and applied to study the hydrolytic degradation of PLA–Con and PLA–Cex at different temperatures. Each hydrolysis cell consisted of a glass vial with a cap, a stainless-steel wire, and glass beads. Samples were cut into 2 cm diameter disks, threaded into the wire with alternating glass beads and stored in the vial filled with 35 mL of test media. The hydrolysis studies were run in two different medias, water and 50% v/v solution of ethanol in water. For the

water condition, the hydrolysis cells were stored at 40, 60, 75, 85, and 95 °C. The samples in 50% ethanol solution were stored at 50, 60, 75, and 85 °C. Three replicates of each sample were collected periodically and dried before analysis. For the characterization of PLA–Con and PLA–Cex during hydrolytic degradation, $M_n$ of samples retrieved periodically were evaluated using GPC. The degree of crystallinity ($\%X_c$) and the *pH* variation of the media were measured using the first heating scan of DSC analysis and a pH meter (Omega Engineering Inc., CT, USA), respectively.

### 3.2.9 Parameter estimation: Rate constant of hydrolytic degradation

For hydrolytic degradation of PLA, the two mathematical models were used to evaluate the rate constant of hydrolytic degradation. The first order reaction equation can be expressed as:

$$M_n = M_{n0}\, exp\,(-k_{1st}t) \qquad (3.8)$$

where $M_n$ is the number average molecular weight (Da), $M_{n0}$ is the initial $M_n$ (Da), $k_{1st}$ is the rate constant of hydrolysis ($h^{-1}$), and $t$ is time (h).

The reference model purposed by Pan [8] was adjusted to the simplified form by considering only the rate constant of autocatalytic degradation (more information is shown in **Section 2.3.1**). The reference equation can be rewritten as:

$$\frac{d\overline{R}_s}{dt} = \left[1 - \left(\alpha(\overline{R}_s)^{\beta} - \overline{\omega}\,(X_C - X_{C_0})\right)\right]\left\{k_{deg}\left[C_{E_0}\cdot\alpha(\overline{R}_s)^{\beta}\cdot\left(\frac{1}{1-X_C}\right)\right]^{0.5}\right\} \qquad (3.9)$$

$$\overline{M}_n = \left(\frac{1+\overline{\omega}Xc_0 - \alpha(\overline{R}_s)^{\beta}}{(1+\overline{\omega}\,Xc_0)\left[1+\frac{C_{E0}}{N_{chain0}}\left(\overline{R}_s - \frac{\alpha}{m}(\overline{R}_s)^{\beta}\right)\right]}\right) \qquad (3.10)$$

where $\overline{R}_s$, $\overline{\omega}$, and $\overline{M}_n$ are the normalized forms expressed as: $\frac{R_s}{C_{E0}}$, $\frac{\omega}{C_{E0}}$, and $\frac{M_n}{M_{n0}}$

$C_{E_0}$ = The initial number of ester units of all the chain per unit volume

= $\frac{\rho_{amorphous}}{M_{unit}} = \frac{1.24\ \text{g/cm}^3}{72\ \text{g/mol}} = 1.72\times10^4\ \text{mol/m}^3$

$\omega$ = The number of ester unit of the crystalline phase per unit volume

= $\frac{\rho_{crystal}}{M_{unit}} = \frac{1.36\ \text{g/cm}^3}{72\ \text{g/mol}} = 1.89\times10^4\ \text{mol/m}^3$

$\alpha$ and $\beta$ = The dimensionless constants represented the relationship between the random and end chain scissions

= 0.4 and 1, respectively

$N_{chain0}$ = The number of the polymer chains per unit volume $= \frac{\rho_{amorphous}}{M_{n0}}$

$m$ = The average degree of polymerization of oligomers = 4

$M_{n0}$, and $M_n$ = The initial, and time-dependent of molecular weight

$X_{C0}$, and $X_C$ = The initial, and time-dependent of the degree of crystallinity

$R_s$ = The total number of chain scission per unit volume

$k_{deg}$ = The rate constant of autocatalytic degradation

### 3.2.10 Parameter estimation: Activation energy of hydrolytic degradation

The Arrhenius equation was used to understand the effect of temperature over the glass transition temperature on the rate constant of hydrolytic degradation and explore the effect of energy on the degradation of modified PLA with chain extender. The temperature dependence of the rate constant ($k$) was expressed as:

$$k = k_0 \exp\left(-\frac{E_a}{RT}\right) \qquad (3.11)$$

where $k$ is the rate constant of hydrolysis ($h^{-1}$), $k_0$ is the pre-exponential factor ($h^{-1}$), $R$ is the gas constant =8.314 J/mol ·K, and $T$ is temperature (K), $E_a$ is the activation energy.

For the basic method, the linear relationship between the natural log of $k$ and the reciprocal of the temperature was used to estimate $E_a$ which can be obtained from the slope of $-E_a/R$. Due to a high correlation between the two parameters, $k_0$ and $E_a$, a parameterization of the Arrhenius equation [9] was introduced by adding the reference temperature ($T_{ref}$) and the rate constant of hydrolysis obtained from the first order reaction at $T_{ref}$ ($k_{ref}$) given as follows:

$$M_n = M_{n_0} \exp\left(-k_{ref} \exp\left[-\frac{E_a}{R}\left(\frac{1}{T}-\frac{1}{T_{ref}}\right)\right] t\right) \qquad (3.12)$$

#### 3.2.10.1 Scaled sensitivity coefficients

A sensitivity coefficient (SE) was used to determine the sensitivity of a dependence variable to a parameter and the correlation among parameters. SE can be obtained by taking the first derivative of a dependent variable with respect to a specific parameter over the change in the independent variable [10]. To compare all parameters, the sensitivity coefficient of each parameter was plotted in the same scale by using a scaled sensitivity coefficient ($X'$):

$$X'_{ij} = \beta_j \frac{\partial \eta}{\partial \beta_j} \qquad (3.13)$$

where $i$ is the temperature index, $j$ is the parameter index.

Since the hydrolysis experiments were conducted at several temperature conditions, a temperature simulation ($T_{sim}$) was generated to plot with $X'_{ij}$ and $\beta_j$:

$$T_{sim} = T_L + \frac{T_H - T_L}{t_{max} - t_{min}} t \qquad (3.14)$$

where $T_L$ and $T_H$ are the lowest and highest temperature (K), $t_{min}$ and $t_{max}$ are the minimum and maximum time duration.

The scaled sensitivity coefficient (SSC) was determined using a forward-difference approximation and initial parameter guesses in MATLAB® 2017b (MathWork, Natick, MA, USA). For the best estimation, the scaled sensitivity coefficients $X'_{ij}$ was expected to be large and uncorrelated.

#### 3.2.10.2 Performing the inverse problem

The inverse problem method was performed using Ordinary Least Square (OLS) estimation. $T_{ref}$ in Eq. (3.11) was assessed by holding $T_{ref}$ at fixed values. The correlation coefficients $k_{ref}$ and $E_a$ were plotted with $T_{ref}$ values. The optimum $T_{ref}$ was the temperature where the correlation was close to zero. For the final estimation, the optimum $T_{ref}$ was used to evaluate the kinetic parameters ($E_a$ and $K_{ref}$ ) and initial molecular weight ($M_{n0}$) in using nonlinear regression (n-linfit function in MATLAB® 2017b).

### 3.2.11 Parameter estimation: The VTF and WLF equation

The VTF model was used to study the hydrolytic degradation of PLA–Con and PLA–Cex over a wide range of temperatures, both above and below $T_g$, which does not follow the Arrhenius law (more information is shown in **Section 2.3.2.2**).

The VTF equation is given as:

$$k = k_0 \exp\left[ -\frac{E_{VTF}}{R\,(T - T_s)} \right] \qquad (3.15)$$

where $E_{VTF}$ is pseudo activation energy, $T_s$ is the temperature at which the conformation entropy induced by segmental motion approaches zero (is about 50 K below the $T_g$).

A parameterization of the VTF equation was proposed to minimize the correlation between two parameters $k_0$ and $E_a$ in the following form:

$$M_n = M_{n0} \exp\left(-k_{ref} \exp\left[-\frac{E_{VTF}}{R}\left(\frac{1}{T - T_s} - \frac{1}{T_{ref} - T_s}\right)\right] t\right) \qquad (3.16)$$

By using parameter estimation techniques following **Section 3.2.10.2**, the kinetic parameters $E_{VTF}$ and $K_{ref}$ and $M_{n0}$ were estimated.

The WLF equation which are mathematically equivalent to the VTF is giving as:

$$\log \alpha_T = -\frac{C_1 (T - T_i)}{C_2 + (T - T_i)} \qquad (3.17)$$

where $T_i$ is the temperature of interest, $C_1$ and $C_2$ are empirical constants. $\alpha_T$ is the factor to shift the data obtained at temperature $T$ to overlap one at $T_i$. By comparing with the VTF equation, $C_1$ and $C_2$ can be obtained as follows:

$$C_1 = \frac{E_{VTF}/R}{2.303\,(T_i - T_s)} \text{ and } C_2 = (T_i - T_s) \qquad (3.18)$$

### 3.2.12 Application of the VTF and WLF equation for predicting hydrolytic degradation of a long-term at temperature of interest

According to Eqs. (3.18), $C_1$ and $C_2$ were estimated using $T_i$ of 40 °C. $\alpha_T$ values were calculated by substituting $C_1$ and $C_2$ into Eq. (3.17) to shift the experimental data curves of 85 °C to construct the master curve at 40 °C based on the time – temperature superposition principal.

# REFERENCES

## REFERENCES


[1] Cailloux J, Santana OO, Franco-Urquiza E, Bou JJ, Carrasco F, Gámez-Pérez J, et al. Sheets of branched poly(lactic acid) obtained by one step reactive extrusion calendering process: Melt rheology analysis. Express Polym Lett 2012;7:304–18.

[2] Derringer G, Suich R. Simultaneous Optimization of Several Response Variables. J Qual Technol 1980;12:214–9.

[3] Kunnan Singh J, Ching Y, Abdullah L, Ching K, Razali S, Gan S. Optimization of Mechanical Properties for Polyoxymethylene/Glass Fiber/Polytetrafluoroethylene Composites Using Response Surface Methodology. Polymers (Basel) 2018;10:338.

[4] Wojdyr M. Fityk: A general-purpose peak fitting program. J Appl Crystallogr 2010;43:1126–8.

[5] ASTM International. ASTM D882: Standard Test Method for Tensile Properties of Thin Plastic Sheeting. ASTM Stand 2012:12.

[6] Fukushima K, Tabuani D, Dottori M, Armentano I, Kenny JM, Camino G. Effect of temperature and nanoparticle type on hydrolytic degradation of poly(lactic acid) nanocomposites. Polym Degrad Stab 2011;96:2120–9.

[7] ASTM International. Standard Test Method for Two-Sided Liquid Extraction of Plastic Materials Using FDA 2018:1–5.

[8] Pan J. Modelling Degradation of Bioresorbable Polymeric Medical Devices. Elsevier Science; 2014.

[9] Iñiguez-Franco F, Auras R, Dolan K, Selke S, Holmes D, Rubino M, et al. Chemical recycling of poly(lactic acid) by water-ethanol solutions. Polym Degrad Stab 2018;149:28–38.

[10] Greiby I, Mishra DK, Dolan KD, Siddiq M. Inverse method to estimate anthocyanin degradation kinetic parameters in cherry pomace during non-isothermal heating. J Food Eng 2017;198:54–62.

# CHAPTER 4

## Results and Discussions

### 4.1 Experimental design for process optimization

#### 4.1.1 Molecular weight properties of modified PLA with chain extender

The processing of polymers can generate thermal and mechanical stresses leading to polymer degradation and weight average molecular weight changes [1]. PLA was found to be severely susceptible to thermal degradation of ester linkage during processing, mostly due to the process temperature, shear rate, and residence time [2,3]. To enhance the thermal stability of processed PLA, a chain modifier with chain extender (Cex), was used. The residence time in the melt blending process and the Cex content were studied using an RSM experimental design. The molecular weight distribution (MWD) of the samples collected from each condition were obtained from GPC. Subsequently, a deconvolution method was applied to analyze the multiple peak distribution by fitting several distributions. The main peak fitting - the highest area fraction of each MWD curve - was used to evaluate the number-average molecular weight ($M_n$) and the weight-average molecular weight ($M_w$) of the PLA presented in **Table 4.1**. Further information regarding the deconvolution technique is provided in **Section 4.4.2**.

**Figure 4.1** shows the $M_n$ and $M_w$ with increasing Cex content and residence time after the melt blending and compression molding. The $M_n$ and $M_w$ of PLA without the Cex collected after the melt blending process slightly decreased with increasing the residence time and dropped again after the compression molding process. The presence of Cex provided a higher $M_n$ and $M_w$ compared with the neat PLA samples. Moreover, the $M_n$ and $M_w$ after the melt blending process increased as the Cex content and residence time

increased, indicating that the multi-functional epoxy group can react with the reactive chain end of PLA and increase the size of the polymer chains. By applying the second steps of thermal process-compression molding, the molecular weight increased further compared with the first thermal step, indicating that more epoxide-reactive groups in the chain extender react with PLA chains and increase the chain lengths as heat was applied.

**Table 4.1** Molecular weight of control and modified PLA after melt-blending and compression molding processes

| Run | $X_1$, Wt % | $X_2$ (min) | Melt-blending process | | Compression molding process | |
|---|---|---|---|---|---|---|
| | | | $M_n$, Da | $M_w$, Da | $M_n$, Da | $M_w$, Da |
| 1 | 0 | 5 | 65901± 689 $^{hi}$ | 106740± 958 $^{G}$ | 64676±1482 $^{hi}$ | 105232±2811 $^{G}$ |
| 9 | 0 | 10 | 64867±1012 $^{i}$ | 106917±2206 $^{G}$ | 62128±1669 $^{i}$ | 105219±1800 $^{G}$ |
| 2 | 0 | 15 | 63828±1533 $^{i}$ | 104539±3842 $^{H}$ | 59347±1101 $^{i}$ | 100760±1607 $^{H}$ |
| 8 | 1 | 5 | 70686±1420 $^{g}$ | 116359±1402 $^{F}$ | 93782±1433 $^{d}$ | 147464±2465 $^{C}$ |
| 5, 6, 7 | 1 | 10 | 83297±1649 $^{f}$ | 127976±3077 $^{E}$ | 106899±2411 $^{c}$ | 164087±2692 $^{B}$ |
| 11 | 1 | 15 | 87793±3251 $^{ef}$ | 139791±1136 $^{D}$ | 111353±3198 $^{acb}$ | 171580±4616 $^{A}$ |
| 3 | 2 | 5 | 70021±2035 $^{gh}$ | 114374±2678 $^{F}$ | 109564±1000 $^{bc}$ | 162879±2947 $^{B}$ |
| 10 | 2 | 10 | 83060±1111 $^{f}$ | 126129±3302 $^{E}$ | 113446±1495 $^{ab}$ | 166361±2124 $^{B}$ |
| 4 | 2 | 15 | 89987±1434 $^{de}$ | 140127±911 $^{D}$ | 116303±2065 $^{a}$ | 171031±2128 $^{A}$ |

**Note:** $X_1$ = Chain extender content (wt%), $X_2$ = Residence time (min)
Values with different lowercase and uppercase letters represent statistically significant differences ($P < 0.05$; Tukey's HSD) of $M_n$ and $M_w$, respectively.

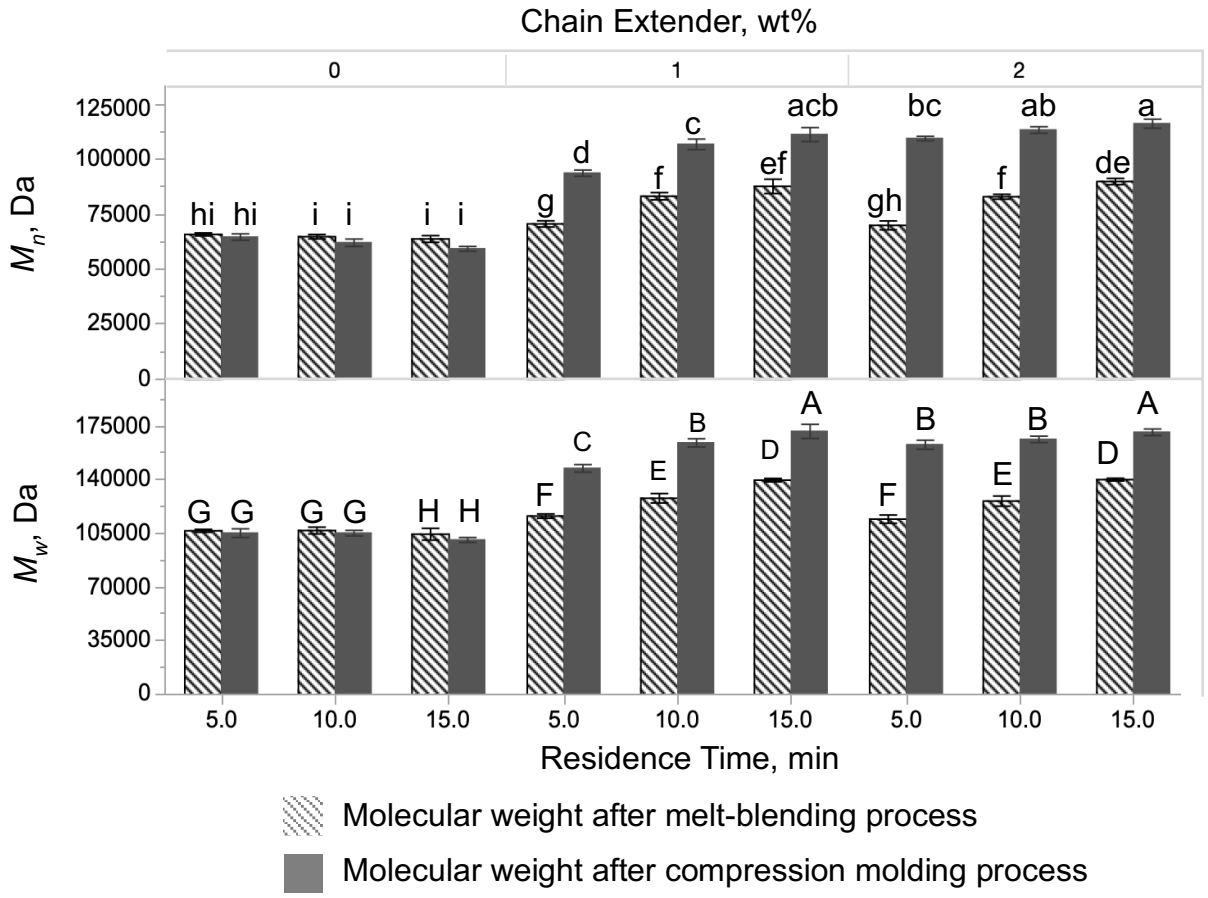


**Figure 4.1** Molecular weight of modified PLA after melt blending and compression molding processes. Values with different lowercase and uppercase letters represent statistically significant differences ($P < 0.05$; Tukey's HSD) of $M_n$ and $M_w$, respectively.

### 4.1.2 Model development using Response Surface Methodology (RSM)

**Figures 4.2** and **4.3** show the linear relationship between $M_n$ and $M_w$ of PLA after melt blending and compression molding processes versus predicted values from RSM with $R^2$ = 0.95 and 0.94, respectively. Additionally, the parameter estimations of $M_n$ and $M_w$ of the two steps (**Tables 4.2–4.5**) indicate that both linear and quadratic main effects of $x_1$ significantly affected the $M_n$ and $M_w$ ($p$ < .025). The positive parameter estimate can be interpreted as indicating that PLA processed with higher Cex concentration and longer residence time has increased average molecular weight. Moreover, the interaction terms of $x_1$ and $x_2$ are significant with positive parameter estimates indicating that the addition of Cex would considerably increase the molecular weight of PLA when processing at longer residence time.

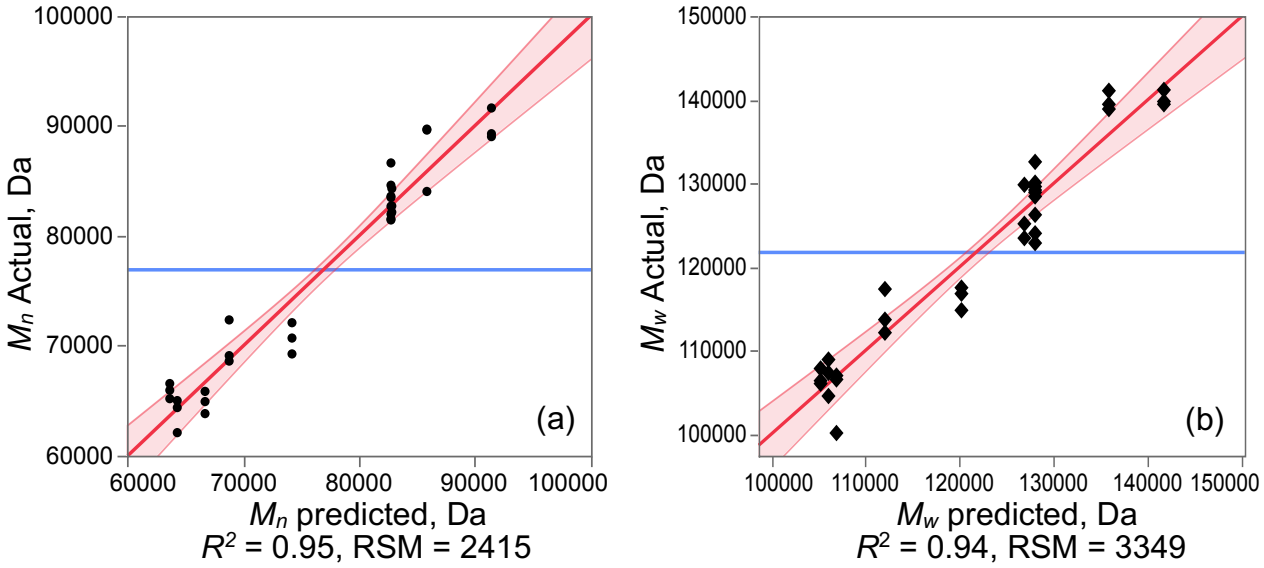


**Figure 4.2** Actual data vs. predicted values for PLA from RSM model after melt blending. The diagonal and the shaded area indicate a line of fit and 95% confidence intervals: (a) actual $M_n$ vs. predictions data, and (b) actual $M_w$ vs. predictions

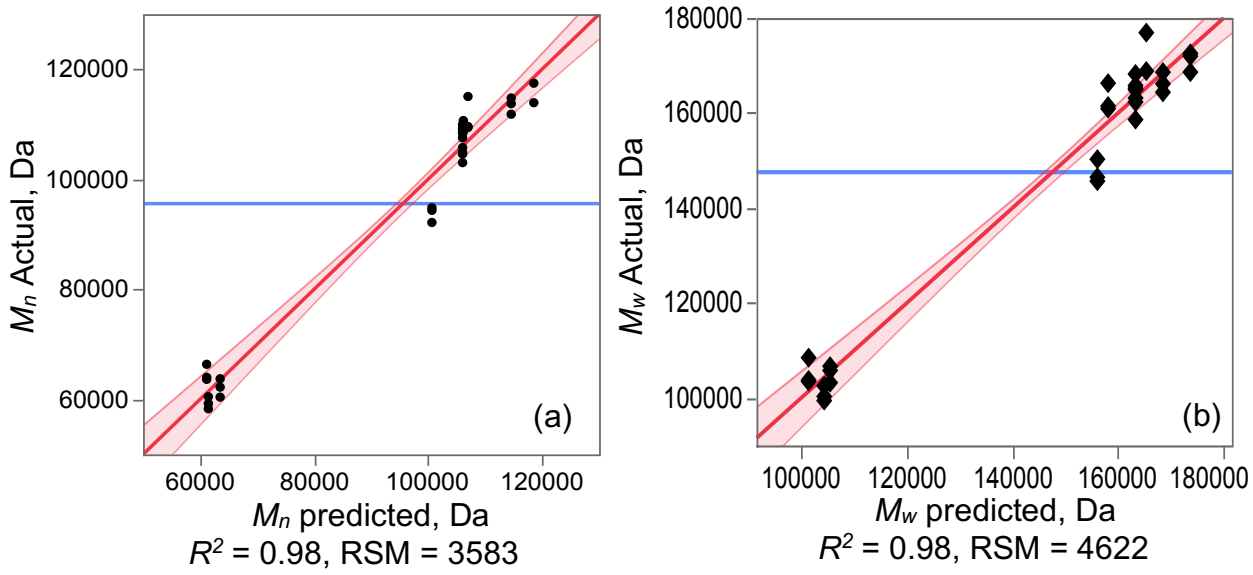


**Figure 4.3** Actual data vs. predicted values for PLA from RSM model after compression molding. The diagonal and the shaded area indicate a line of fit and 95% confidence intervals: (a) actual $M_n$ vs. predictions, and (b) actual $M_w$ vs. predictions

**Table 4.2** Statistical analysis of $M_n$ of modified PLA after melt blending process

**Analysis of Variance**

| Source | DF | Sum of Squares | Mean Square | F Ratio |
|---|---|---|---|---|
| Model | 5 | 2831588914 | 566317783 | 97.1 |
| Error | 27 | 157507101 | 5833596 | **Prob > F** |
| Total | 32 | 2989096015 | | <.001* |

**Parameter Estimates**

| Term | Estimate | Std Error | t Ratio | Prob>\|t\| |
|---|---|---|---|---|
| Intercept | 82765 | 715 | 116 | <.001* |
| $x_1$ (0,2) | 8079 | 569 | 14.2 | <.001* |
| $x_2$ (5,15) | 5833 | 569 | 10.2 | <.001* |
| $x_1$* $x_2$ | 5510 | 697 | 7.90 | <.001* |
| $x_1$* $x_1$ | -8001 | 876 | -9.13 | <.001* |
| $x_2$* $x_2$ | -2727 | 876 | -3.11 | .004* |

**Note:** $x_1$ = Chain extender content (wt%), $x_2$ = Residence time (min)

* indicates statistical significance at type I error ($\alpha$) of 0.05

**Table 4.3** Statistical analysis of $M_w$ of modified PLA after melt-blending process

**Analysis of Variance**

| Source | DF | Sum of Squares | Mean Square | F Ratio |
|---|---|---|---|---|
| Model | 5 | 4729330736 | 945866147 | 84.33 |
| Error | 27 | 302822428 | 11215645 | **Prob > F** |
| Total | 32 | 5032153164 | | <.001* |

**Parameter Estimates**

| Term | Estimate | Std Error | t Ratio | Prob>\|t\| |
|---|---|---|---|---|
| Intercept | 128013 | 992 | 129 | <.001* |
| $x_1$ (0,2) | 10405 | 789 | 13.18 | <.001* |
| $x_2$ (5,15) | 7831 | 789 | 9.92 | <.001* |
| $x_1 * x_2$ | 6988 | 967 | 7.23 | <.001* |
| $x_1 * x_1$ | -11546 | 1215 | -9.50 | <.001* |
| $x_2 * x_2$ | 6.00 | 1215 | 0.00 | .10 |

**Note:** $x_1$ = Chain extender content (wt %), $x_2$ = Residence time (min)

* indicates statistical significance at type I error ($\alpha$) of 0.05

**Table 4.4** Statistical analysis of $M_n$ of modified PLA after compression molding process

**Analysis of Variance**

| Source | DF | Sum of Squares | Mean Square | F Ratio |
|---|---|---|---|---|
| Model | 5 | 14587000000 | 2917500000 | 190.4 |
| Error | 27 | 413675828 | 1532132 | **Prob > F** |
| Total | 32 | 15001000000 | | <.001* |

**Parameter Estimates**

| Term | Estimate | Std Error | t Ratio | Prob>\|t\| |
|---|---|---|---|---|
| Intercept | 106053 | 1159 | 91.5 | <.001* |
| $x_1$ (0,2) | 25527 | 922 | 27.7 | <.001* |
| $x_2$ (5,15) | 3163 | 922 | 3.43 | .002* |
| $x_1 * x_2$ | 3017 | 1130 | 2.67 | .013* |
| $x_1 * x_1$ | -16998 | 1420 | -12.0 | <.001* |
| $x_2 * x_2$ | -2217 | 1420 | -1.56 | 0.13 |

**Note:** $x_1$ = Chain extender content (wt%), $x_2$ = Residence time (min)

* indicates statistical significance at type I error ($\alpha$) of 0.05

**Table 4.5** Statistical analysis of $M_w$ of modified PLA after compression molding process

**Analysis of Variance**

| Source | DF | Sum of Squares | Mean Square | F Ratio |
|---|---|---|---|---|
| Model | 5 | 24399000000 | 4879900000 | 186 |
| Error | 27 | 706466518 | 26165427 | Prob > F |
| Total | 32 | 25106000000 | | <.001* |

**Parameter Estimates**

| Term | Estimate | Std Error | t Ratio | Prob>\|t\| |
|---|---|---|---|---|
| Intercept | 163297 | 1515 | 107 | <.001* |
| $x_1$ (0,2) | 31510 | 1206 | 26.1 | <.001* |
| $x_2$ (5,15) | 4633 | 1206 | 3.84 | .007* |
| $x_1 * x_2$ | 3156 | 1477 | 2.14 | .042* |
| $x_1 * x_1$ | -26323 | 1855 | -14.19 | <.001* |
| $x_2 * x_2$ | -2591 | 1855 | -1.40 | .17 |

**Note:** $x_1$ = Chain extender content (wt %), $x_2$ = Residence time (minute)

* indicates statistical significance at type I error (α) of 0.05

The interaction effects of the Cex content and residence time for the melt blending process on the molecular weight properties were determined by plotting surface response curves. The 3D surface curves and 2D contour plots from the interactions obtained from the two thermal processes are shown in **Figures 4.4** and **4.5**. The horizontal axes show the independent variables, whereas the vertical axis represents the predicted response of the $M_n$ and $M_w$. The unshaded area in the contour plots is the intersection of the desirable response values showing that the maximum response of the $M_n$ and $M_w$ could be reached at the combination of the higher Cex content and reaction time.

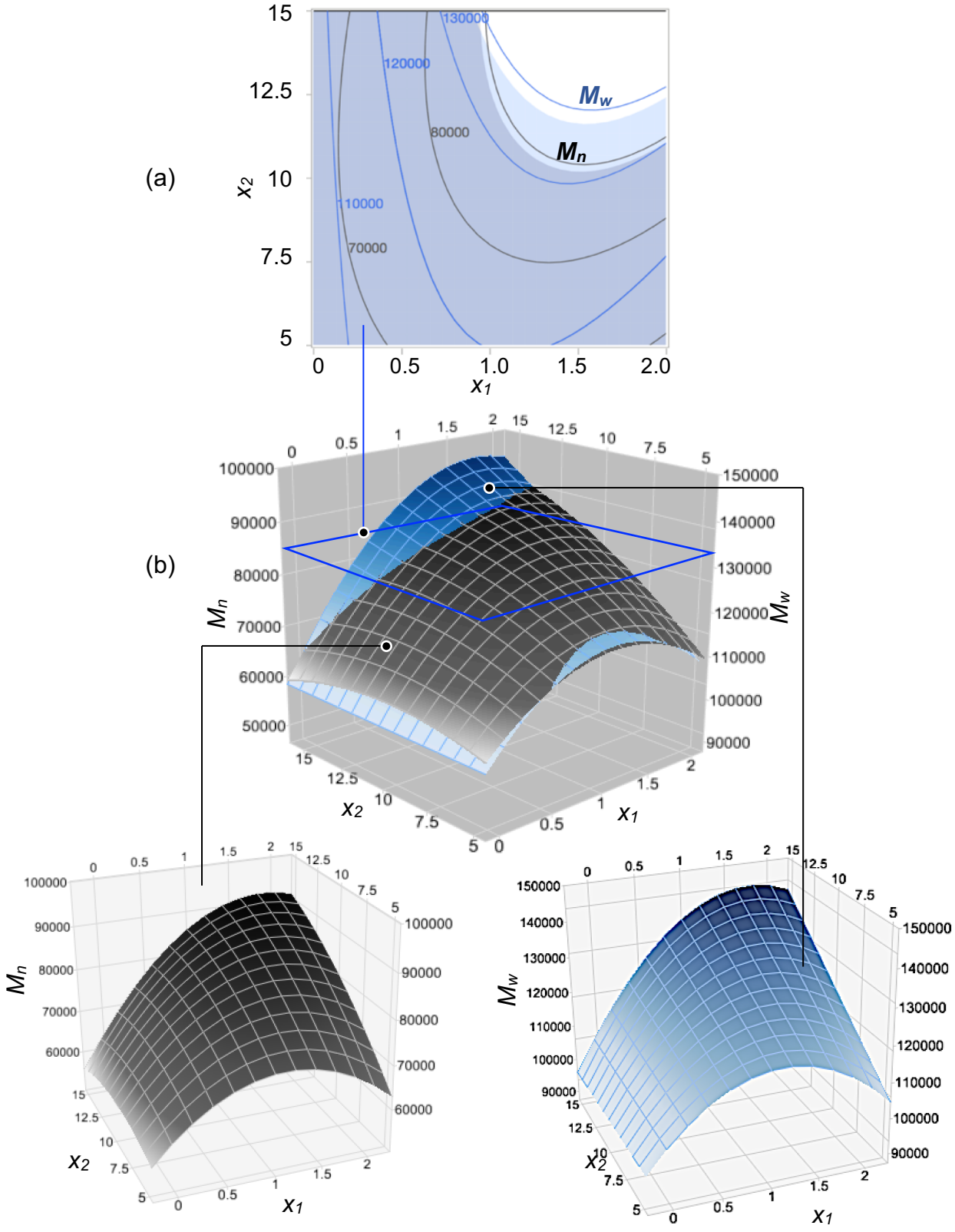


**Figure 4.4** (a) 2D contour and (b) 3D response surface plots of the effects of chain extender content and residence time on $M_n$ and $M_w$ after melt blending process.

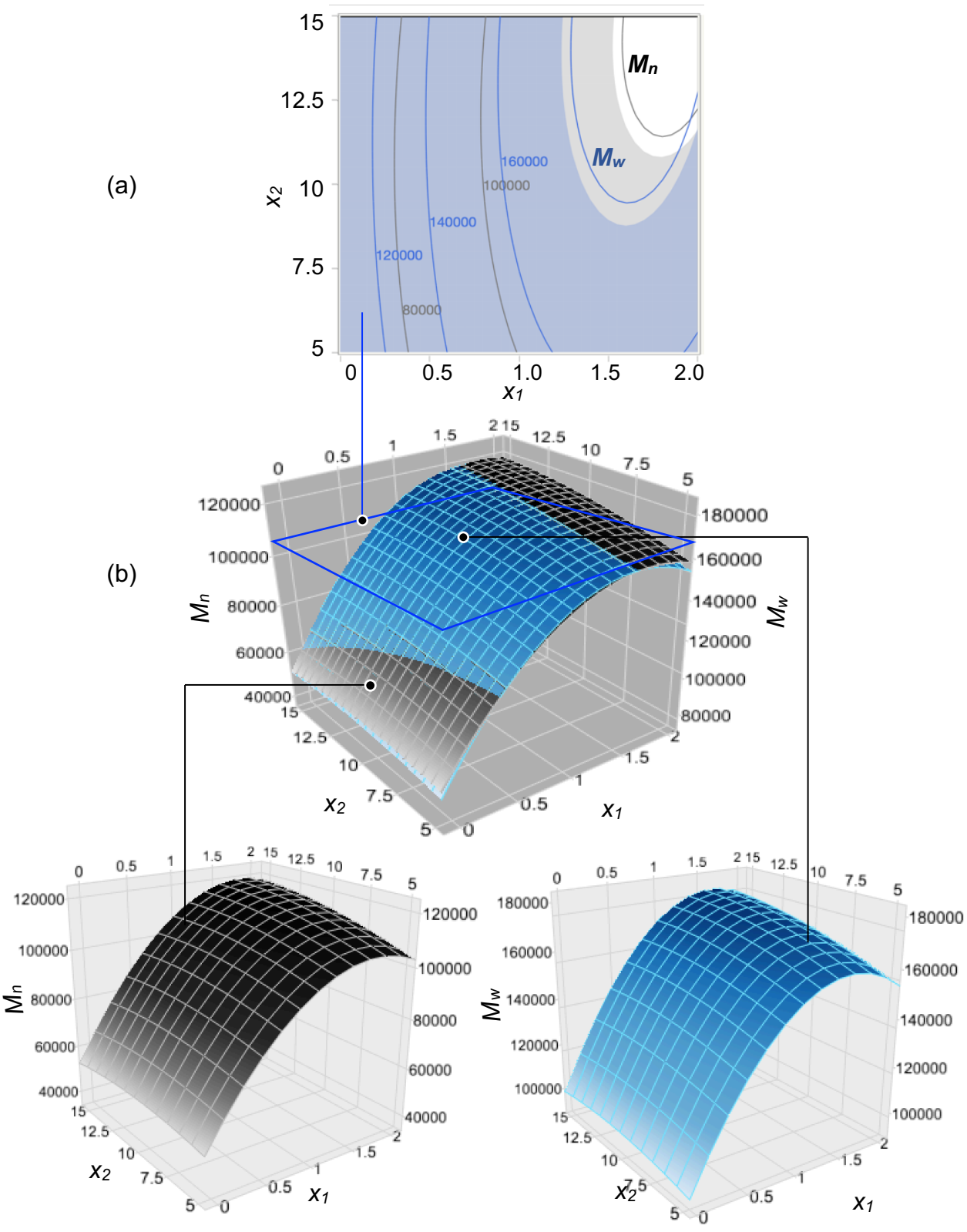


**Figure 4.5** (a) 2D contour and (b) 3D response surface plots of the effects of chain extender content and residence time on $M_n$ and $M_w$ after compression molding process

### 4.1.3 Optimization of molecular weight properties

The $M_n$ and $M_w$ were simultaneously evaluated and maximized to quantify the optimized conditions of the two processes using a desirability function. As shown in **Figure 4.6**, for the melt blending process, a maximum $M_n$ of 91622±2220 Da and $M_w$ of 142373±3078 Da were achieved with a Cex content of 1.80 wt%. When the compression molding step was applied, the optimum of Cex content was determined as 1.74 wt%, which provided the maximum $M_n$ of 118812±3491 Da and $M_w$ of 176579±4562 Da. For both methods, the optimum conditions were reached at a residence time of 15 min which was the upper boundary of the experimental design. It is apparent that with higher Cex content, the reaction needs a longer reaction time to achieve the optimal average molecular weight.

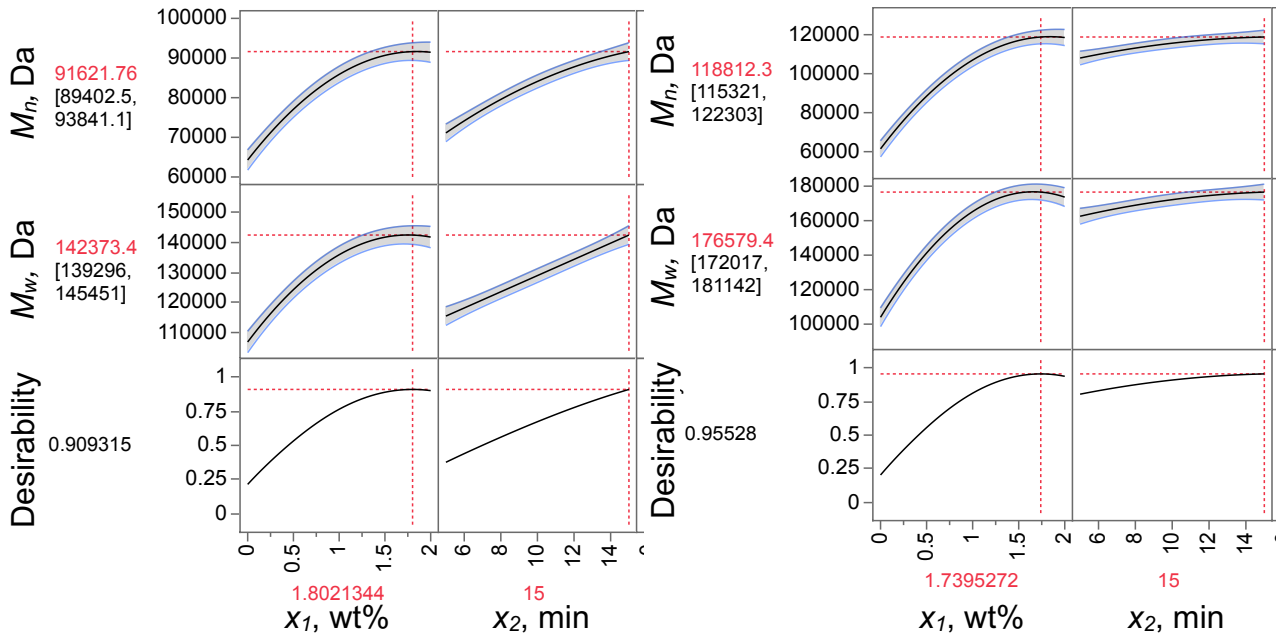


**Figure 4.6** Optimum condition and responses of $M_n$ and $M_w$ measured after (a) melt blending and (b) compression molding using the desirability function.

### 4.1.4 Additional experiments to expand the prediction of the residence time

As reported in the optimization study, the optimal Cex content for processing the modified PLA using melt blending and compression molding processes was determined as 1.74 wt%. This concentration was adjusted to 1.5 wt% due to concerns about processability of modified PLA with a high concentration of Cex. This issue was mentioned by Frenz et al. [4] where they found that a high concentration of chain extender can cause materials to be highly cross-linked and impossible to be processed.

The modified PLA with 1.5 wt% chain extender was processed with an expanded range of residence time for the purpose of achieving the highest possible $M_n$ and $M_w$ after compression molding process and the optimum residence time. The molecular weight of PLA with 1.5 wt% Cex at three levels of residence time, 5, 10, and 15 min, was predicted from the previous experimental models as shown in **Table 4.6**. The additional experimental runs were processed at residence times of 15, 20, and 25 min. The result obtained from each condition is presented in **Table 4.7**.

**Table 4.6** The predicted $M_n$ and $M_w$ of PLA-Cex after compression molding process at the residence time of 5, 10, and 15 min

| Chain extender, wt% | Residence time, min | The predicted average molecular weight | |
|---|---|---|---|
| | | $M_n$, Da | $M_w$, Da |
| 1.5 | 5 | 107678 ± 3298 | 163670 ± 4311 |
| 1.5 | 10 | 114567 ± 2321 | 172472 ± 3033 |
| 1.5 | 15 | 117022 ± 3298 | 176091 ± 4310 |

**Table 4.7** The experimental $M_n$ and $M_w$ of PLA-Con and PLA-Cex after compression molding process of the additional runs processed at the residence time of 15, 20, and 25 min

| Chain extender, wt% | Residence time, min | The experimental average molecular weight | |
|---|---|---|---|
| | | $M_n$, Da | $M_w$, Da |
| 0 | 15 | 66587 ± 358 | 98567 ± 273 |
| 0 | 20 | 65071 ± 454 | 98546 ± 442 |
| 0 | 25 | 61956 ± 1772 | 93275 ± 4242 |
| 1.5 | 15 | 118671 ± 2076 | 170692 ± 3395 |
| 1.5 | 20 | 123813 ± 998 | 169055 ± 448 |
| 1.5 | 25 | 120990 ± 1201 | 168931 ± 1164 |

The predicted and experimental molecular weight properties were plotted as a function of residence time (**Figure 4.7**). The result indicates that the quadratic model well represents the actual data given a $R^2$ of 0.77 for the $M_n$ and 0.56 for the $M_w$. To clarify a well-fitting regression, the predicted against actual plots and the residue plots of the $M_n$ and $M_w$ were performed as shown in **Figure 4.8**, which represents a good fit to the experimental data. The statistical analysis of $M_n$ and $M_w$ shown in **Table 4.8** can be interpreted that the non-significant lack-of-fit of both variables ($P > .05$) indicated that the fitted quadratic models were adequate to predict the data. Additionally, the quadratic terms of both $M_n$ and $M_w$ were significantly different showing that the curvature of the molecular weight response occurred in the range of the additional residence time.

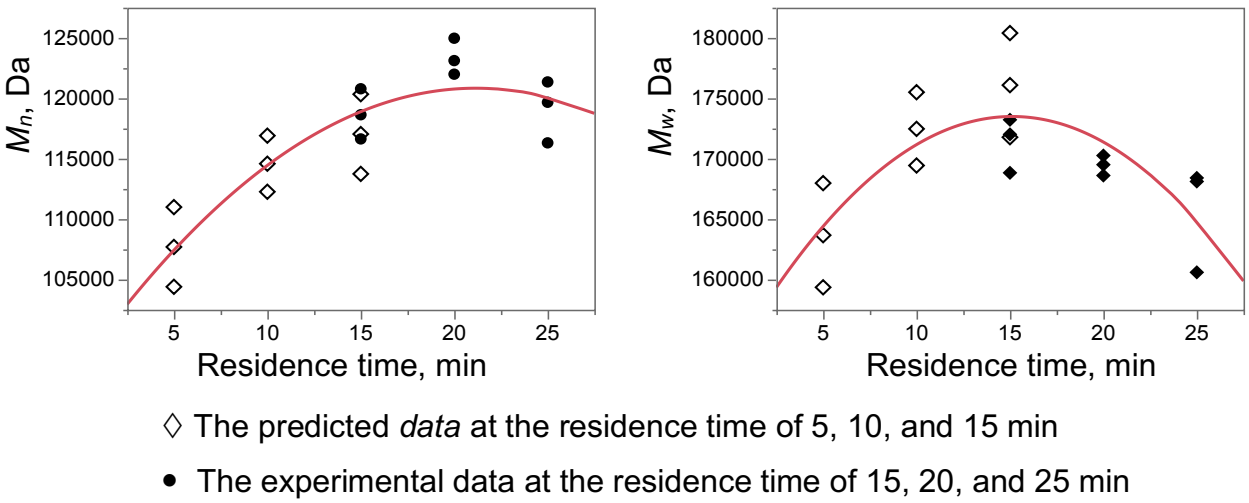


**Figure 4.7** Predicted and experimental data of (a) $M_n$ and (b) $M_w$ vs. residence time

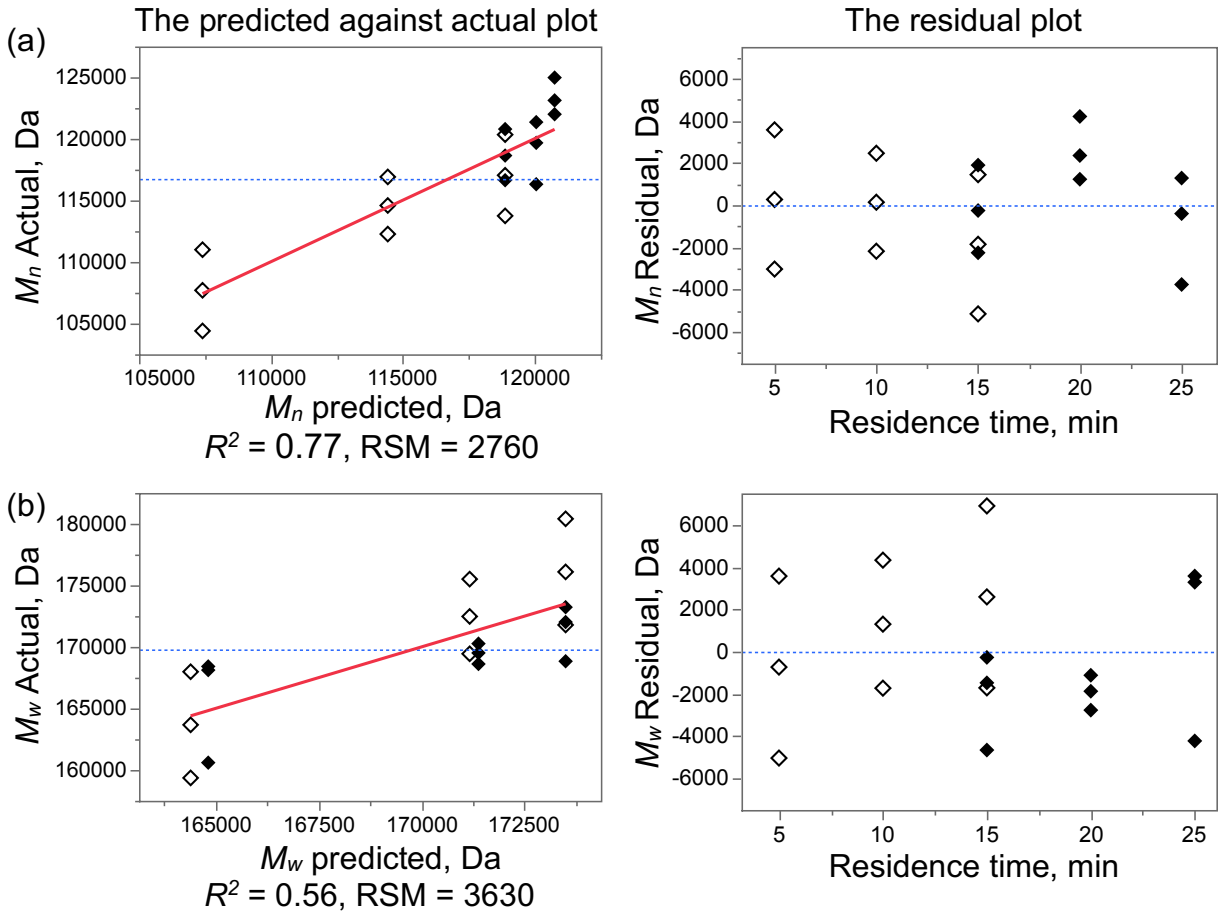


**Figure 4.8** Graphical residual analysis: the predicted against actual plots and the residual plot of (a) $M_n$ and (b) $M_w$

**Table 4.8** Statistical analysis for $M_n$ and $M_w$ of modified PLA with 15 wt% Cex

| Term | $M_n$ | $M_w$ |
|---|---|---|
| Intercept | 109389* | 173174* |
| Residence time | 632* | 21.34 |
| (Residence time-15) $^2$ | -51.4* | -88.8* |
| $R^2$ | 0.77* | 0.56 |
| ANOVA, Prob > F | <.001* | .002* |
| Lack of fit, Prob > F | 0.14 | 0.49 |

* indicates statistical significance at type I error ($\alpha$) of 0.05

In this processing method, the chain extension reaction took place during the melt blending and also during the compression molding process. Therefore, increasing the residence time in the melt blending process can prolong the reaction time and allow the reactive epoxy groups to react with the PLA end-chains. **Figure 4.7** demonstrates that at the residence time of 5–15 minutes, the increment of $M_n$ and $M_w$ increased, but after that, they slightly decreased. As mentioned, the higher amount of Cex needed a longer thermal process time to be stabilized. However, after the chain extension, the extended molecular length could restrict the accessibility of the chain ends to connect with epoxy functional groups in the reactive sites. Therefore, the free ends could not react with Cex and increase the molecular weight. Moreover, degradation of PLA could also be generated by random chain scission reactions and accelerated due to heat accumulation and increased viscosity with the incorporation of chain extender [3,5]. As a result, the $M_n$ and $M_w$ apparently dropped at the residence time between 20 and 25 minutes. The optimal residence time was estimated to simultaneously enhance the greatest $M_n$ and $M_w$ of PLA–Cex. **Figure 4.9** shows the optimal condition achieved at the residence time as 16.73 min. The estimated $M_n$ and $M_w$ were estimated as 119814±1757 Da and 173265±2312 Da, respectively.

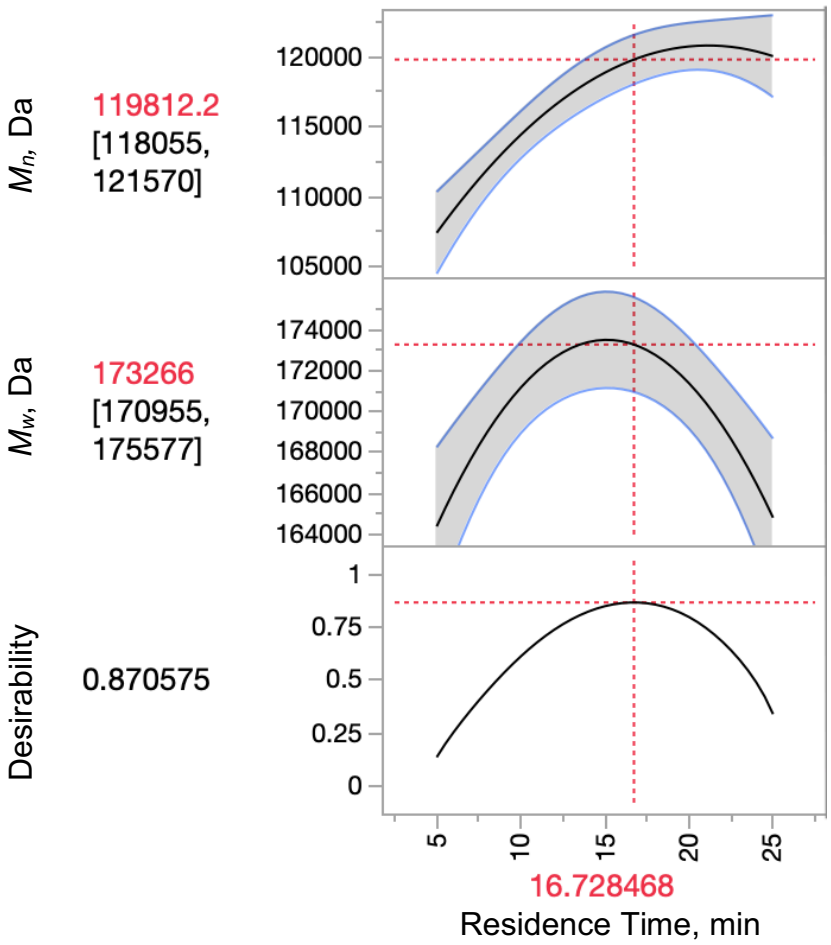


**Figure 4.9** The optimum condition of the $M_n$ and $M_w$ of modified PLA using the desirability function

## 4.2 Processing condition for cast film extrusion of modified PLA

PLA–Cex film was produced using the casting method with selected Cex concentration of 1.5 wt%. The efficiency of the chain extension reaction was influenced by the thermal conditions of the processing method as mentioned in **Section 4.1**. To process PΩLA–Cex film to be as efficient as possible, the residence time distribution was considered by varying the screw speeds (10, 20, and 40 rpm). In general, the duration that the polymer stays inside an extruder mixing and reacting with chain extender increases when the screw speed is reduced. The molecular weight determination was used to select the appropriate experimental condition.

The $M_n$ result of PLA–Con and PLA–Cex obtained from each screw speed condition is shown in **Figure 4.10** representing the effect of the residence time on the degradation of PLA–Con and the chain extension reaction of PLA–Cex. The molecular weight of PLA significantly increased with the addition of Cex. By decreasing screw speeds of 40, 20, and 10 rpm, the $M_n$ of PLA–Cex increased to 177084$\pm$642,187721$\pm$1031, and 187939$\pm$1913 Da, respectively. However, the $M_n$ values of PLA–Cex produced with the screw speeds of 10 and 20 rpm were not significantly different. In this case, it could be attributed to the higher degradation of PLA chains in the unreacted regions corresponding to the noticeable decreasing of $M_n$ of PLA–Con processed at the longer residence time. Therefore, the PLA–Cex produced with the screw speed of 20 rpm was selected for further processing to study the properties and also the effect on hydrolytic degradation because when produced at lower speeds, the inconsistent flow of material could cause problems in processing.

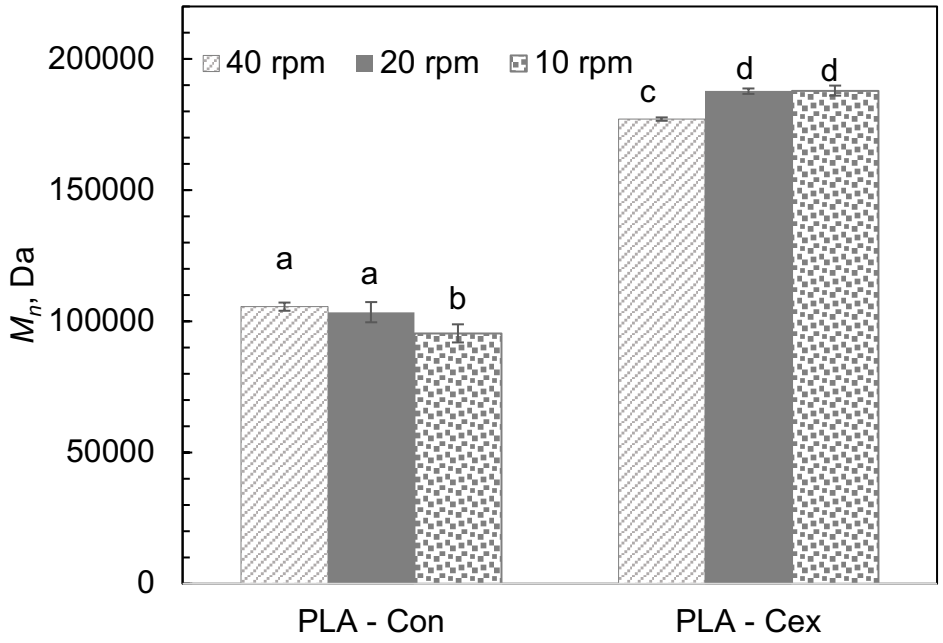


**Figure 4.10** $M_n$ of PLA–Con and PLA–Cex film processed with screw speed at 40, 20 and 10 rpm. Values with different lowercase letters represent statistically significant differences ($P < 0.05$; Tukey's HSD) of $M_n$.

## 4.3 Initial characterization of the modified PLA with the chain extender

### 4.3.1 Thermal properties

The thermal gravimetric analysis (TGA/DTA) of PLA–Con and PLA–Cex was studied to measure the change in the weight (%) as a function of temperature representing the decomposition process, thermal characteristics and also predicted properties of the polymers. The TGA and DTG thermograms of PLA–Con and PLA–Cex are shown in **Figure 4.11**. The curve of PLA–Con showed an initial temperature of decomposition ($T_i$) at 260°C, whereas the $T_i$ of PLA–Cex was found at a lower temperature of 253°C. The temperatures of maximum weight loss ($T_{max}$) of PLA–Con and PLA–Cex were 366°C and 363°C, respectively. Although the TGA curves of both samples were very similar, this reduction could be evidence that the incorporation of Cex into PLA could achieve long branched structures contributing to an increase in chain mobility. Therefore, the thermal stability of

PLA slightly decreased when reacted with the chain extender, which is in general agreement with previous studies [6–8]. Baimark and Cheerarot [7] studied the effect of chain extension on the thermal stability of PLA and explained that the architecture of PLA had a significant impact on the thermal stability. The modified PLA with a higher ratio of Cex presented a greater degree of branching structures exhibiting lower thermal stability compared to the linear long molecular chains of PLA–Con.

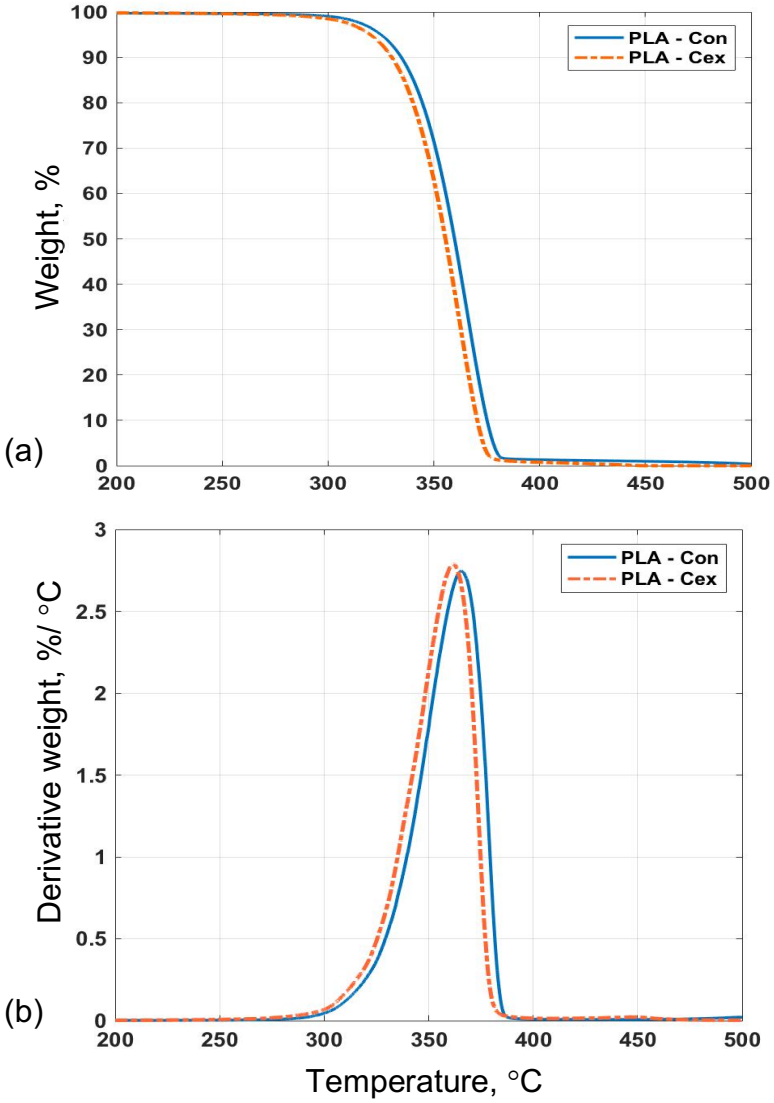


**Figure 4.11** Thermal stabilities of PLA–Con and PLA–Cex: a) TGA thermogram b) DTG thermogram

The effect of the chain extender on the thermal properties of PLA was also examined using differential scanning calorimeter (DSC). The second scan of the heating curves of PLA–Con and PLA–Cex are shown in **Figure 4.12**, and the thermal properties, $T_c$, $T_g$ , $T_m$, and $\%X_C$ are shown in **Table 4.9**. $T_g$ and $T_c$ of the PLA–Con and PLA–Cex were not significantly different. The decrease in the $T_m$ indicates that the presence of long chain branches of PLA–Cex can affect the packing efficiency and cause the formation of imperfect crystal morphologies compared to the neat PLA [9,10]. The initial degree of crystallinity does not show any difference. Moreover, it can be assumed that both samples were entirely amorphous.

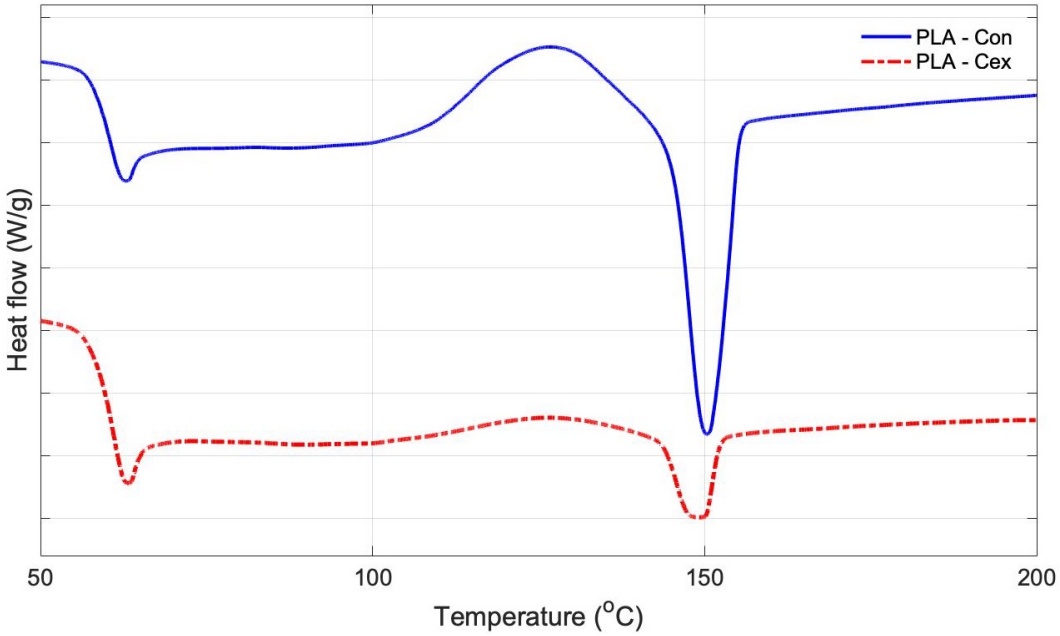


**Figure 4.12** DSC thermograms of PLA–Con and PLA Cex (the 2nd heating scan).

**Table 4.9** Thermal properties of the second heat scan of PLA–Con and PLA–Cex films

| Samples | $T_g$, °C | $T_c$, °C | $T_m$, °C | $X_c$,% |
|---|---|---|---|---|
| PLA–Con | 60.8 ± 0.2[a] | 127.1 ± 0.4[a] | 150.7 ± 0.2[a] | 0.1 ± 0.1[a] |
| PLA–Cex | 61.0 ± 0.3[a] | 125.4 ± 0.9[a] | 149.5 ± 0.2[b] | 0.1 ± 0.1[a] |

Values with different lowercase letters represent statistically significant differences ($P < 0.05$; Tukey's HSD).

### 4.3.2 Mechanical properties

The mechanical properties of PLA–Con and PLA–Cex film were evaluated by tensile testing measured in the machine direction. **Figure 4.13** compares the strain-stress curves of PLA–Con and PLA–Cex while **Table 4.10** reports the Young's modulus, tensile strength and elongation at break. PLA–Con clearly presents a brittle behavior showing poor elongation at break of around 2%. The tensile stress and the Young's modulus were approximately 49 MPa and 2.8 GPa, respectively. This behavior results from the lack of energy absorbing capability of PLA, which cannot dissipate the kinetic energy during deformation and the lack of the chain entanglement during the crack propagation [11]. Addition of the chain extender significantly increased the elongation at break to ~108%, average tensile stress of 62 MPa and the Young's modulus of around 3.62 GPa. This indicates that the higher molecular weight and branched molecular chains produced with the presence of chain extender enhance the tensile strength and toughness of PLA–Cex.

**Table 4.10** Mechanical properties of PLA–Con and PLA–Cex films

| Samples | Modulus, GPa | Tensile stress, MPa | Elongation at break, % |
|---|---|---|---|
| PLA–Con | $2.8 \pm 0.1^{a}$ | $49.1 \pm 0.7^{a}$ | $2.3 \pm 0.1^{a}$ |
| PLA–Cex | $3.6 \pm 0.1^{b}$ | $62.2 \pm 9.9^{b}$ | $108.5 \pm 16.1^{b}$ |

Values with different lowercase letters represent statistically significant differences ($P < 0.05$; Tukey's HSD).

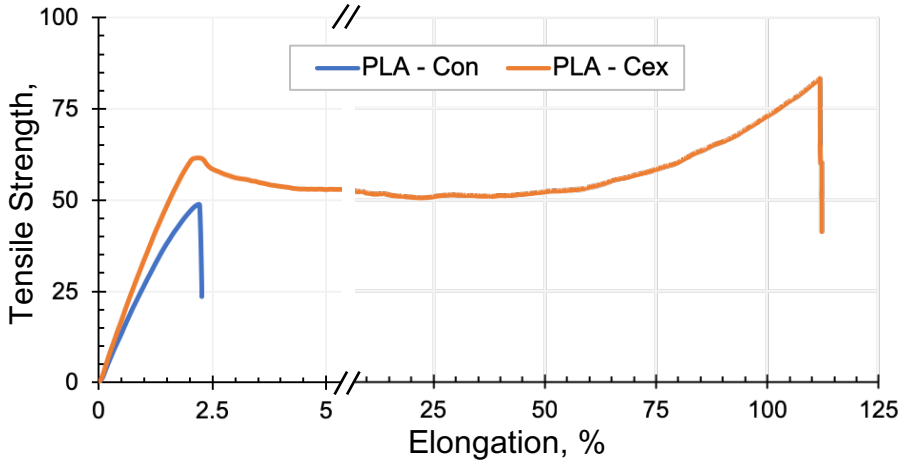


**Figure 4.13** Tensile properties of PLA–Con and PLA–Cex

### 4.3.3 Dynamic mechanical analysis

Dynamic mechanical analysis (DMA) is a general technique to measure the thermal transition of materials under a mechanical stress which relates to the internal motions of the molecules of polymers. In this study, the PLA film was tested in both dry and wet conditions to investigate the initial $T_g$ and also the $T_g$ of film while immersed in water and in 50% ethanol. The $T_g$ was determined as the temperature at which the tanδ value reaches a maximum. As reported in **Table 4.11**, the initial $T_g$ of PLA–Con was 61.1±0.5 °C and PLA–Cex was 60.4±0.5 °C, which were not significantly different. Additionally, there was no difference in $T_g$ measured by DSC and DMA under dry conditions as shown in **Table 4.9**.

**Figures 4.14** and **4.15** represent the tanδ curves of PLA–Con and PLA–Cex immersed in water and in 50% ethanol, respectively. **Table 4.11** shows that the $T_g$ values of the films immersed in water decreased to approximately 53 °C for PLA–Con and 54°C for PLA–Cex due to the plasticization effect of the water penetrating the polymer matrix and making the molecular chains more flexible. The $T_g$ of PLA–Con immersed in 50% ethanol decreased to 37 °C due to the stronger plasticization effect of ethanol solution compared to water. For PLA–Cex film immersed in 50% ethanol, the peaks of tanδ curve appears at two

temperatures of approximately 50 °C and 38 °C indicating the existence of two phases. The relaxation at the higher temperature, which is the main peak, affected the $T_g$ of the fraction PLA incorporating the chain extender, while the lower temperature locating near $T_g$ of PLA–Con representing the $T_g$ of the neat PLA fraction.

**Table 4.11** The $T_g$ of PLA–Con and PLA–Cex films from DMA under the dry and wet conditions (water and 50% ethanol)

| solution | PLA–Con, °C | PLA–Cex, °C |
|---|---|---|
| - | 61.1 ± 0.5 $^{Aa}$ | 60.4 ± 0.5 $^{Aa}$ |
| pure water | 52.9 ± 0.4 $^{Ba}$ | 53.7 ± 1.2 $^{Ba}$ |
| 50% ethanol | 36.8 ± 0.8 $^{Ca}$ | 38.0 ± 0.3 $^{Ca}$ (the 1st peak)<br>50.3 ± 0.3 $^{Db}$ (the 2nd peak) |

The values within a column followed by the same uppercase letters and the values within a row followed by the same lowercase letters are not significantly different ($\alpha$=0.05).

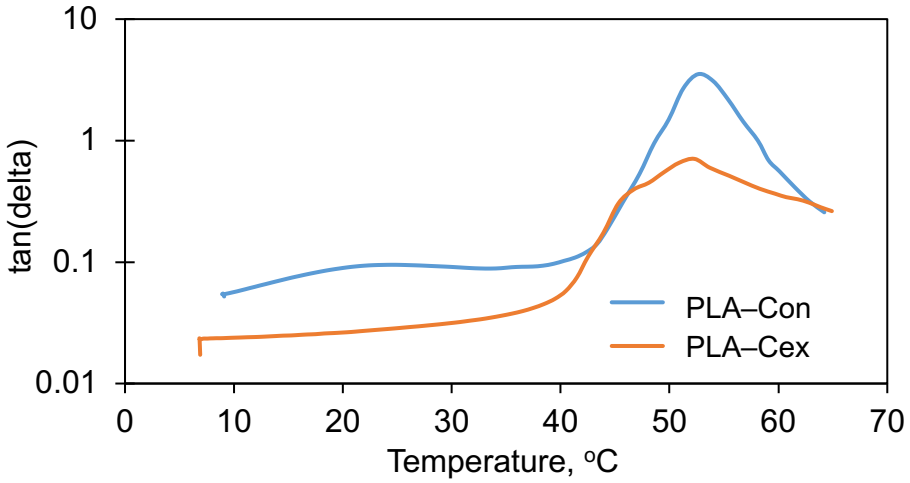


**Figure 4.14** The thermal transition of PLA–Con and PLA–Cex immersed in water obtained from DMA under wet conditions

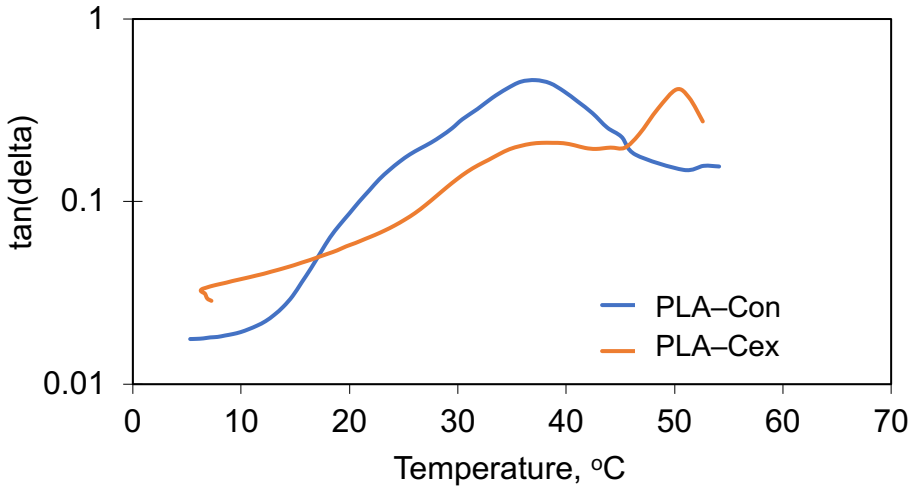


**Figure 4.15** The thermal transition of PLA–Con and PLA–Cex immersed in 50% ethanol obtained from DMA under wet conditions

### 4.4 Hydrolytic degradation study of control and modified PLA

The effect of temperature on the degradation of modified PLA with chain extender was studied in two kinds of media, water and 50% ethanol. The hydrolysis experiments were designed to be carried out the selected temperature ranges related to the $T_g$ of the samples. According to the result obtained from DMA, $T_g$ of PLA–Con and PLA–Cex films immersed in water were approximately 52.9 °C and 53.7 °C, respectively. Therefore, the experiments were set at 40 °C, which represented a temperature condition lower than $T_g$, and at 60, 75, 85, and 95 °C for the temperature conditions above $T_g$. When PLA was immersed in 50% ethanol, the $T_g$ values decreased to 36.8 °C for PLA–Con, and 38.0 and 50.3 °C for PLA–Cex. The hydrolysis in 50% ethanol was conducted at temperatures of 50, 60, 75 and 85 °C which are assumed to be conditions above $T_g$. Visual images during hydrolytic degradation in water at 75 °C of PLA–Con and PLA–Cex film are presented in **Figure A.1,** Appendix A as an example for the comparison of the structure change between both samples.

### 4.4.1 The pH and crystallinity variation during the hydrolytic degradation

The hydrolytic degradation in water and in 50% ethanol was conducted at neutral pH. During the hydrolysis, the acidic degradation products were formed from the chain scission reaction of PLA chain had an effect to decrease the pH inside PLA matrix, then released to outside of the surface and the media solution. The pH variation of the hydrolysis media was monitored as a function of time as shown in **Figures 4.16** and **4.17**. The initial pH values of the water at different hydrolysis temperature conditions were measured to be 7.48–8.16 due to the hydrolysis temperature could plays a significant role on pH measurement. As seen in **Figures 4.16,** the pH measured over the hydrolysis at 40 °C varied between 7.09 and 7.87 for PLA–Con and 7.72 and 8.42 for PLA–Cex. For temperatures above $T_g$, the initial pH rapidly dropped and reached a plateau value at about 3.06 for PLA–Con and 3.25 for PLA–Cex. These terminal pH values corresponded to the pKa of lactic acid oligomers reported as 3.86 at 25 °C [12–14]. In comparison, the pH of water measured from the water-mediated hydrolysis of PLA–Cex proceeded slightly slower than PLA–Con. A similar result was obtained from the hydrolysis in 50% ethanol. The initial pH of 50% ethanol was measured as 7.44–7.60 and finally reached the values of 3.63 and 2.99 for PLA–Con and PLA–Cex, respectively.

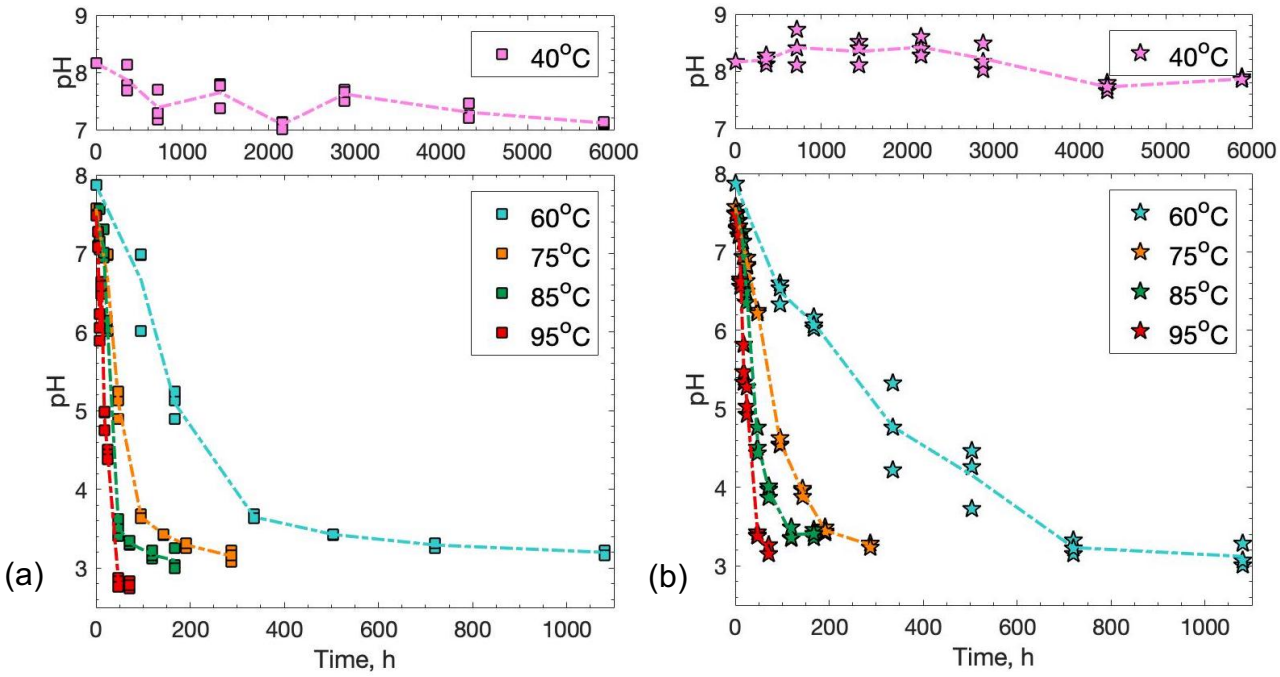


**Figure 4.16** pH variation during hydrolytic degradation in water (a) PLA–Con and (b) PLA–Cex. Markers (■, ★) indicate the pH values and lines (– - –) indicates fitted points at the average values.

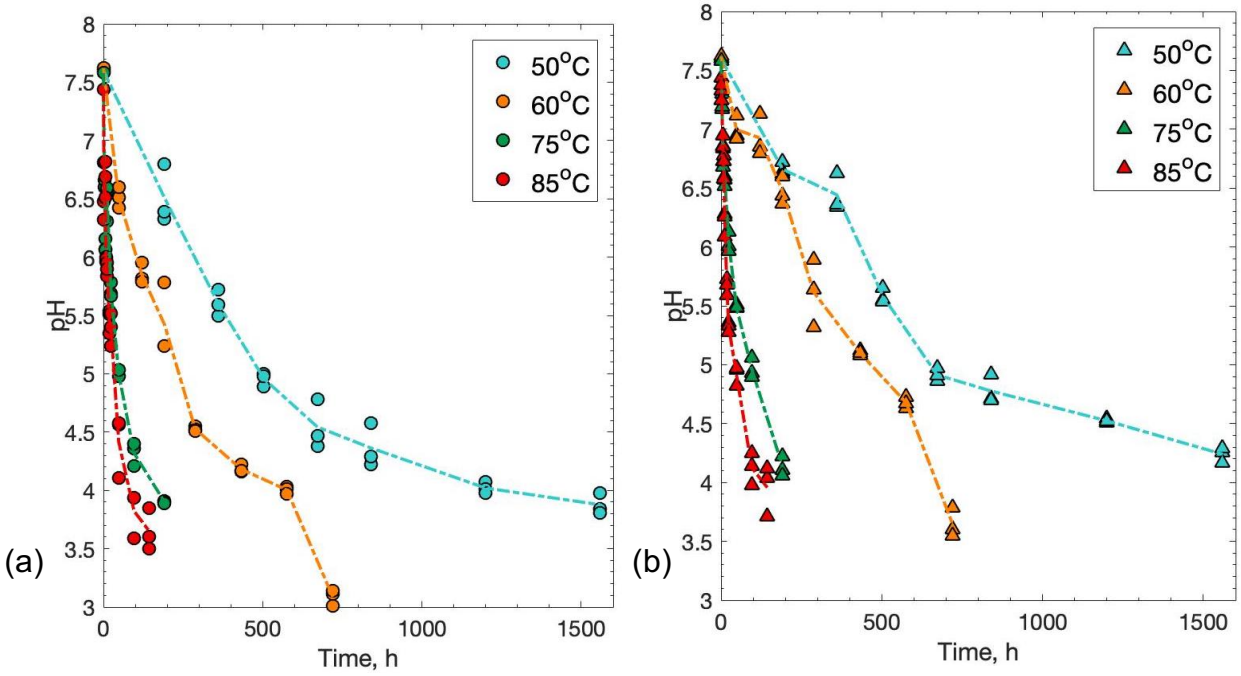


**Figure 4.17** pH variation during hydrolytic degradation in 50% ethanol (a) PLA–Con and (b) PLA–Cex Markers (●, ▲) indicate the pH values and lines (– - –) indicates fitted points at the average values.

The DSC technique was used to determine the thermograms and variation of crystallinity of the PLA film during the hydrolytic degradation process. **Figures 4.18–4.20** show the thermograms of PLA–Con and PLA–Cex from the first heating cycle to investigate the structural changes during the common chain scission-induced crystallization process. The $T_m$ and $T_c$ were determined from the endothermic melting peaks and the exothermic cold-crystallization peak, respectively. The thermograms of PLA film exposed to hydrolysis at 40 °C represented the temperature condition below $T_g$ shown in **Figures 4.18**. The $T_c$ of PLA film before degradation decreased with the presence of chain extender while the $T_{m,}$ which indicated the thermal stability of the crystalline structure, occurred at a similar location. When PLA experiences hydrolytic degradation, $T_c$ tends to decrease for several reasons such as an increase in the segmental mobility of the hydrolyzed molecular chains, and an occurrence of local crystalline structures, which can facilitate the nucleation and crystal growth during the heating scan [15]. The existence of double peaks of $T_m$ were shown in PLA–Con film, which could be attributed to the difference in crystal structures, crystal perfection and the thickness of lamellas [16] whereas $T_m$ of PLA–Cex exhibited as one peak over the hydrolysis process indicating less mobility and mode of crystallization may be due to the longer chains. **Figures 4.19** and **4.20** show the thermograms of PLA–Con and PLA–Cex during hydrolysis at 75 °C in water and in 50% ethanol, respectively, selected as examples for the high hydrolytic degradation temperature conditions. Similar trends of $T_m$ were observed from both thermograms. Unlike the degradation at low temperature, $T_c$ of hydrolyzed PLA during hydrolysis at 75 °C disappeared in the first heating scan as can be seen in **Figures 4.21** and **4.22**.

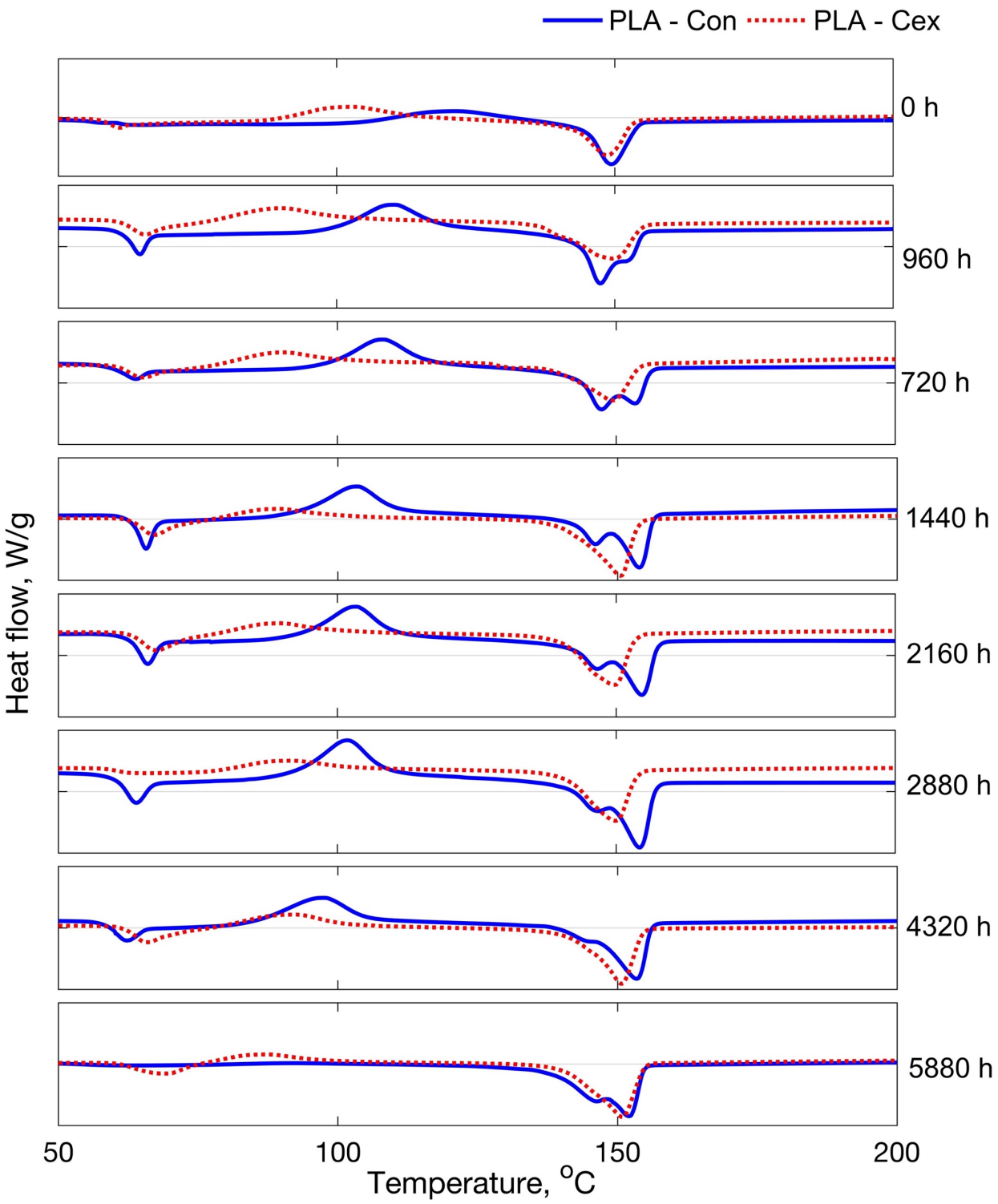


**Figure 4.18** Thermograms of PLA–Con and PLA–Cex film during hydrolytic degradation in water at 40 °C

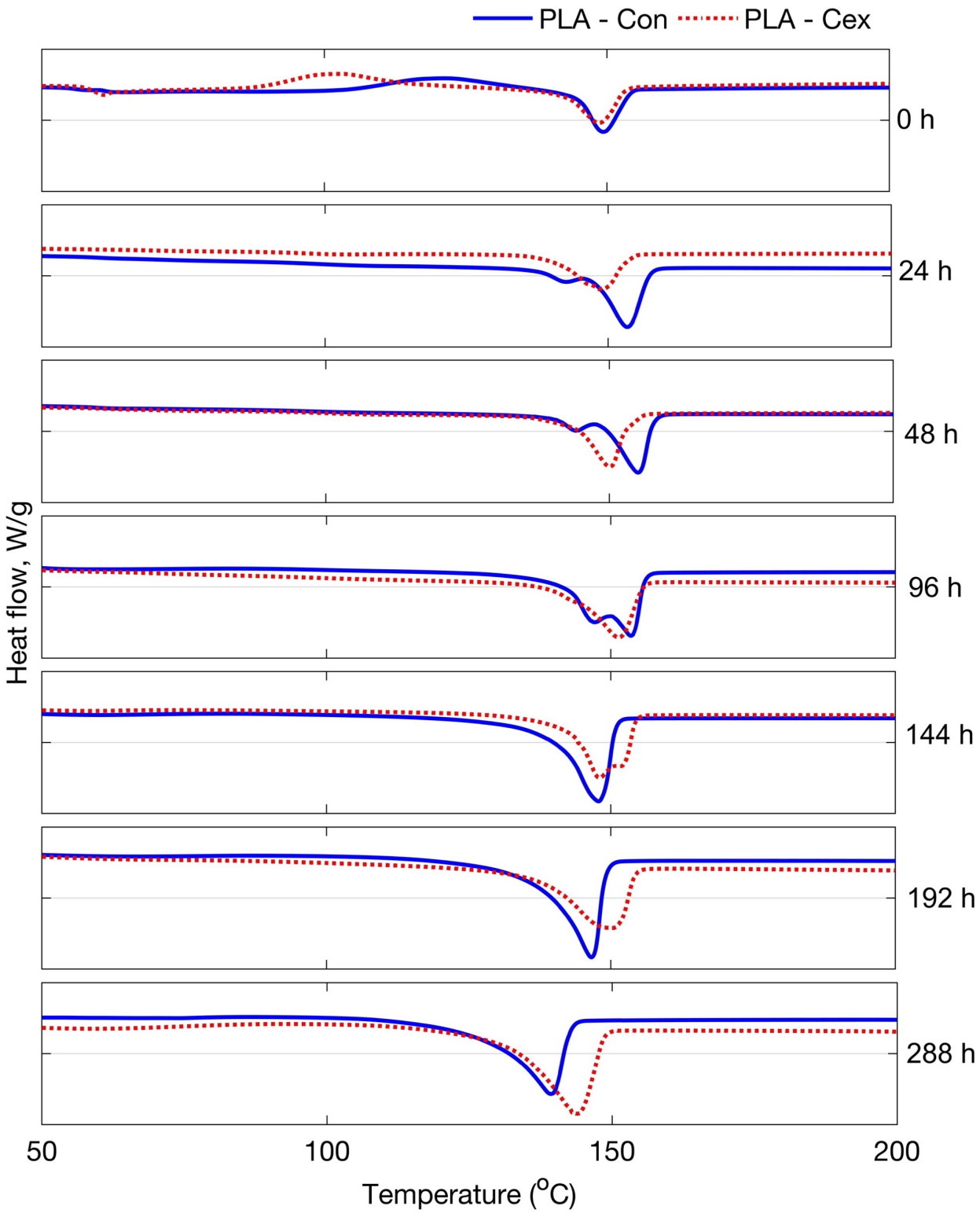


**Figure 4.19** Thermograms of PLA–Con and PLA–Cex film during hydrolytic degradation in water at 75 °C

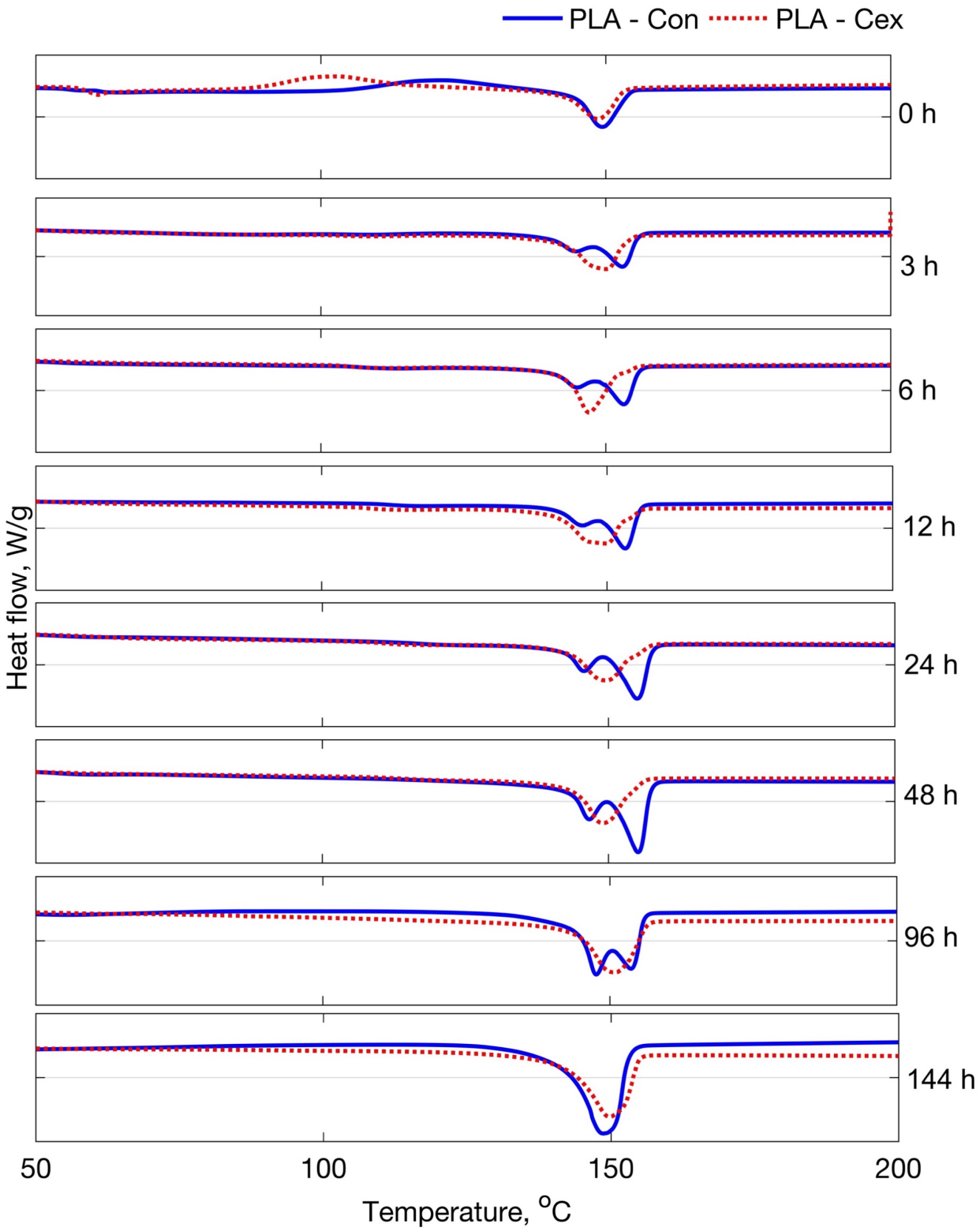


**Figure 4.20** Thermograms of PLA–Con and PLA–Cex film during hydrolytic degradation in 50% ethanol at 75 °C

The crystalline volume fraction ($X_c$) of the samples during the hydrolysis in water and 50% ethanol calculated from **Eq. (3.6)** are illustrated in **Figures 4.21** and **4.22.** The crystalline volume fraction after immersion in 40°C water increased from 1.2% to 14.5% at 245 days for PLA-Con and from 1.1% to 12.7% for PLA-Cex during the hydrolysis, as shown in **Figure 4.21**. For the hydrolysis at the higher temperature, the crystallinity was considerably increased and reached approximately 63.7–73.3 % and 57.2–76.6% for the PLA–Con and PLA–Cex, respectively. Similar results were found in the experiments in 50% ethanol plotted in **Figure 4.22**. The $X_c$ values of the PLA–Con and PLA–Cex reached approximately 56.2–76.2% and 47.7–56.5% respectively. The degree of crystallinity of the hydrolyzed PLA was significantly increased during the chain scission process due to the extra mobility of the molecular chains to form the crystalline structure.

The amorphous regions are more susceptible to hydrolytic degradation than the crystalline regions. Therefore, as the hydrolysis time increases, the crystallinity induced from the chain scission had a significant effect on the degradation process. When the molecular weight of PLA chain reduces to approximately 4 kDa which is assumed as a solubility limit of PLA oligomer [17,18], the amorphous phase could dissolve first and leave the crystalline residues remaining in the matrix. The Avrami equation was applied to estimate crystallization processes during the hydrolytic degradation. The $X_c$ values of the degraded samples with the average $M_n$ less than 4 kDa, represented in symbols (✳), were excluded from the parameter estimation because they could overestimate the crystallization process during hydrolytic degradation.

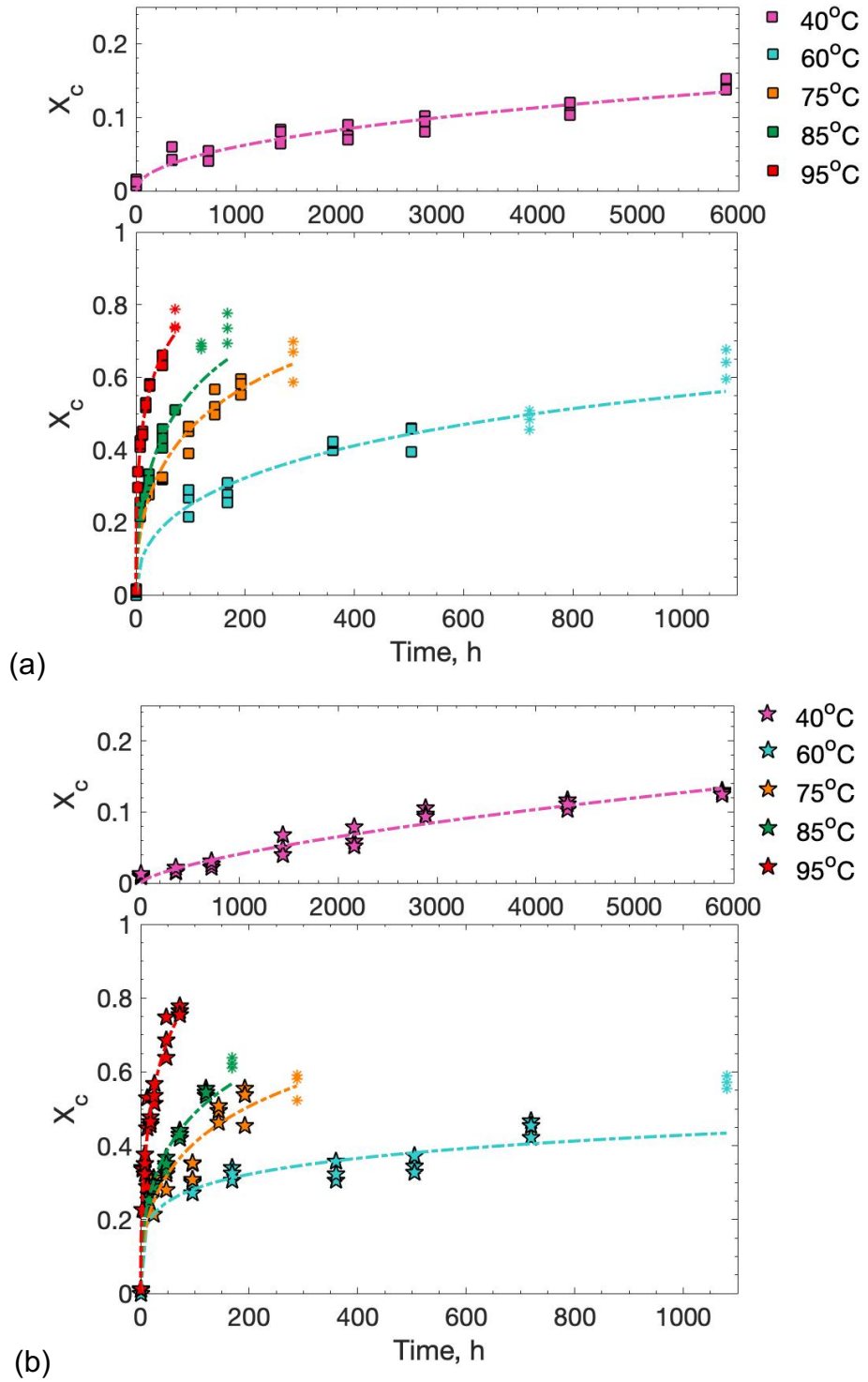


**Figure 4.21** Variation of the crystalline volume fraction ($X_c$) of (a) PLA–Con and (b) PLA–Cex film during hydrolytic degradation in water at 40, 60, 75, 85, and 95 °C. Symbols (✳) represent the $X_c$ values of the PLA film with the average $M_n$ less than 4 kDa.

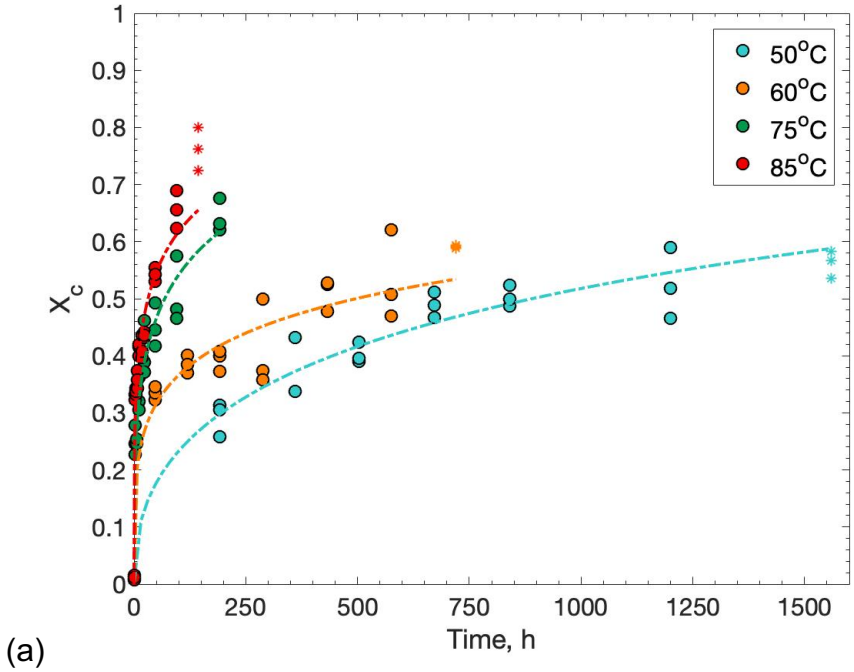


(a)

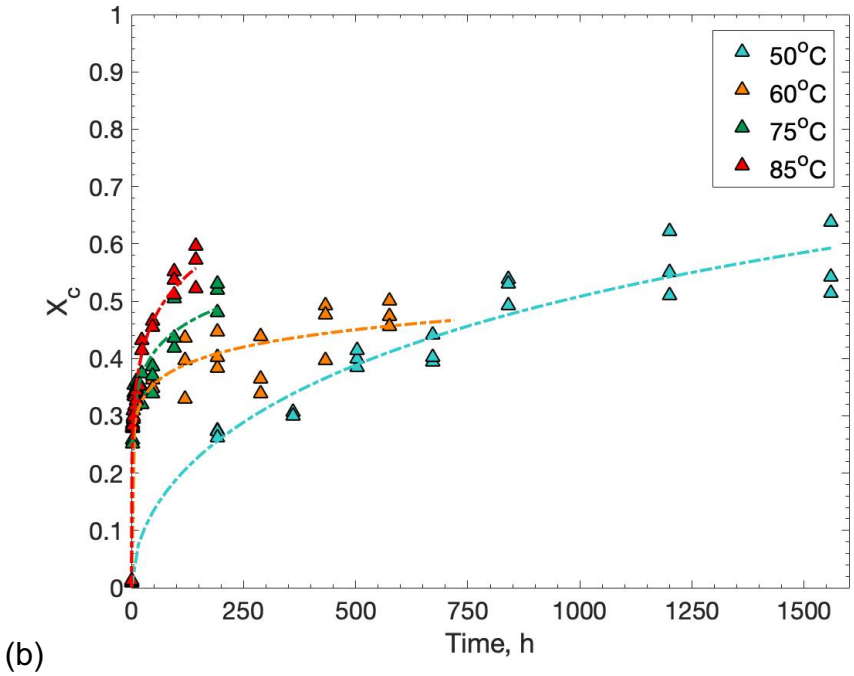


(b)

**Figure 4.22** Variation of the crystalline volume fraction ($X_c$) of (a) PLA–Con and (b) PLA–Cex film during hydrolytic degradation in 50% ethanol at 50, 60, 75, and 85 °C. Symbols (✳) represent the $X_c$ values of the PLA film with the average $M_n$ less than 4 kDa.

### 4.4.2 MWD and deconvolution of MWD of PLA

**Figures 4.23** and **4.24** show the series of MWDs of PLA–Con and PLA–Cex exposed to hydrolytic degradation in water at various temperatures, respectively. As seen in all MWD profiles, when the degradation time increased, the MWD profiles shifted to the left side representing the increasing of the smaller molecular chains due to chain scission degradation. From a visual comparison between the series of MWDs of PLA–Con and PLA–Cex, it can be noticed that the shift of molecular weight distribution curves of PLA–Cex toward lower molecular weight was slower compared to ones of PLA–Con.

The MWD of the polymer contains a number of the polymer chains with unequal lengths. During the degradation, the MWD curves gradually broadened and then changed from a monomodal into a bimodal or a multimodal distribution. When the MWD transforms into multimodal shape, it can imply that there is a mixture of two or more separating populations. Many studies explain that the multimodal distribution apparently found at the late stage of hydrolysis can be developed from the crystal residues forming during the chain scission reaction and remaining stable while the amorphous fraction hydrolyzed [19–21]. A deconvolution technique was performed to assess the main population of the molecular chains to evaluate the average molecular weight which represented the properties of the modified PLA. **Figure 4.27** shows examples of the initial MWD and deconvolution of MWD of PLA–Con and PLA–Cex film. The distribution curve of PLA–Cex shifted to a higher molecular weight and also showed a bimodal distribution with a little shoulder peak due to the increase of molecular chains and the presence of long chain branches of modified PLA.

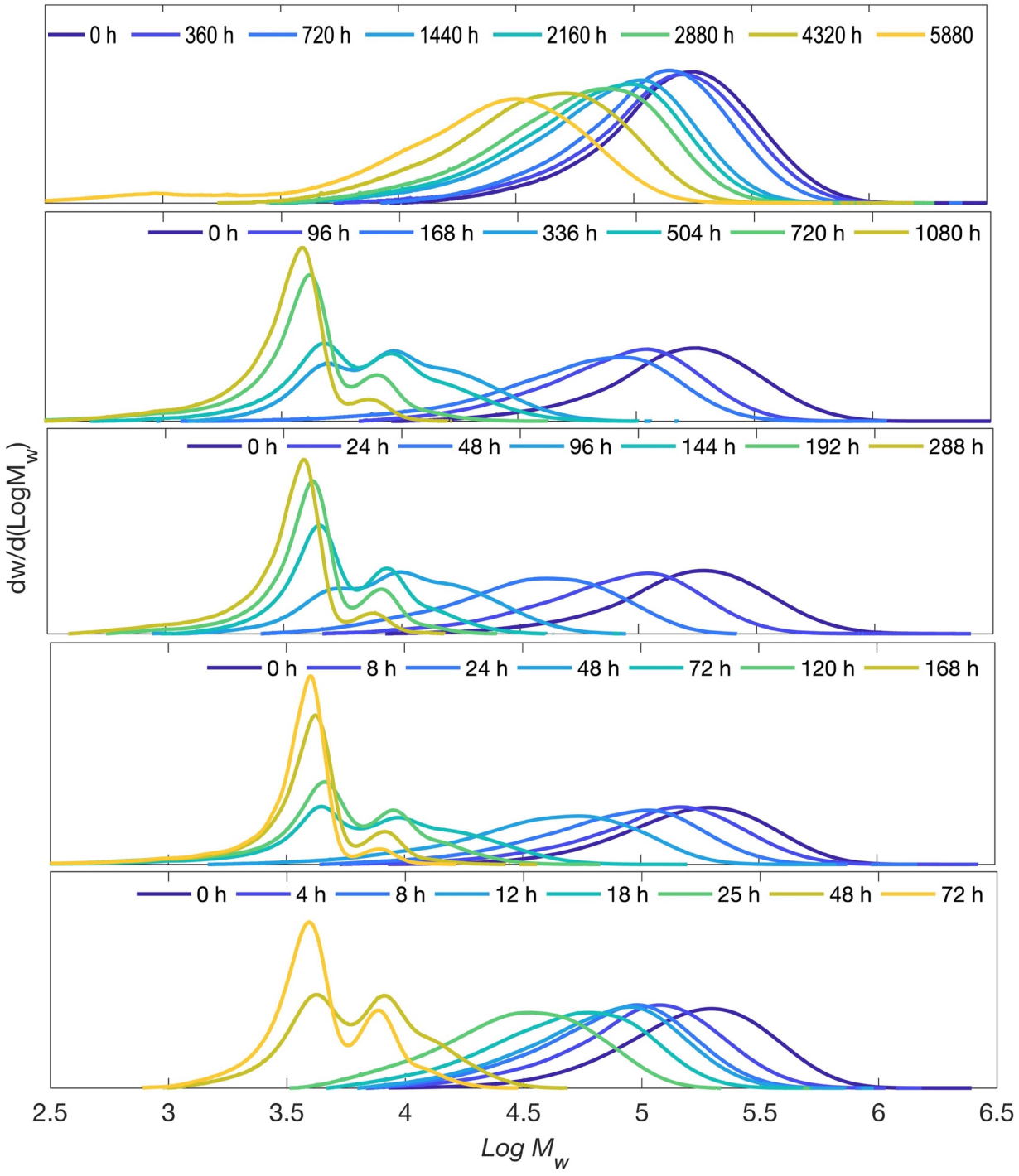


**Figure 4.23** MWD of PLA–Con film during hydrolytic degradation in water at (a) 40, (b) 60, (c) 75, (d) 85, and (e) 95 °C

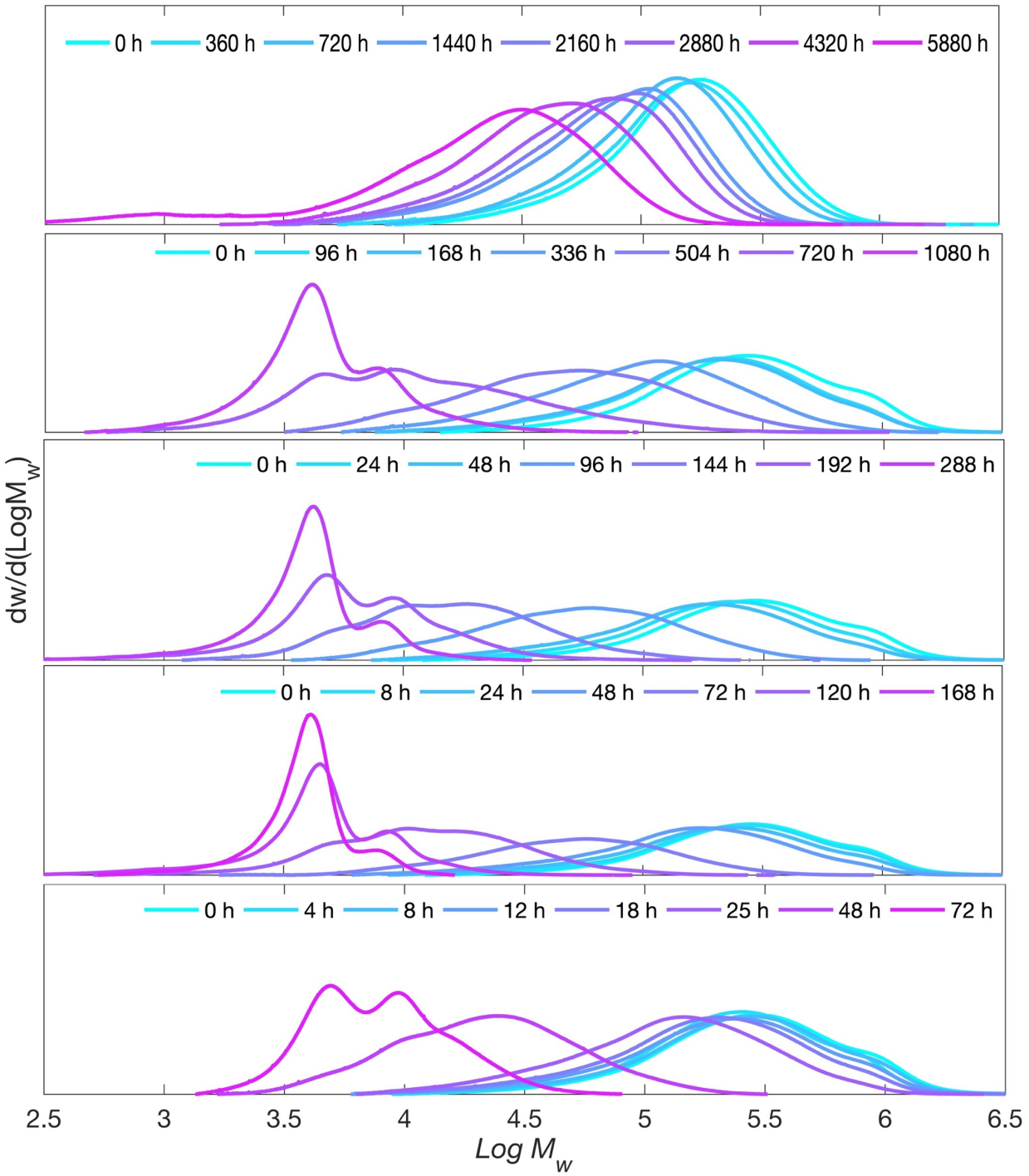


**Figure 4.24** MWD of PLA–Cex film during hydrolytic degradation in water at (a) 40, (b) 60, (c) 75, (d) 85, and (e) 95 °C

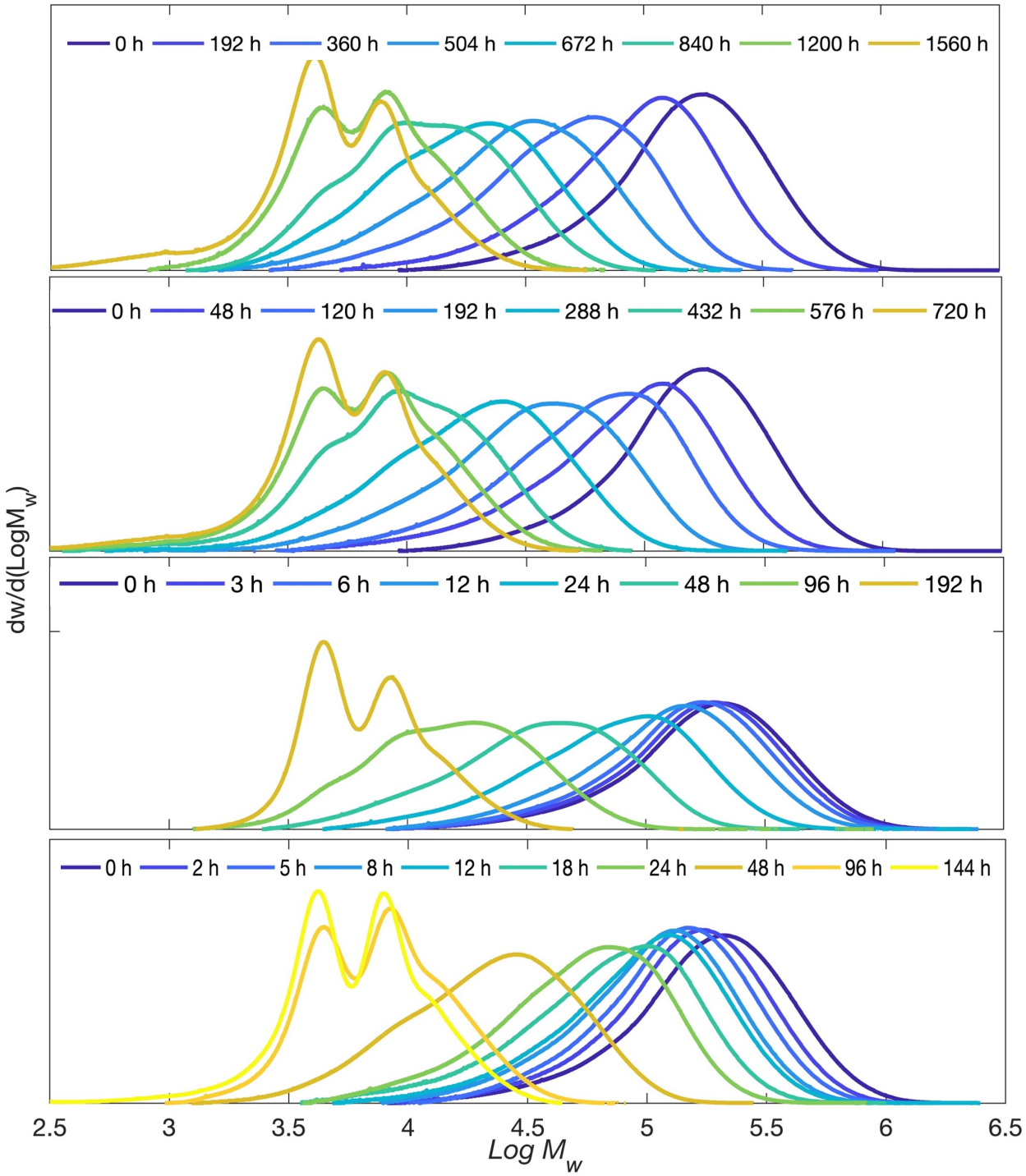


**Figure 4.25** MWD of PLA–Con film during hydrolytic degradation in 50% ethanol at (a) 50, (b) 60, (c) 75, and (d) 85 °C

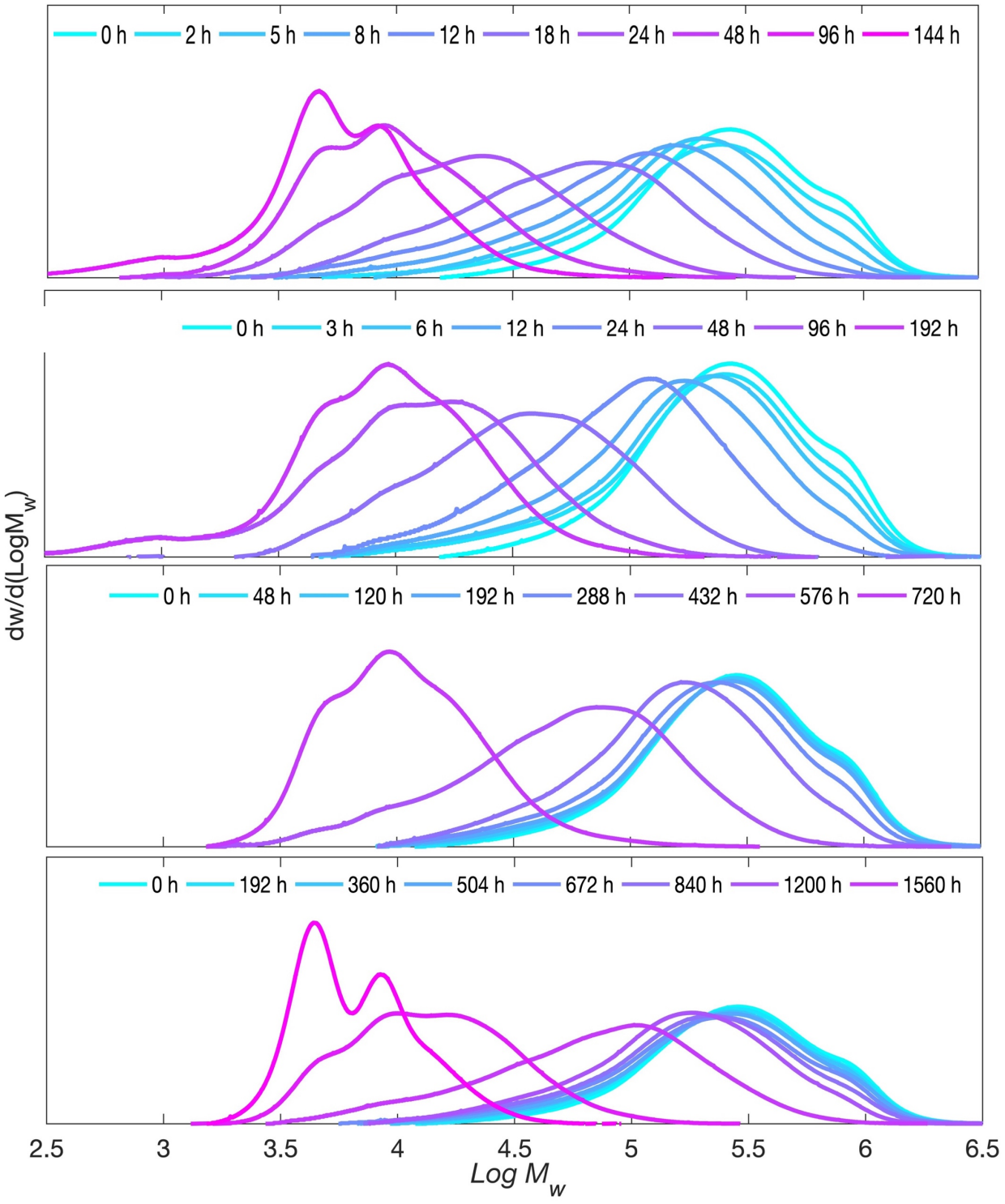


**Figure 4.26** MWD of PLA–Cex film during hydrolytic degradation in 50% ethanol at (a) 50, (b) 60, (c) 75, and (d) 85 °C

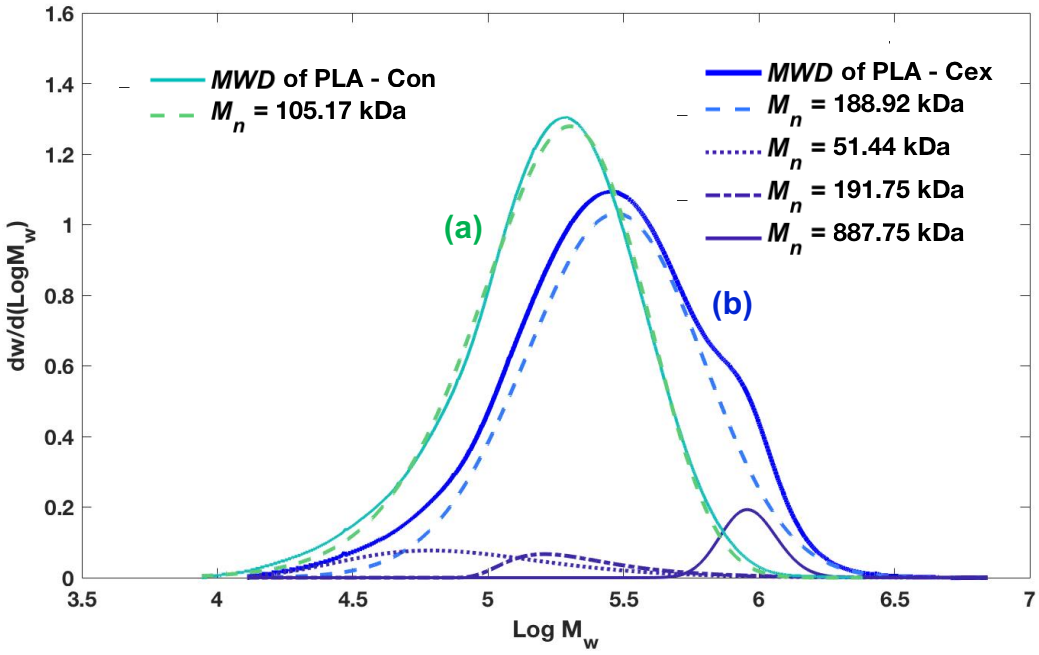


**Figure 4.27** The initial MWD and deconvolution of MWD of (a) PLA–Con and (b) PLA - Cex before the hydrolytic degradation

**Figures 4.28** and **4.29** show examples of deconvolution of MWD series of PLA–Con and PLA–Cex films during hydrolytic degradation in water at 60°C. The MWD of PLA–Con films after hydrolytic degradation at 0 and 96 h could be considered close to a normal distribution curve, so that only one main peak was obtained from the deconvolution. Later after the hydrolytic degradation proceeded, distortion from the symmetrical curve was observed and it developed into a multi-modal distribution. The deconvolution of MWD curves of PLA after 168 h was needed to determine the subpopulations of PLA chains shown in **Figure 4.28b – f**. For PLA–Cex films, the deconvolution of MWD curves was used to determine the molecular weight of subpopulations since the beginning of the degradation shown in **Figures 4.27** and **4.29**. Furthermore, the series of MWD indicate that the distribution profiles of PLA–Cex at all temperatures moved to the lower $M_n$ slower than the ones of PLA–Con. Therefore, it can be preliminarily concluded that the chain extender effects on delaying the hydrolytic degradation of PLA films.

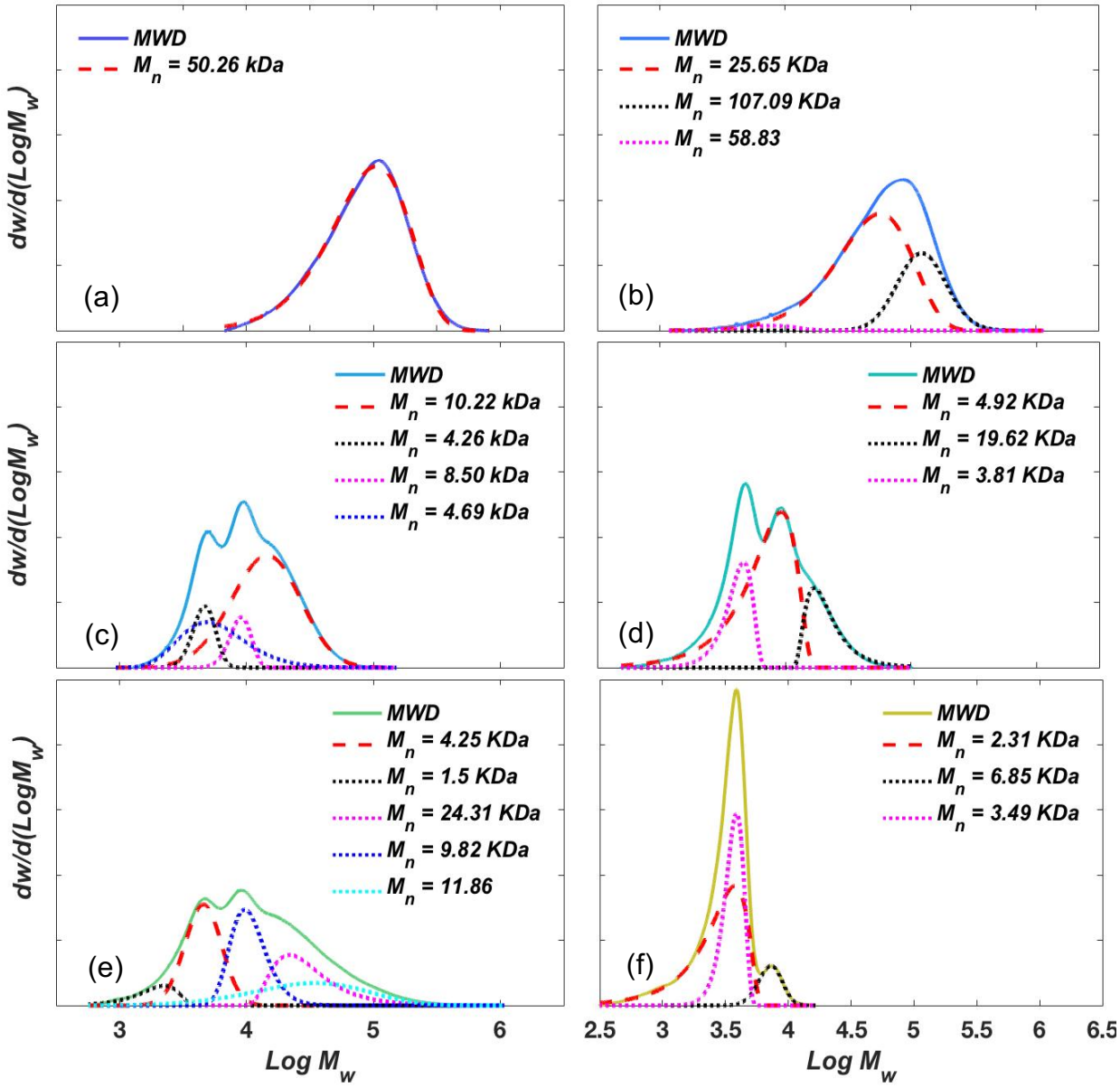


**Figure 4.28** Deconvolution of MWD of PLA–Con films during the hydrolytic degradation in water at 60°C:(a) 96 h, (b) 168 h, (c) 336 h, (d) 504 h, (e) 720 h, and (f) 1080 h. ( — ) Lines represent the MWD curves obtained from GPC, (---) lines correspond the main peak fitting, and (…) lines represent the other fitted curves with smaller peak area.

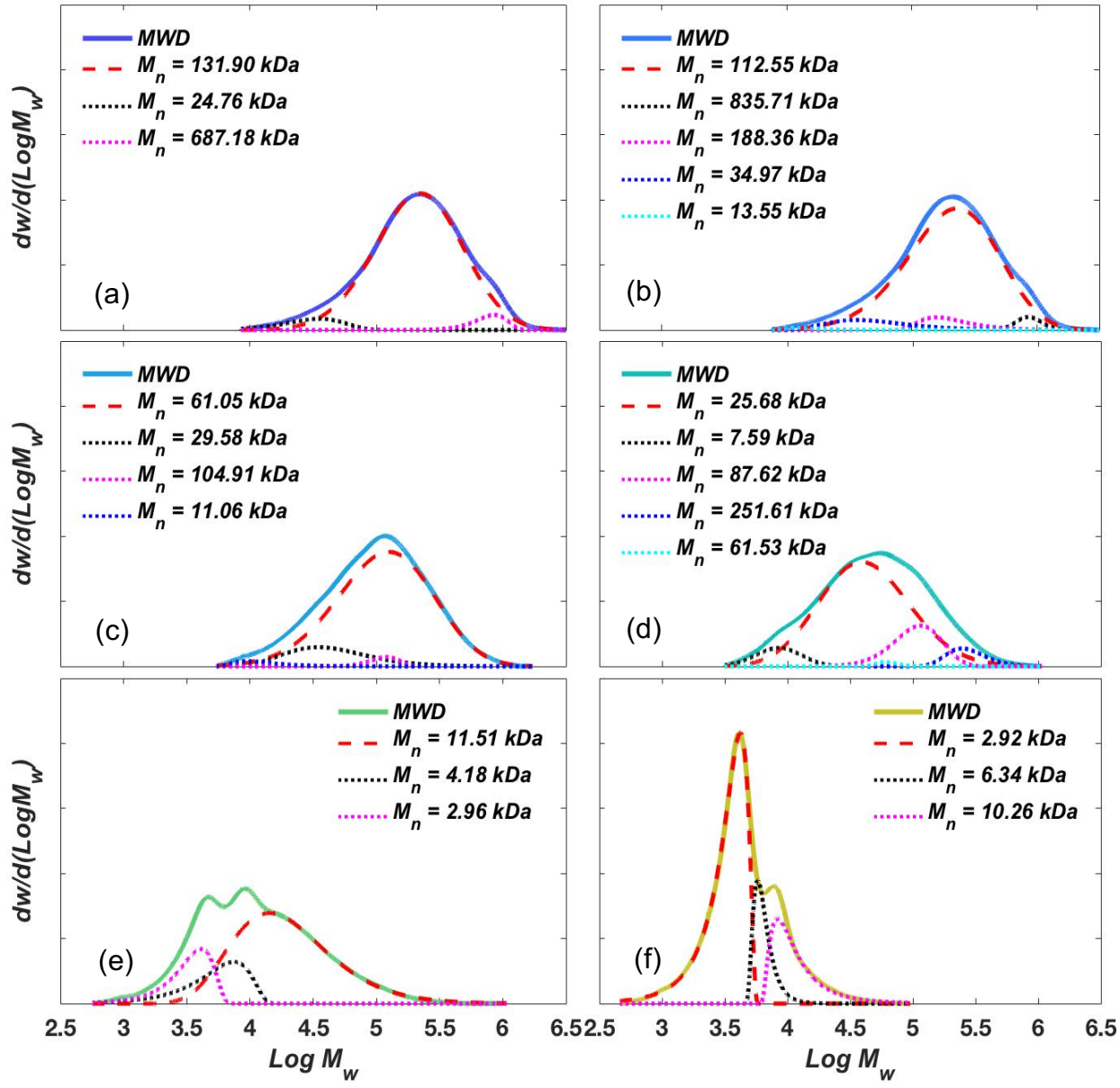


**Figure 4.29** Deconvolution of MWD of PLA - Cex films during the hydrolytic degradation in water at 60 °C:(a) 96 h, (b) 168 h, (c) 336 h, (d) 504 h, (e) 720 h, and (f) 1080 h. (—) Lines represent the MWD curves obtained from GPC, (---) lines correspond the main peak fitting, and (…) lines represent the other fitted curves with smaller peak area.

### 4.4.3 Hydrolytic degradation study of modified PLA–Cex

#### 4.4.3.1 Molecular weight variation and estimation of the rate constant of hydrolysis using first order reaction

$M_n$ values of PLA during hydrolytic degradation were obtained from the main peak of the deconvolution of MWDs. To predict the pathway of the hydrolysis of PLA, a first order fitting was used to establish the relationship of $M_n$ as a function of hydrolysis time. **Figures 4.30–4.31** show the reduction of $M_n$ of PLA–Con and PLA–Cex over hydrolysis time in water at 40, 60, 75, 85 and 95 °C and in 50% ethanol at 50, 60, 75 and 85 °C, respectively. Temperature obviously showed a significant effect on the reduction of $M_n$. For the hydrolytic degradation at 40 °C in water, PLA–Con film of molecular weight of approximately 106 kDa slowly degraded to 12 kDa and PLA–Cex degraded from 190 kDa to 28 kDa after 245 days. At the highest temperature condition of 95 °C, the $M_n$ of PLA–Con and PLA–Cex were entirely degraded to around 3 kDa and 9 kDa after 72 hours. This indicates that the higher the temperature, the faster the degradation. Meanwhile, the comparison of pathways between PLA–Con and PLA–Cex of each temperature is shown in **Figures 4.32–4.33.** The chain extender has a significant effect on increasing the initial $M_n$ of PLA–Cex. Moreover, the $M_n$ values of PLA–Cex at the middle stages of the hydrolytic degradation process were higher than ones of PLA–Con. However, at the terminal stage of the hydrolytic reaction, the $M_n$ values of PLA–Cex and PLA–Con tend to level off beyond approximately 3-5 kDa at which PLA molecules became soluble in water.

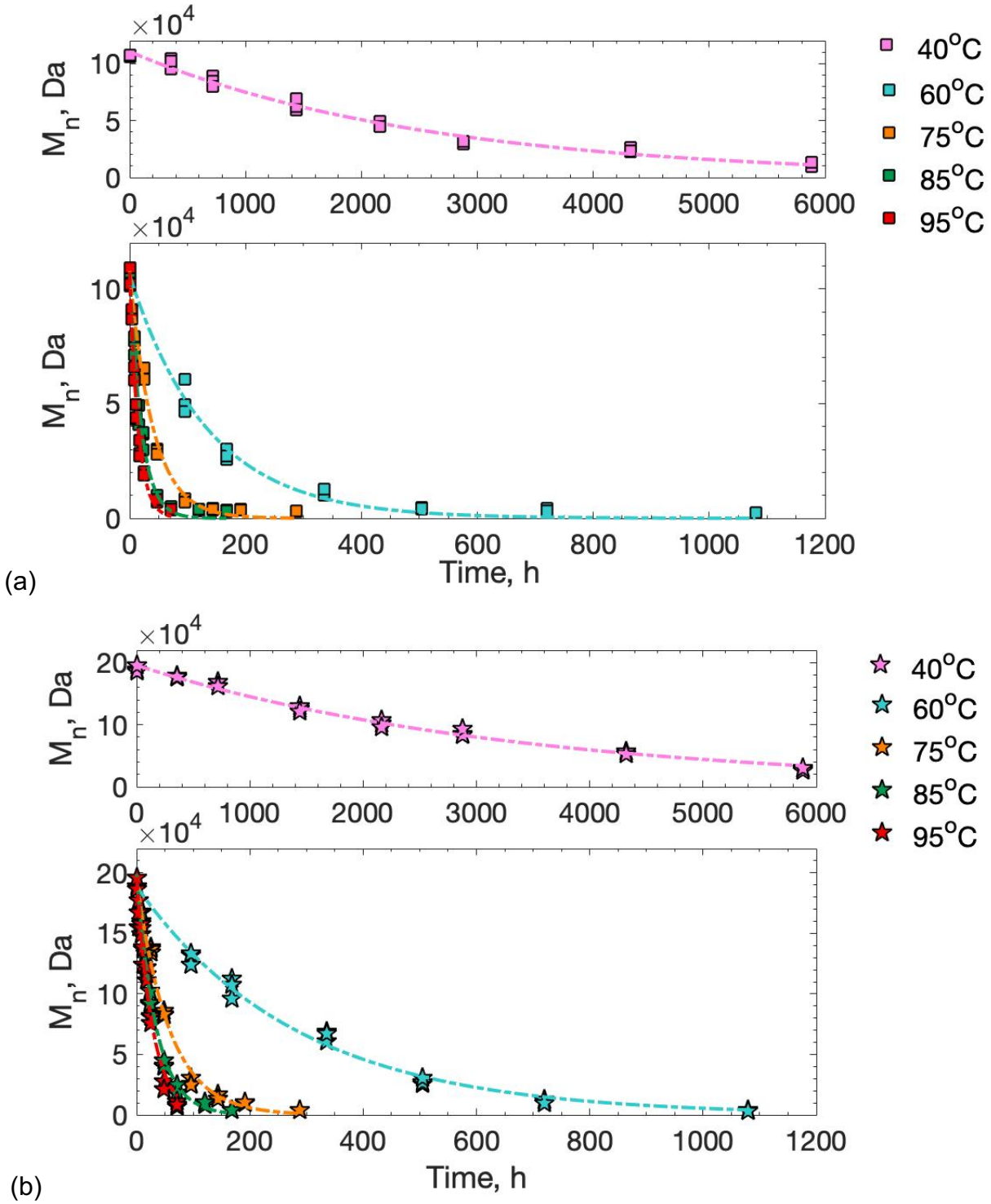


**Figure 4.30** $M_n$ as a function of time during hydrolytic degradation in water at 40, 60, 75, 85, and 95 °C: (a) PLA–Con and (b) PLA–Cex

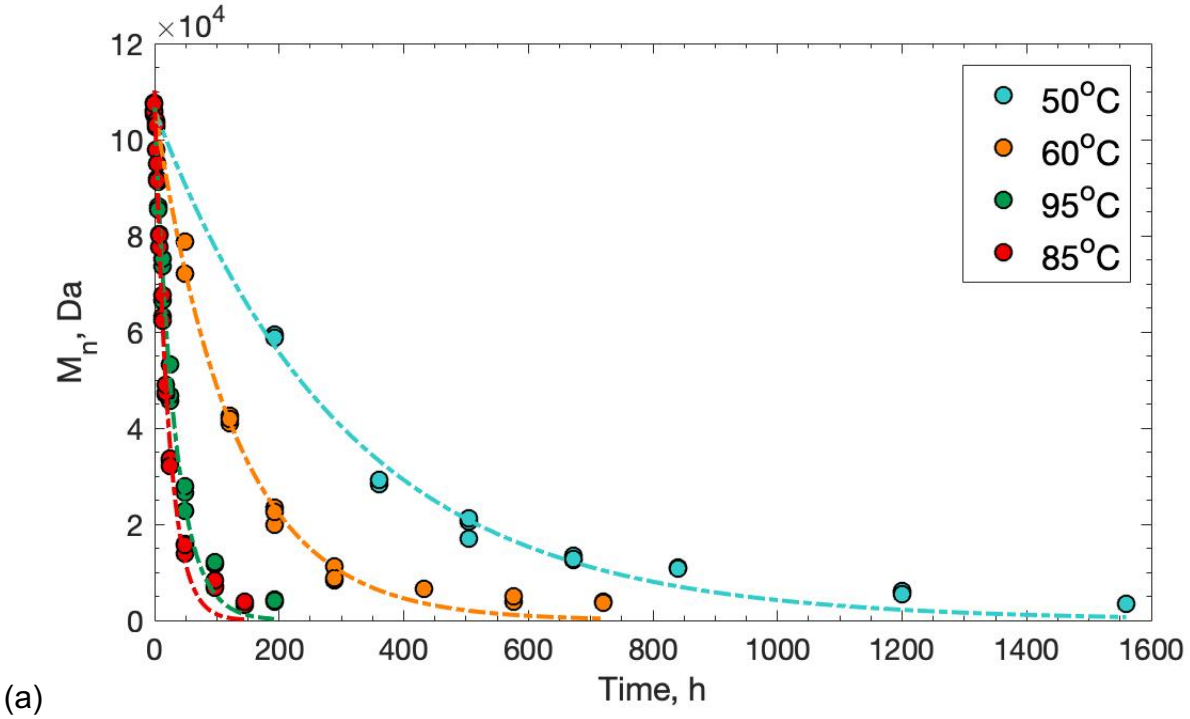


(a)

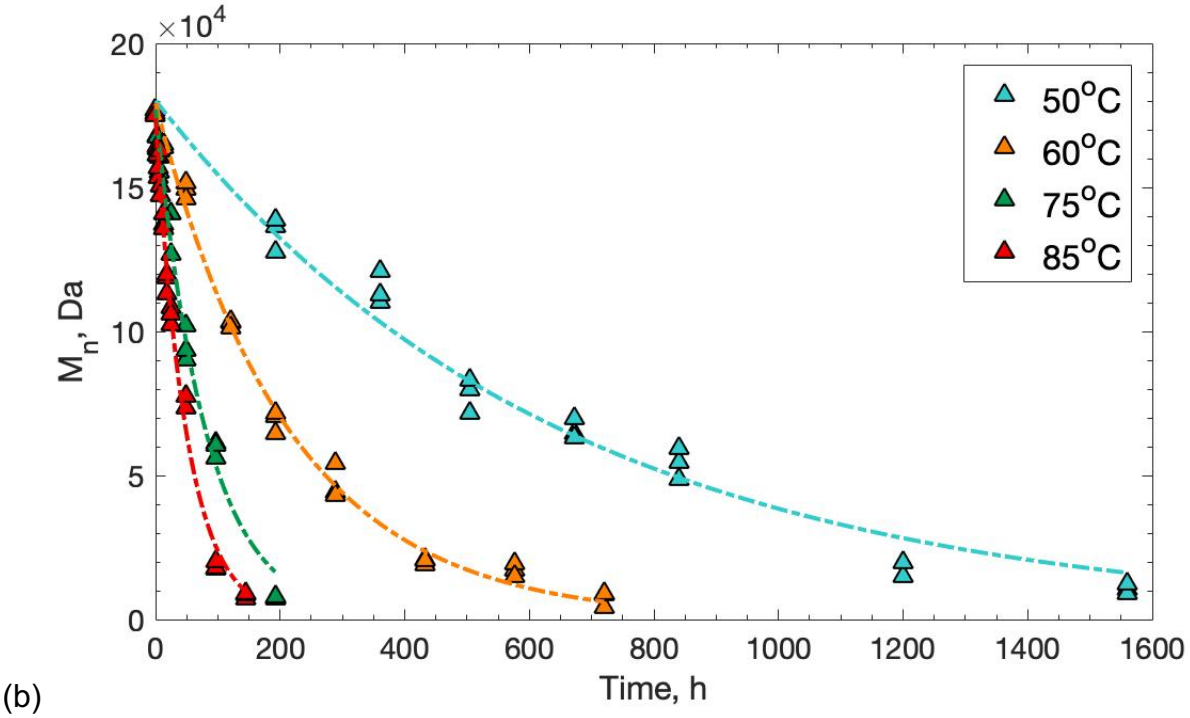


(b)

**Figure 4.31** $M_n$ as a function of time during hydrolytic degradation in 50% ethanol at 50, 60, 75, and 85 °C: (a) PLA–Con and (b) PLA–Cex

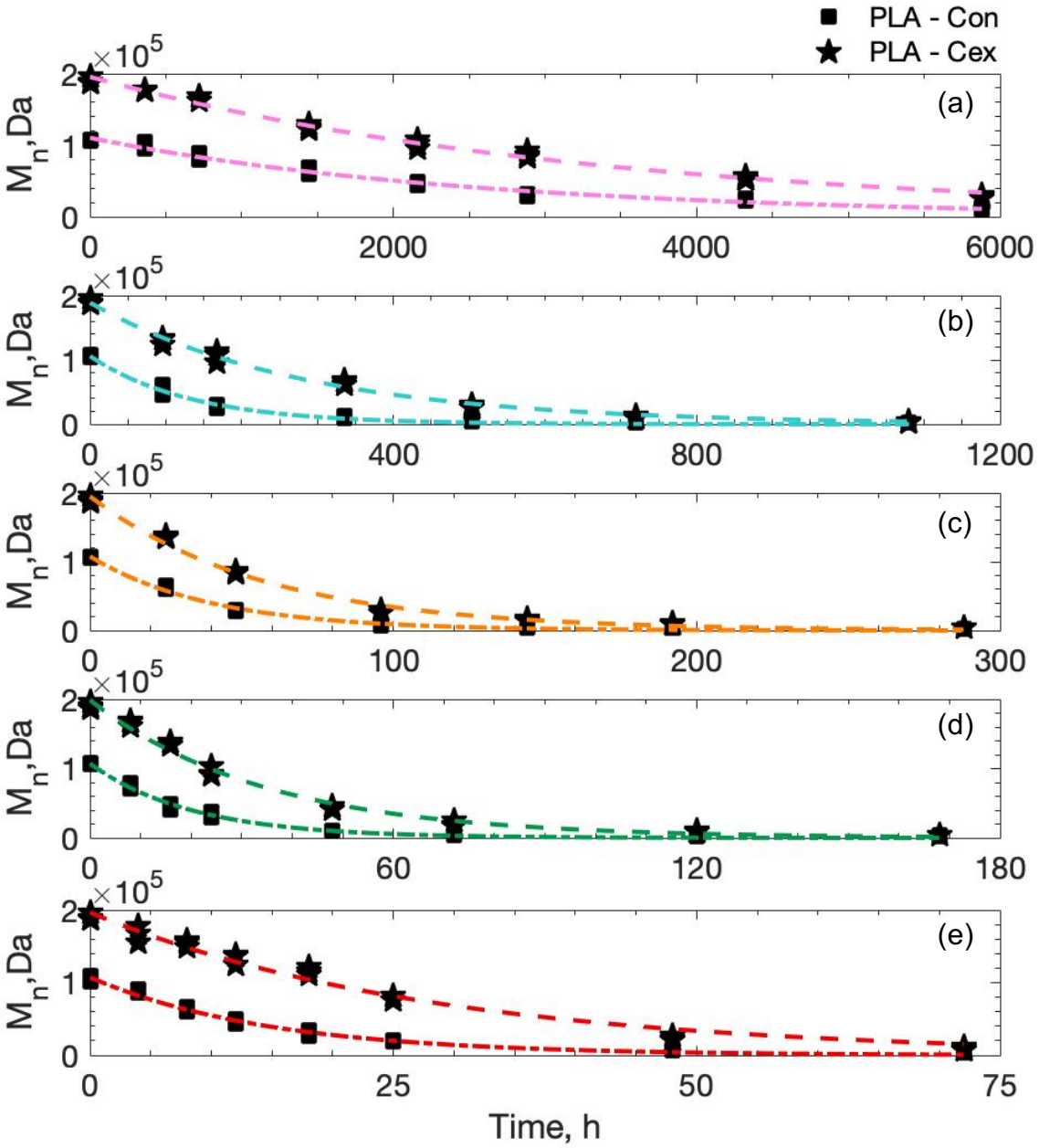


**Figure 4.32** Comparison of $M_n$ as a function of time during hydrolytic degradation of PLA–Con and PLA–Cex in water at (a) 40, (b) 60, (c) 75, (d) 85, and (e) 95 °C

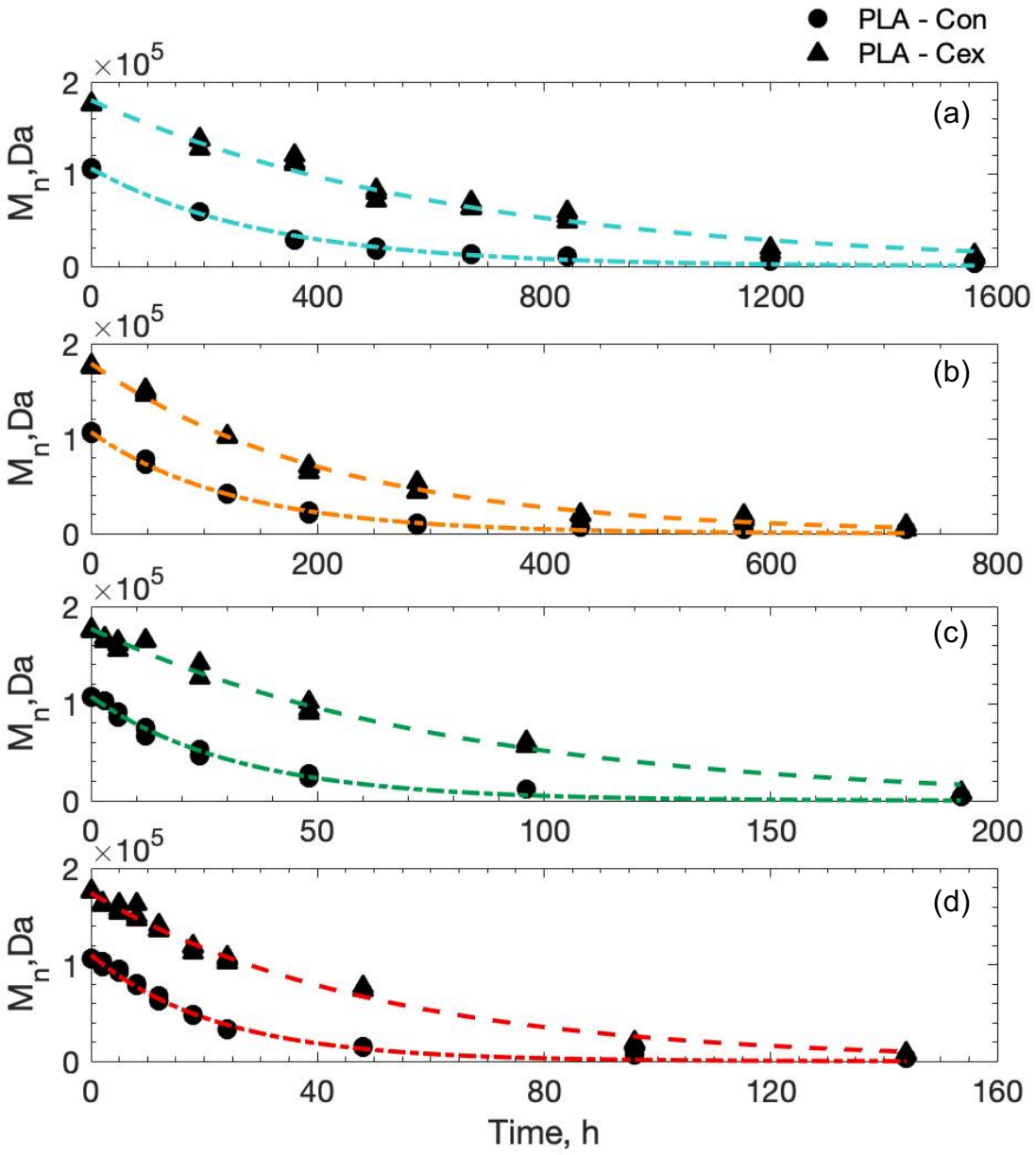


**Figure 4.33** Comparison of $M_n$ as a function of time during hydrolytic degradation of PLA–Con and PLA–Cex in 50% ethanol at (a) 50, (b) 60, (c) 75, and (d) 85°C

**Table 4.13** shows the rate constants calculated using the first order reaction equation (**Eq. 3.8**). The rate of hydrolytic degradation ($k_{1st}$, $h^{-1}$) of PLA–Cex was lower than that of PLA–Con at all temperatures. The presence of chain extender in the PLA matrix significantly enhanced PLA's stability during the hydrolytic degradation. Additionally, the $k_{1st}$ values of the two materials increased with increasing temperature. The $k_{1st}$ value of hydrolysis at the temperature of 60, 75 and 85 °C were used to compare the effect of the media. The hydrolysis of PLA–Con in 50% ethanol at 60 and 75 °C were faster than in contact with water, but they were not significantly different when exposed in water at 85 °C. While the fragment hydrolysis of PLA–Cex in 50% ethanol was faster only at 60 °C, but significantly slower at 75 and 85 °C. **Figure 4.34** shows $k_{1st}$ values of PLA–Con and PLA–Cex in both types of media increased exponentially with increasing temperature. The $k_{1st}$ values of PLA–Cex were lower than ones of PLA–Con in all temperature conditions.

**Table 4.12** Rate constant ($k_{1st}$, $h^{-1}$) of hydrolytic degradation of PLA–Con and PLA–Cex in water and 50% ethanol

| Temp | Water | | 50% Ethanol | |
|---|---|---|---|---|
| (°C) | PLA - Con | PLA - Cex | PLA - Con | PLA - Cex |
| 40 | 0.00039± 0.00001$^{Aa}$ | 0.00030±0.000 01$^{Ab}$ | - | |
| 50 | - | | 0.0032±0.0001 $^{Aa}$ | 0.0015± 0.0001$^{Ab}$ |
| 60 | 0.0075±0.0003 $^{Bb}$ | 0.0035±0.0001 $^{Bd}$ | 0.0081±0.0002 $^{Ba}$ | 0.0047±0.0001 $^{Bc}$ |
| 75 | 0.0249±0.0009 $^{Cb}$ | 0.0175±0.0004 $^{Cc}$ | 0.0307±0.0015 $^{Ca}$ | 0.0129±0.000 7$^{Cd}$ |
| 85 | 0.0470±0.00 20$^{Da}$ | 0.0290±0.001 2$^{Db}$ | 0.0452± 0.0016$^{Da}$ | 0.0209± 0.0009$^{Dc}$ |
| 95 | 0.0673±0.0029 $^{Ea}$ | 0.0353±0.0017 $^{Eb}$ | - | |

The values within a column followed by the same uppercase letters and the values within a row followed by the same lowercase letters are not significantly different ($\alpha$=0.05).

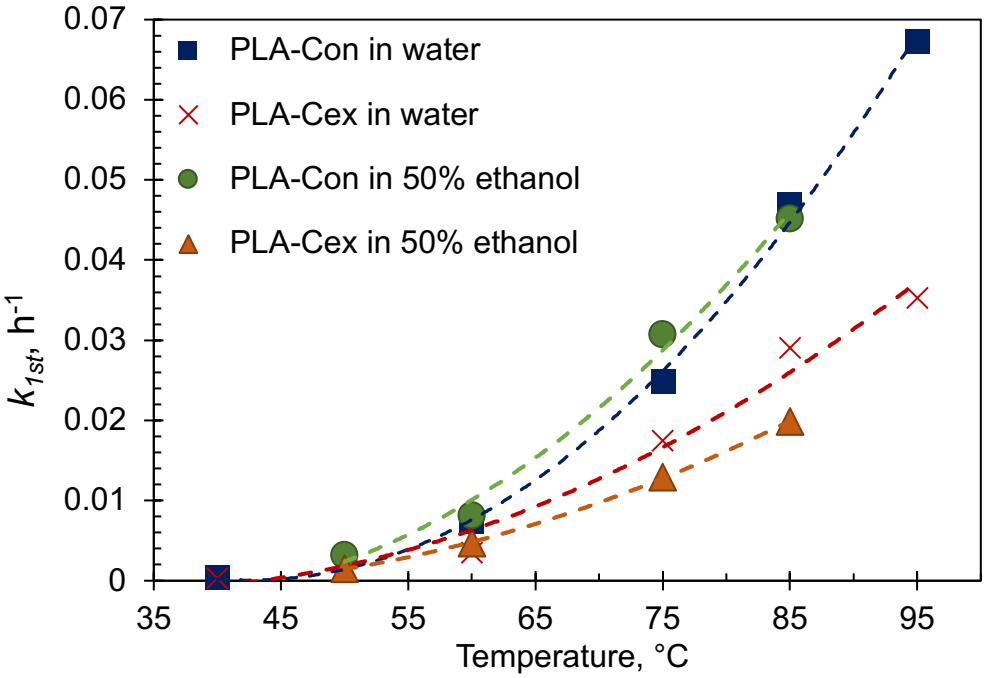


**Figure 4.34** Rate constant ($k_{1st}$) of hydrolytic degradation of PLA–Con and PLA–Cex in water and 50% ethanol as a function of temperature

The first order reaction has been acceptable for modeling kinetic mechanism for Polyester hydrolysis [22]. However, it was assumed that the concentration of the ester bonds remains constant throughout the hydrolytic experiment. In fact, the semi-crystalline polymer matrix is composed of the crystalline and amorphous phases. As the chain scission reaction proceeded, the amorphous phase with higher mobility can rearrange and form into crystallites. Moreover, in the amorphous phase, there is a combination of the different size of molecules as identified from the molecular weight distribution. The long polymeric chains are hydrolyzed to shorter chains and finally to soluble oligomers. Thus, the concentration of ester bonds available for hydrolysis decreases with an increase in the degradation time. Therefore, in order to have a better understanding, the hydrolytic degradation model has to be modified by considering the change in the concentration of ester bonds.

#### 4.4.3.2 Molecular weight variation and estimation of the rate constant of hydrolysis using a reference model for hydrolytic degradation

The result obtained from the hydrolytic degradation was determined using the mathematical model proposed by Pan [23]. The simplified hydrolytic degradation model shown in **Eq. (3.9)–(3.10)** was used to determine the rate constant for the auto-catalytic degradation. **Table 4.13** shows the parameters used to fit the model.

**Table 4.13** Parameters used in the model to fit the experimental data

| Material parameters* | | |
|---|---|---|
| $\rho_{PLA}$ | (g $cm^{-3}$) | 1.24 |
| $\rho_{Crystal}$ | (g $cm^{-3}$) | 1.36 |
| $X_{c_0}$ | - | 0.01 |
| $C_{E_0}$ | (mol $m^{-3}$) | $1.72\times10^{4}$ |
| $\omega$ | (mol $m^{-3}$) | $1.89\times10^{4}$ |
| $C_{ol_0}$ | (mol $m^{-3}$) | $C_{E_0}\times10^{-12}$ |
| $\alpha$ | - | 0.4 |
| $\beta$ | - | 1 |
| $m$ | - | 4 |
| $n$ | - | 0.5 |

*Note*: See **Section 3.2.9** for the description of each parameter.

**Figures 4.35–4.42** show the examples of the variation in polymer chains during the hydrolytic degradation of PLA–Con and PLA–Cex in water and 50% ethanol at 60 °C obtained from the reference model. During the hydrolytic degradation, the reduction of $M_n$ and the increase in $X_c$ of PLA film were tracked over hydrolysis time. The $M_n$ was expressed in the normalized form while the change in $X_c$ was estimated by the Avrami equation. **Figure 4.35** shows the fitting between the model and variation of $M_n$ and $X_c$ of PLA–Con immersed in water. The crystals, which were formed and gradually grew, were assumed to not be subject to hydrolysis. For the amorphous phase, which can be degraded and crystallized, it can be separated into two constituents, the long molecular chains and the short molecular chains. As the chain scission proceeded, the total number of ester units of the long chains ($C_E$) decreased, while the total number of ester units of the short chains ($C_{ol}$) increased as shown in **Figure 4.36**. **Figures 4.37** and **4.38** show the fitting between the model and variation of $M_n$ and $X_c$ of PLA–Cex and the prediction of the $C_E$ and $C_{ol}$ of PLA–Cex at the same condition, which illustrates the different number of ester units and the total number of chain scissions, respectively. For the hydrolysis of PLA–Con the $C_E$ dropped below zero before the final stage of the experiment. This phenomenon indicates that part of a crystalline region was dissolved and degraded at the late stage of hydrolysis [24]. The total number of chain scissions was stable at the late stage of the experiment. For the hydrolysis of PLA–Cex, the final $C_E$ decreased, while the $C_{ol}$ increased to approximately 4 kmol/m$^3$, and the chain scission substantially proceeded after 45 days. For the hydrolysis in 50% ethanol, **Figures 4.39** and **4.41** show the variation of $M_n$ and $X_c$ with the model prediction, while **Figures 4.40** and **4.42** show the prediction of the $C_E$ and $C_{ol}$ during the hydrolysis of PLA–Con and PLA–Cex, respectively. Similar results were observed from the samples immersed in 50% ethanol, but they occurred in shorter periods of hydrolysis time.

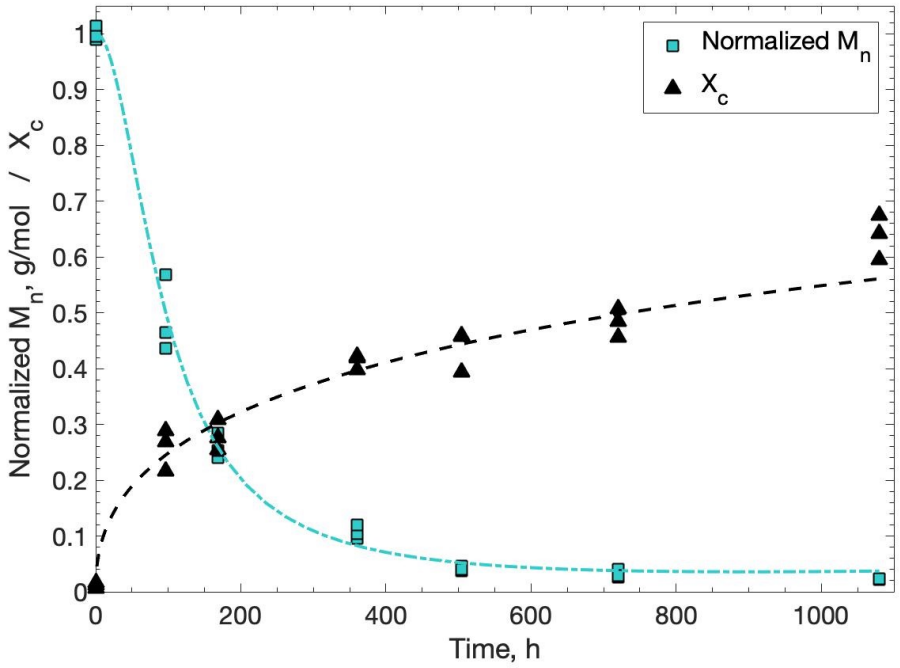


**Figure 4.35** The normalized $M_n$ and $X_c$ of PLA–Con during the hydrolytic degradation in water at 60 °C

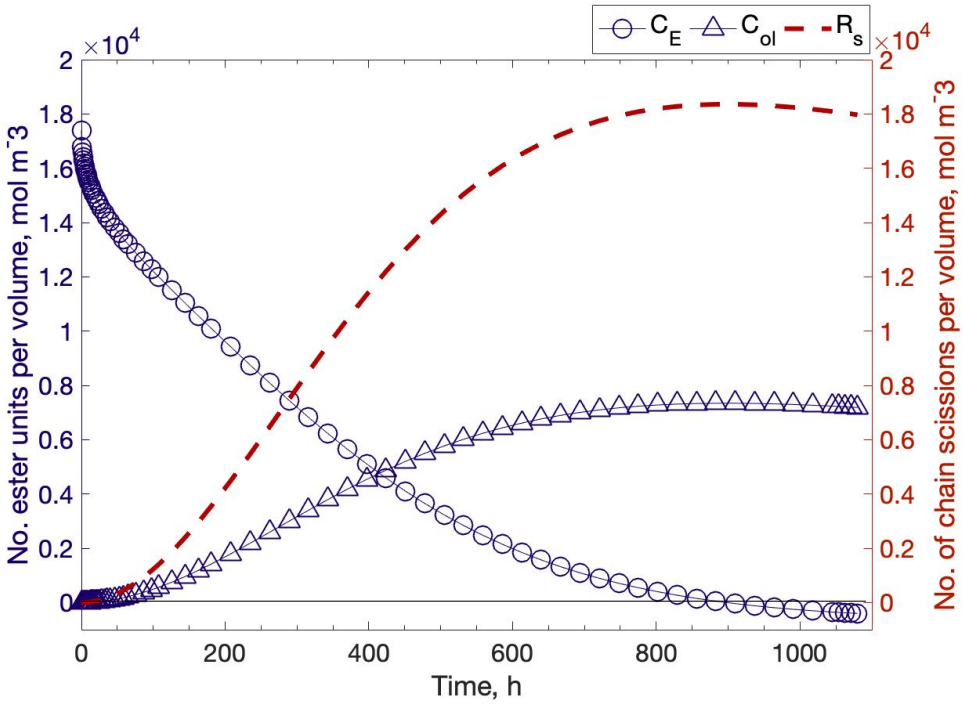


**Figure 4.36** Number of total ester units of all the polymer chains, long and short chains, and the total number of chain scissions of PLA–Con per unit volume during the hydrolytic degradation in water at 60 °C : (○, △) symbols correspond the $C_E$ and $C_{ol}$ and (– – –) line represents the $R_s$.

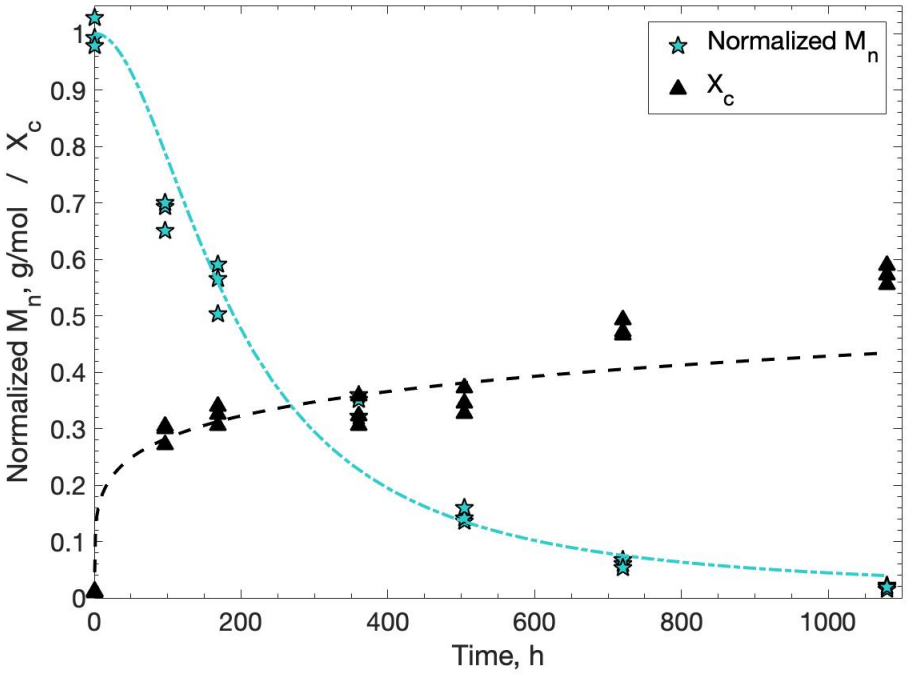


**Figure 4.37** The normalized $M_n$ and $X_c$ of PLA–Cex during the hydrolytic degradation in water at 60 °C

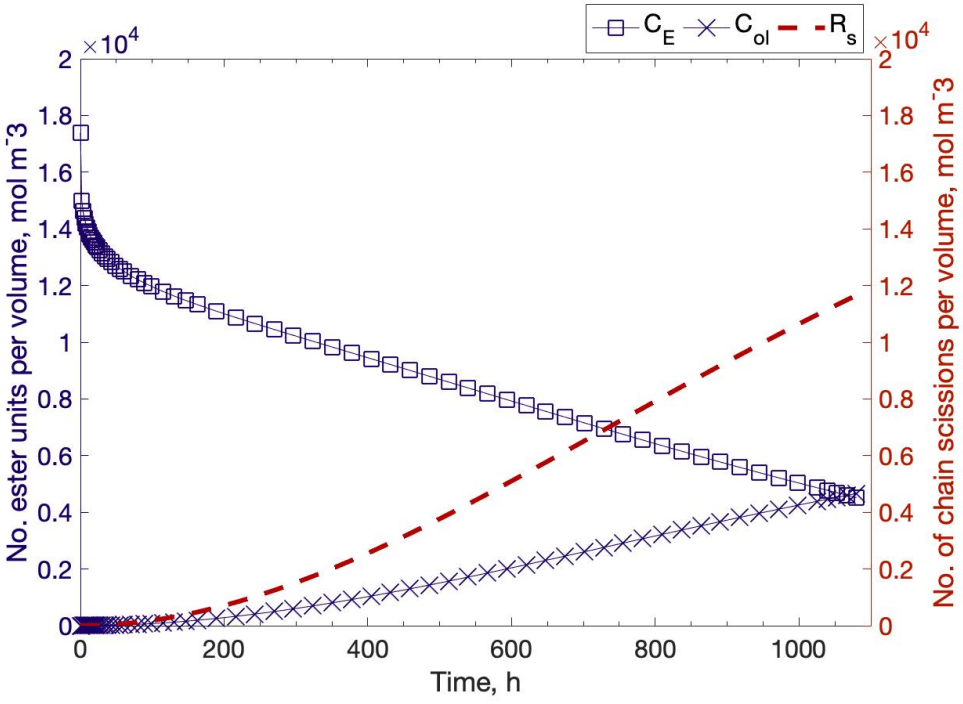


**Figure 4.38** Number of total ester units of all the polymer chains, long and short chains, and the total number of chain scissions of PLA–Cex per unit volume during the hydrolytic degradation in water at 60 °C : (⊟, ✕) symbols correspond the $C_E$ and $C_{ol}$ and (– – –) line represents the $R_s$

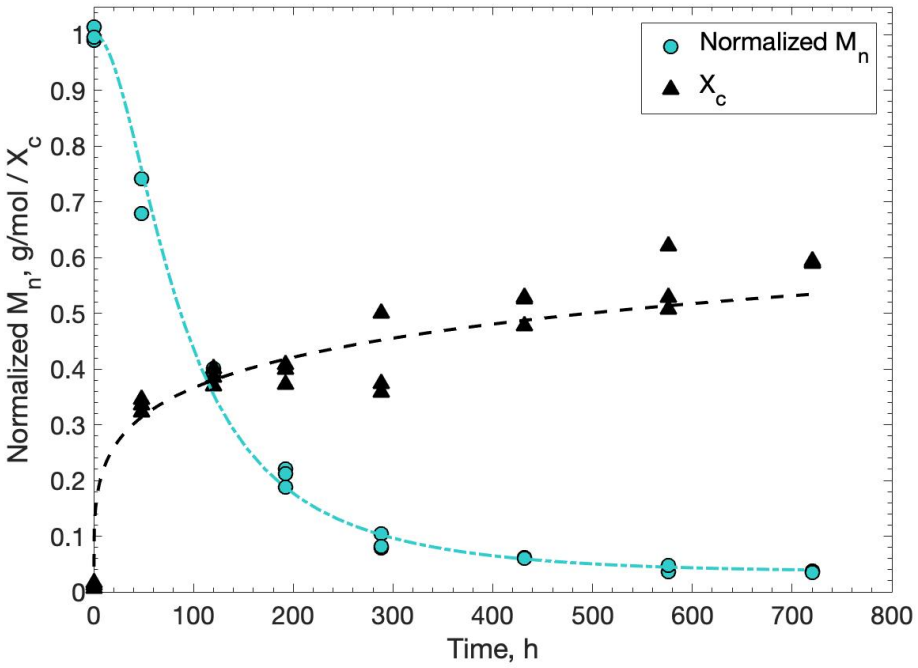


**Figure 4.39** The normalized $M_n$ and $X_c$ of PLA–Con during the hydrolytic degradation in 50% ethanol at 60 °C

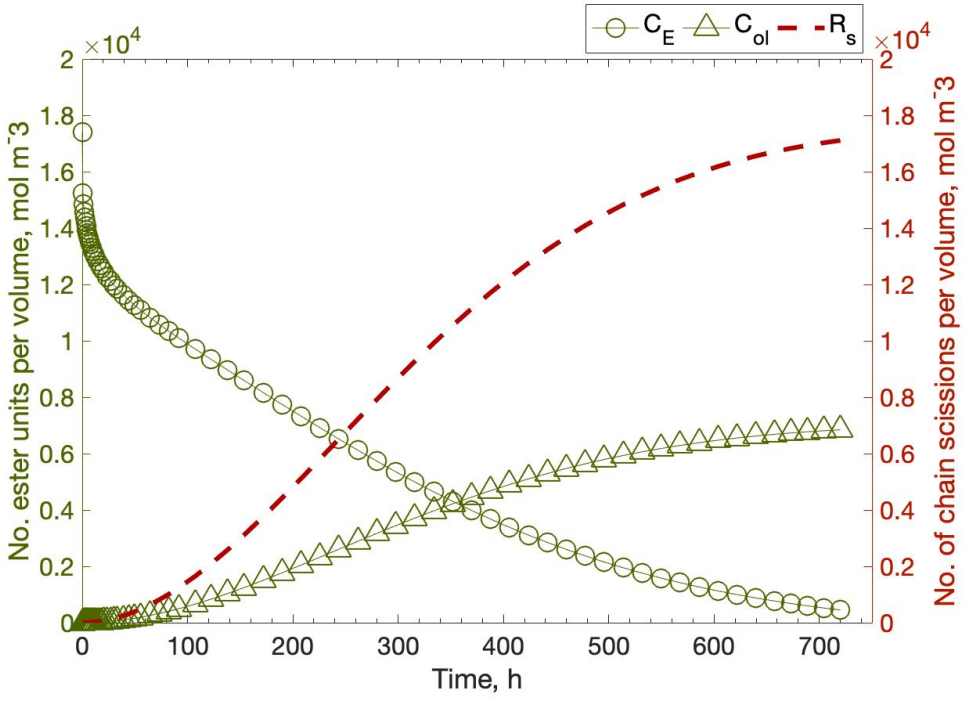


**Figure 4.40** Number of total ester units of all the polymer chains, long and short chains, and the total number of chain scissions of PLA–Con per unit volume during the hydrolytic degradation in 50% ethanol at 60 °C:(○, △) symbols correspond the $C_E$ and $C_{ol}$ and (– – –) line represents the $R_s$

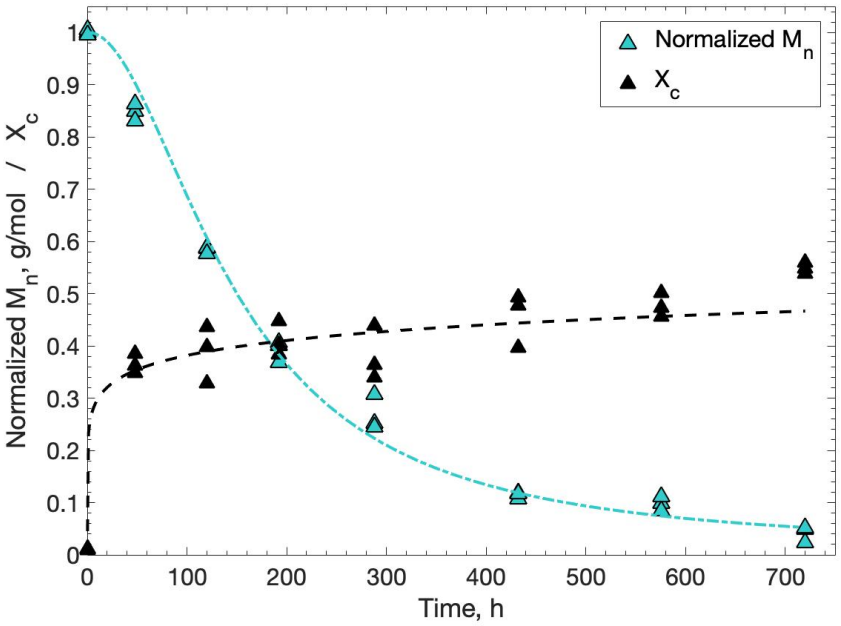


**Figure 4.41** The normalized $M_n$ and $X_c$ of PLA–Cex during the hydrolytic degradation in 50% ethanol at 60 °C

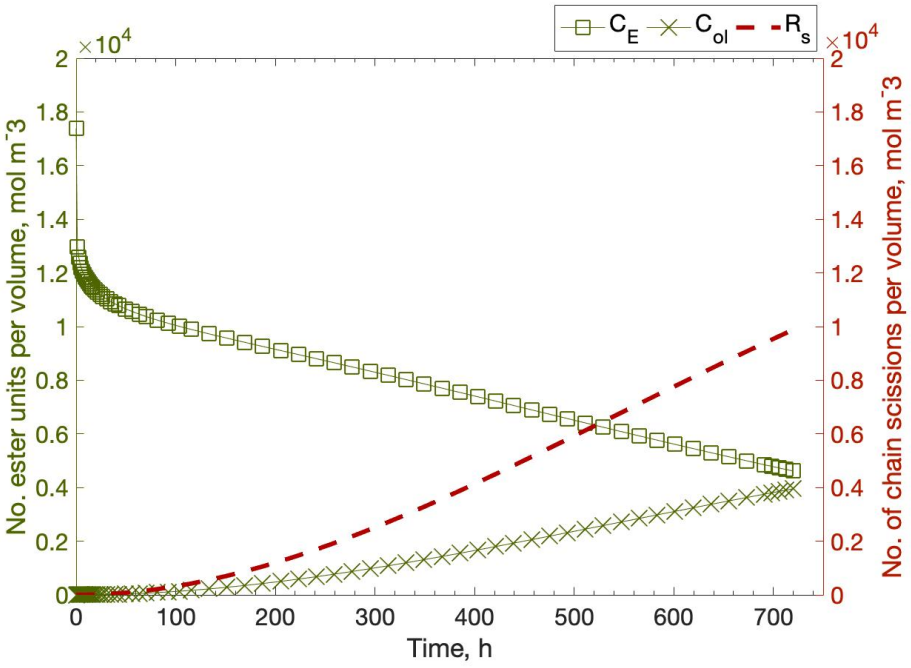


**Figure 4.42** Number of total ester units of all the polymer chains, long and short chains, and the total number of chain scissions of PLA–Cex per unit volume during the hydrolytic degradation in 50% ethanol at 60 °C:( (⊟,X) symbols correspond the $C_E$ and $C_{ol}$ and (– – – ) line represents the $R_s$

The comparison between the model and experimental data for normalized $M_n$ of PLA of different hydrolysis temperatures in water and 50% ethanol are shown in **Figures 4.43** and **4.44.** The model fit with the experimental data of $M_n$ obtained during the hydrolysis process by considering the chain scission-induced crystallization and the transition from the long molecules to the short chains. The estimated $k_{deg}$ in the unit of molar concentration per unit of time (mol $m^{-3}$ $h^{-1}$) obtained from the degradation model was converted to $\bar{k}_{deg}$ with a simple rate constant unit of $h^{-1}$ and shown in **Table 4.14**. The $\bar{k}_{deg}$ obtained from this model was compared to the one obtained from $k_{1st}$ of the first order reaction model. In one sense, the result from both models could be interpreted in the same aspect that the temperature was one of the major factors in hydrolytic degradation. The PLA–Cex had a significant effect of decreasing the hydrolytic degradation process at a variety of temperatures. In this study, the characterization of chain morphology has not been investigated; however, it can be expected that the multifunctional epoxy chain extender could lead to a higher degree of branching and increase the molecular weight. For the lower molecular weight molecules, they have a higher number of chains and also more chain ends, which increase the rate of end scission, accordingly, generating more monomers. Moreover, the epoxide-reactive group preferentially reacts with the carboxylic end. The modified PLA, therefore, has hydroxy free ends, which do not affect the autocatalytic degradation. The influence of hydrolytic media between water and 50% ethanol in the hydrolysis of PLA–Con was shown in a decrease in the $T_g$ which affected the higher sorption of water in the 50% ethanol [19,25]. At low temperature, the hydrolysis in ethanol was faster than water. However, when PLA–Con was exposed to higher temperature, in this case at 85 °C, the effect of sorption became less significant. The $T_g$ after immersion in 50% ethanol of PLA–Cex which was found slightly lower that one of water affected on increase in the rate at the only low temperature of 60 °C.

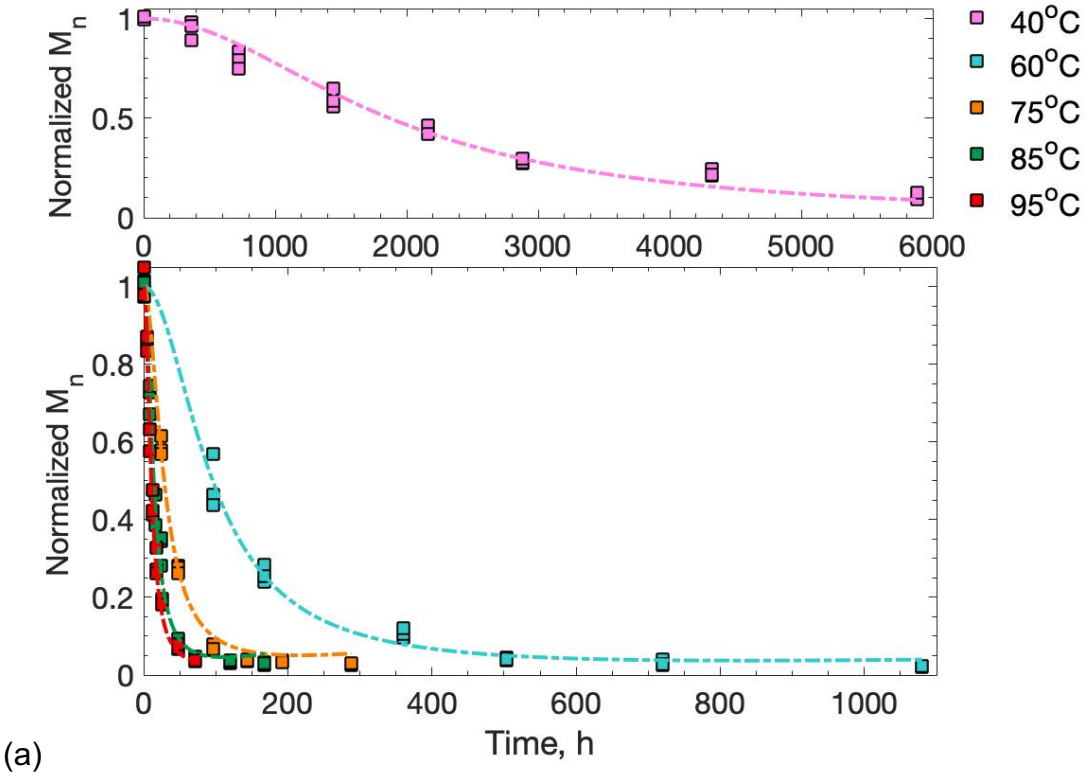


(a)

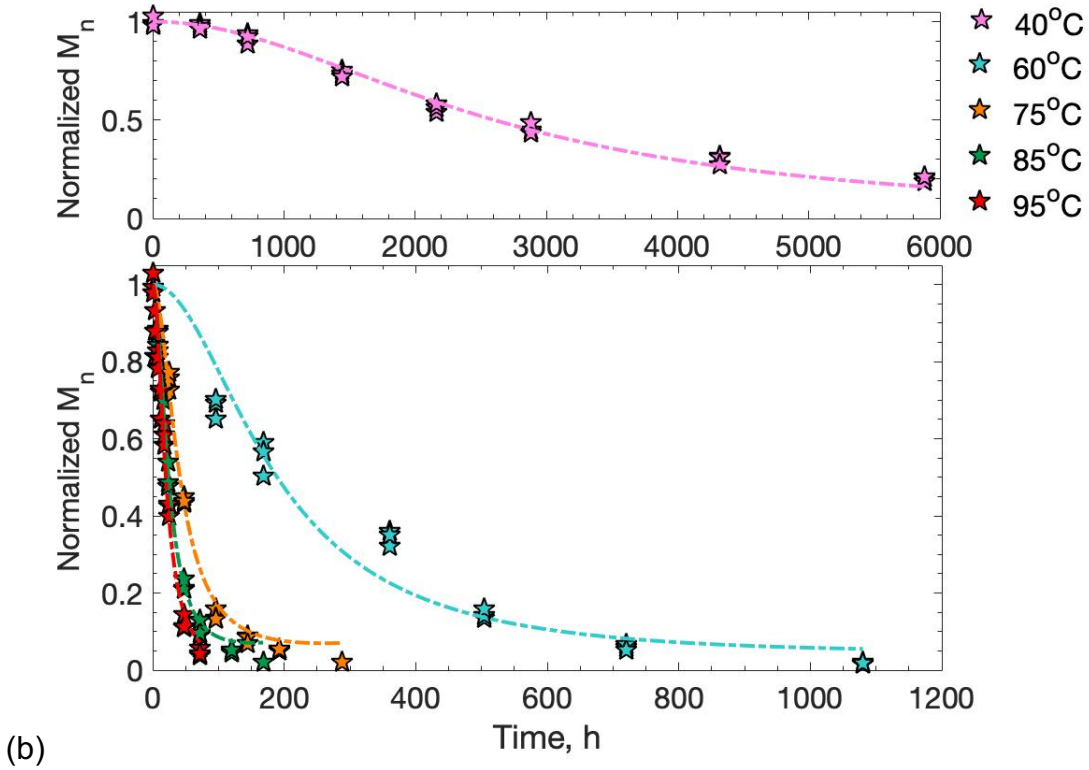


(b)

**Figure 4.43** Normalized $M_n$ as a function of time during hydrolytic degradation in water at 40, 60, 75, 85, and 95 °C: (a) PLA–Con and (b) PLA–Cex

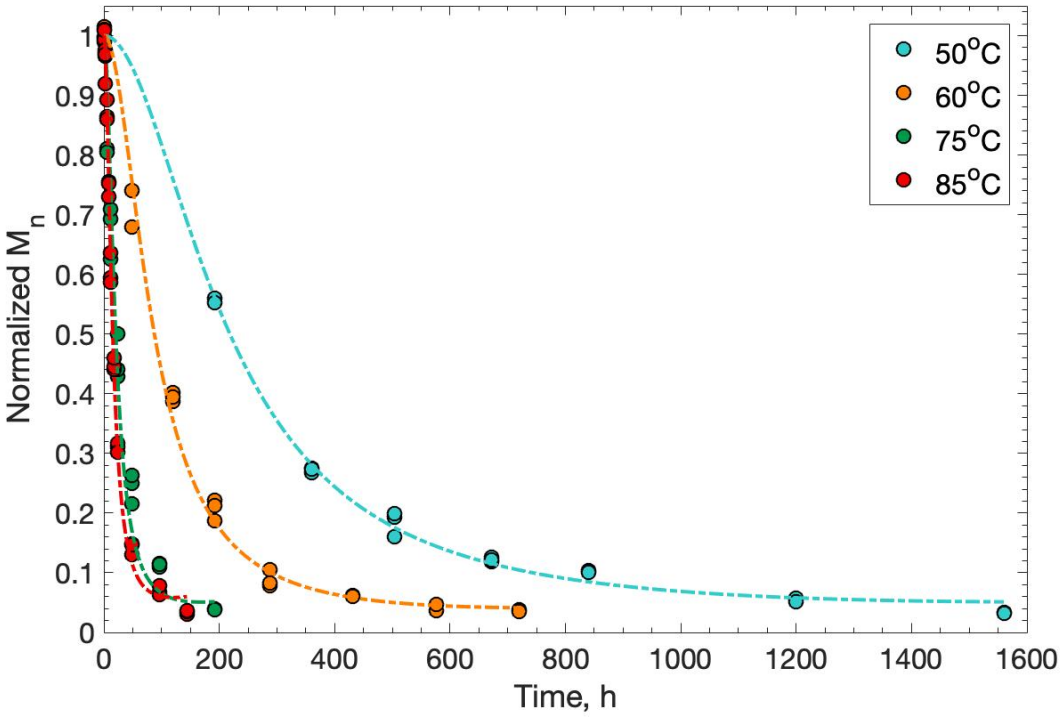


(a)

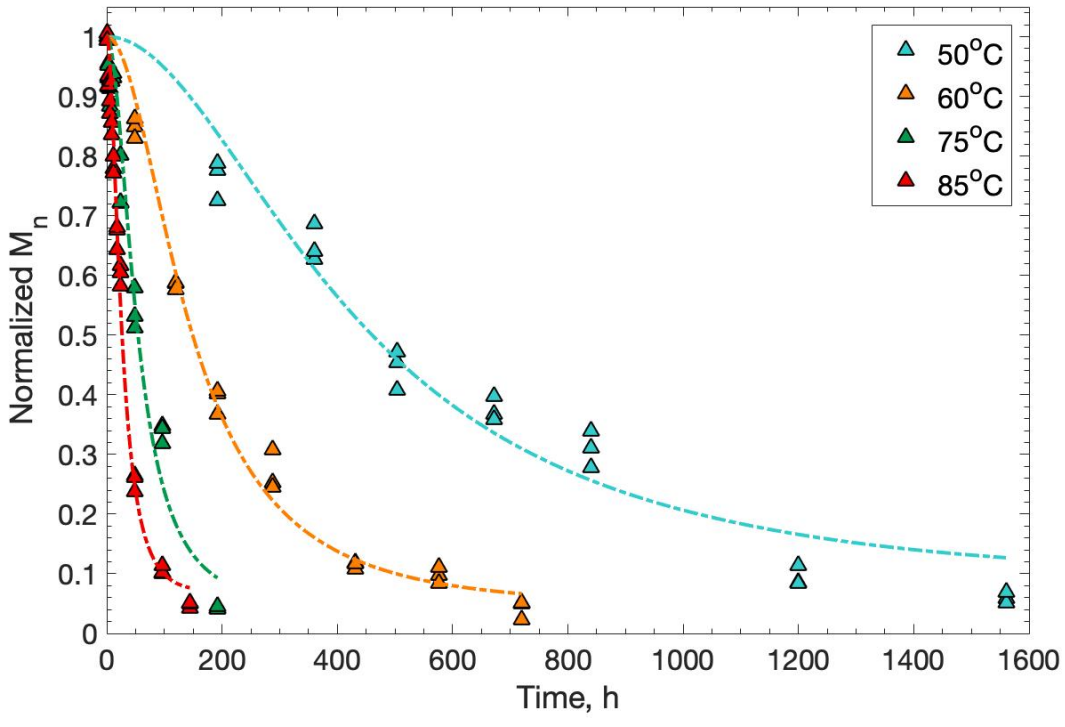


(b)

**Figure 4.44** Normalized $M_n$ as a function of time during hydrolytic degradation in 50% ethanol at 50, 60, 75, and 85°C: (a) PLA–Con and (b) PLA–Cex

The $\bar{k}_{deg}$ was compared against the $k_{1st}$ presented in **Table 4.12** and it was found that the $\bar{k}_{deg}$ values obtained from each temperature conditions considerably increased compared to $k_{1st}$ due to the effect of crystallization induced during degradation except the hydrolysis of PLA–Cex at 40 °C which only approximately 12% crystallinity was formed after 245 days resulting in the less effect of crystallinity on the estimation of the rate constant.

**Table 4.14** Rate constant ($\bar{k}_{deg}$, $h^{-1}$) of hydrolytic degradation of PLA–Con and PLA–Cex in water and 50% ethanol

| Temp | Water | | 50% Ethanol | |
|---|---|---|---|---|
| °C | PLA - Con | PLA - Cex | PLA - Con | PLA - Cex |
| 40 | $0.00046\pm0.00001^{Aa}$ | $0.00024\pm0.00001^{Ab}$ | - | - |
| 50 | - | - | $0.0044\pm0.00004^{Aa}$ | $0.0017\pm0.00005^{Ab}$ |
| 60 | $0.0096\pm0.0002^{Bb}$ | $0.0039\pm0.0002^{Bd}$ | $0.0116\pm0.0003^{Ba}$ | $0.0056\pm0.0001^{Bc}$ |
| 75 | $0.0336\pm0.0006^{Cb}$ | $0.0158\pm0.0005^{Cc}$ | $0.0497\pm0.0021^{Ca}$ | $0.0153\pm0.0008^{Cc}$ |
| 85 | $0.0674\pm0.0018^{Da}$ | $0.0296\pm0.0005^{Dc}$ | $0.0701\pm0.0010^{Da}$ | $0.0301\pm0.0010^{Dc}$ |
| 95 | $0.0952\pm0.0019^{Ea}$ | $0.0349\pm0.0012^{Eb}$ | - | - |

The values within a column followed by the same uppercase letters and the values within a row followed by the same lowercase letters are not significantly different ($\alpha$=0.05).

**Figure 4.45** shows $\bar{k}_{deg}$ of PLA–Con and PLA–Cex as a function of temperature. The curves of the $\bar{k}_{deg}$ are slightly different compared to ones of $k_{1st}$ shown in **Figure 4.34**.. The higher $\bar{k}_{deg}$ was observed in the hydrolysis in 50% ethanol over in water.

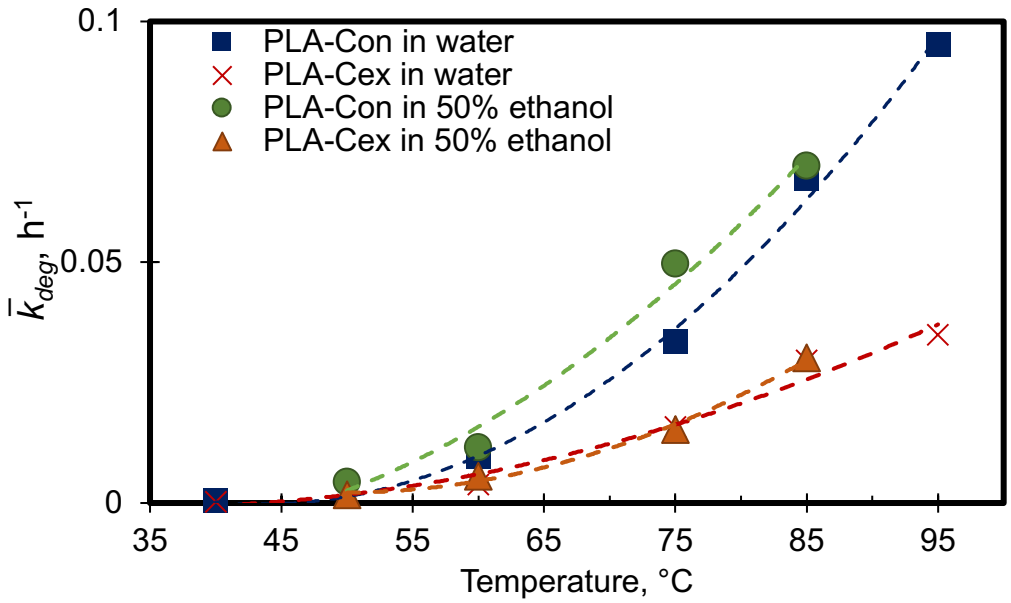


**Figure 4.45** Rate constant ($\bar{k}_{deg}$) of hydrolytic degradation of PLA–Con and PLA–Cex in water and 50% ethanol as a function of temperature

In this study, the effect of chain scission-induced crystallization and the production of short chain were considered in modeling of hydrolytic degradation using a two-phase model which polymers comprise crystalline and amorphous regions. Due to the hydrolysis preferentially occurs in the amorphous phase, the crystalline fraction increased during hydrolysis was assumed to be more resistant and cannot be hydrolyzed. In fact, the amorphous phase should be separated into two fractions, the mobile amorphous fraction (MAF) and the rigid amorphous fraction (RAF) according to the three-phase model theory [26,27]. The RAF exhibits different behaviors compared to the MAF depending on the $T_g$ of RAF, which is located in the wide range between the $T_g$ of MAF and $T_m$, difficult to examine [28]. In general, the formation of RAF, which can occur during isothermal crystallization, limits the mobility due to the fixation of parts of molecules with the crystalline phase [29,30]. The increase in RAF can restrict the diffusion and solubility of the permeant through PLA film and minimize the hydrolytic degradation, while at lower temperatures below its $T_g$, the RAF could behave in the opposite manner by enhancing the formation of microvoids and

increasing the free volume fraction [31,32]. In this study, the existence of the rigid amorphous phase has not been investigated, but it should be unquestionable that the formation of RAF could affect the hydrolysis of PLA.

### 4.4.4 Effect of temperature on the hydrolytic degradation of PLA

The hydrolytic degradation of PLA is profoundly affected by temperature. As reported in the previous section, the hydrolysis rate of both PLA–Con and PLA–Cex was slow at low temperature and rose exponentially with temperature increase. The Arrhenius equation was used to determine the effect of temperature on the hydrolysis. The Arrhenius plots of ln($k_{1st}$) and ln($\bar{k}_{deg}$,) versus 1/T are shown in **Figures 4.46** and **4.47***,* respectively. For the hydrolysis in water, the experiment conducted at 40°C which is lower than the $T_g$ of the samples, *ln($k_{1st}$)* and *ln($\bar{k}_{deg}$,)* did not exhibit the same linear trendline as ones tested over the $T_g$. While all the hydrolysis condition in ethanol run at temperatures above $T_g$ followed the Arrhenius behavior. Therefore, the result obtained from the hydrolysis at 60–95°C in water and at 50–85°C in 50% ethanol were selected to determine $E_a$.

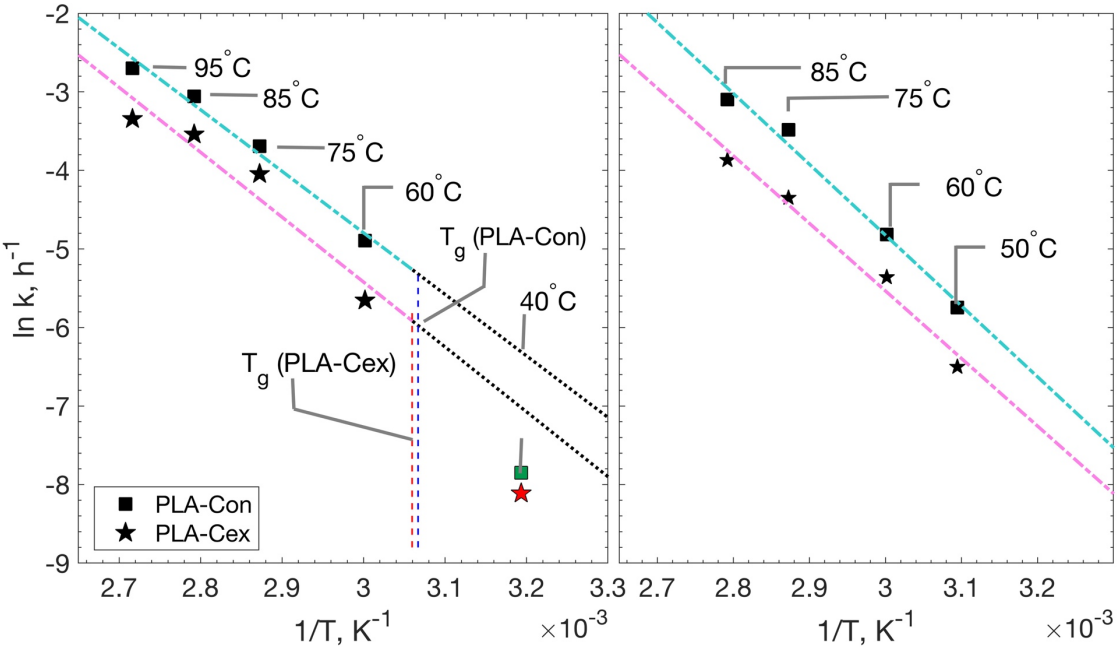


**Figure 4.46** Arrhenius plots of natural logarithm of the rate constant ($k_{1st}$) versus the reciprocal temperature of hydrolytic degradation of PLA–Con and PLA–Cex in (a) water and (b) 50% ethanol: symbols (■,★) represent the ln($k_{1st}$), and (– - –) line correspond the linear fit on Arrhenius plot and (…) line represents the comparison linear trendline.

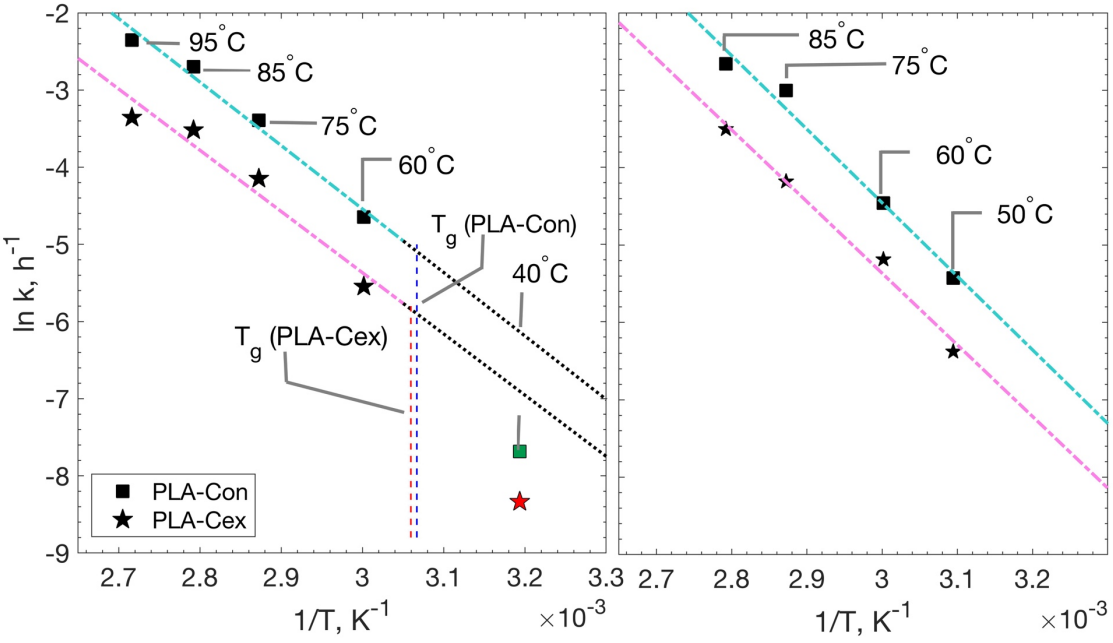


**Figure 4.47** Arrhenius plots of the rate constant ($\bar{k}_{deg}$) versus the reciprocal temperature of hydrolytic degradation of PLA–Con and PLA–Cex in (a) water and (b) 50% ethanol : symbols (■,★) represent the ln($k_{1st}$), and (– - –) line correspond the linear fit on Arrhenius plot and (…) line represents the comparison linear trendline.

The determination of the $E_a$ as described by the first order reaction rate constant used the reparameterization of the Arrhenius equation as shown in Eq. (3.12). Plots of the scaled sensitivity coefficient (SSC) of each condition (Figure B.1 and Figure C.1, Appendix B, C) indicated that the three parameters were uncorrelated. To eliminate the high correlations between $E_a$ and $k_0$, the $T_{ref}$ value were determined as shown in Figure B.2 and Figure C.2, Appendix B, C. Then, the $M_{n0}$, $k_{ref}$, and $E_a$ were estimated simultaneously shown in Table 4.15. The correlation matrix of the kinetic parameters of PLA–Cex after using $T_{ref}$ are presented in Tables B.1–B.2 and C.1–B.2, Appendix B, C. The $E_a$ of PLA–Cex and PLA–Con were not significantly different.

For the hydrolytic degradation process obtained from the Pan's model, the determination of the $E_a$ was evaluated using the slope of the Arrhenius plot. $E_a$ values were calculated (see **Table 4.16**) and concluded that the estimated activation energy for the hydrolysis of PLA and PLA–Cex were not significantly different in both water and 50% ethanol. It can predict that the chain extender can slow the rate of hydrolytic degradation at all temperatures without altering the activation energy of the hydrolytic degradation. The molecular chain requires a similar amount of energy for the reaction to proceed; however, the change in molecular structure can delay the hydrolytic degradation.

**Table 4.15** The reparameterization of the Arrhenius equation and the first order reaction

| Parameters | Water | | 50% Ethanol | |
|---|---|---|---|---|
| | PLA–Con | PLA–Cex | PLA–Con | PLA–Cex |
| $T_{ref}$, °C | 80.70 | 78.84 | 66.39 | 62.97 |
| $M_{n0}$, Da | 106740±1240 | 196430±3220 | 107080±1580 | 177510±5780 |
| $k_{ref}$, $h^{-1}$ | 0.0324±0.0008 | 0.0160±0.0006 | 0.0126±0.0005 | 0.0048±0.0001 |
| $E_a$, J/mol | 63541±1685$^A$ | 65716±2374$^A$ | 72072±1388$^B$ | 73403 ±1331$^B$ |

Values within a row followed by the same letters are not significantly different ($\alpha$=0.05).

**Table 4.16** The estimation of the Activation energy using slope of the Arrhenius plot

| Parameters | Water | | 50% Ethanol | |
|---|---|---|---|---|
| | PLA–Con | PLA–Cex | PLA–Con | PLA–Cex |
| $E_a$, J/mol | 67924±3007$^A$ | 66266±5161$^A$ | 79043±3508$^B$ | 79485±4003$^B$ |

Values within a row followed by the same letters are not significantly different ($\alpha$=0.05).

### 4.4.5 Determination of the hydrolytic stability over a wide range of temperatures

As shown in **Figures 4.46–4.47**, the hydrolytic degradation in water over the wide range of temperature condition from 40 to 95 °C did not obey the Arrhenius equation. An alternative approach to evaluating the effect of temperature around a range crossing $T_g$ can be described with the Vogel-Tammann-Fulcher (VTF) model as described in **Eq. (3.15)**. The $T_g$ values of PLA-Con and PLA-Cex (see **Table 4.11**) were determined using the DMA method under wet condition. The $T_s$ values used in the VTF equation for PLA-Con and PLA-Cex calculated as 50 K below their $T_g$,52.9 and 53.7 °C, were 2.9 and 3.7 °C (276.1 and 276.9 K), respectively. The linear relationship of ln $k_{1st}$ and $1/T\text{-}T_s$ was observed in **Figure 4.48**. The parameterized model of the first order reaction and the VTF model as shown in **Eq. (3.16)** were used to estimate $E_{VTF}$, which is the pseudo activation energy describing the effect of temperature over a wide range of experimental condition crossing the $T_g$. Then, the $E_{VTF}$ can be estimated to be about 2698 J/mol for PLA–Con and 2492 J/mol for PLA–Cex shown in **Table 4.18.**

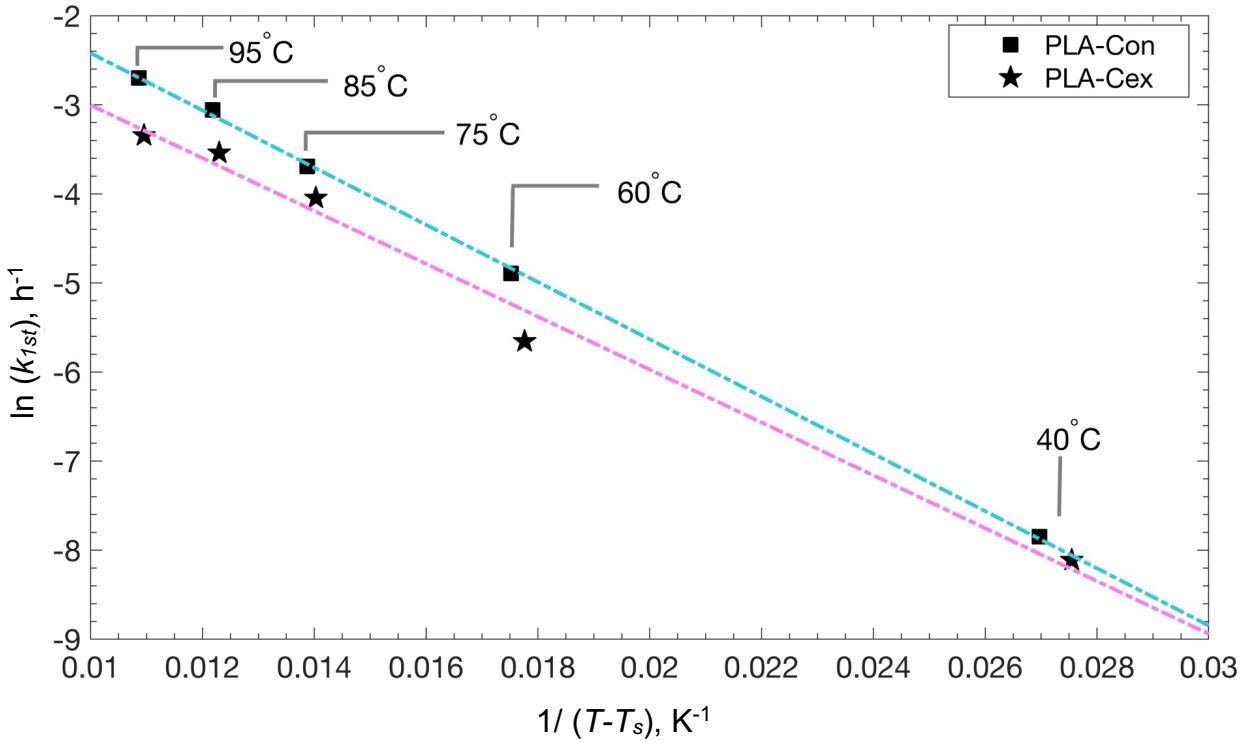


**Figure 4.48** VTF plots of the ln ($k_{1st}$) versus 1/ ($T$-$T_s$) of PLA–Con and PLA–Cex in water

**Table 4.17** The parameterization of the first order reaction and the VTF equation

| Parameters | PLA–Con | PLA–Cex |
|---|---|---|
| $T_s$, °C (K) | 52.9-50 (276.1) | 53.7-50 (276.9) |
| $T_{ref}$, °C (K) | 62.4 (335.6) | 63.50 (336.7) |
| $M_{n_0}$, Da | 107830± 892 | 196430±2167 |
| $k_{ref}$, h$^{-1}$ | 0.0101± 0.0002 | 0.0066±0.0002 |
| $E_{VTF}$, J/mol | 2699±19 | 2493±27 |

The VTF equation can be converted to the Williams-Landel-Ferry (WLF) equation giving in **Eq. (3.17)** using the estimated $E_{VTF}$. $C_1$ and $C_2$ were calculated by **Eq. (3.18)** in order to obtain the shift factors ($\alpha_T$) to shift the experimental data at one temperature condition ($T$) to construct a master curve to predict the data at the temperature of interest ($T_i$). **Figure 4.49** shows the $log\alpha_T$ as a function of $T$. The symbols (■,★) represent the $log\alpha_T$ to shift the data at $T$ of 40, 60, 75, 85, and 95 °C and the line (—) shows the WLF curves of shift factors of $T$ from 40 to 95 °C for construct the master curves at the $T_i$ of 40 °C. For this demonstration, the experimental data of $T$ at 85 °C, which had been done in 7 days as shown in **Figure 4.50a** and **Figure 4.51a** for PLA–Con and PLA–Cex, respectively, were chosen for the reference data. The shift factors $\alpha_T$ were used to horizontally shift the experimental data at 85 °C to construct the master curves of 40°C shown in **Figure 4.50b** and **Figure 4.51b** (for PLA–Con and PLA–Cex, respectively). The actual data of 40 °C was plotted to compare with the predicted data set which was found to be overlapped. See APPENDIX D for the example calculation to construct a master curve. The hydrolytic degradation in the accelerated degradation testing was used to predict the long-term hydrolytic degradation at the lower temperatures. It was found that PLA–Con and PLA–Cex would take approximately 368 and 634 days, respectively, to degrade to the $M_n$ of 4 kDa when the PLA oligomers are assumed to become soluble in water.

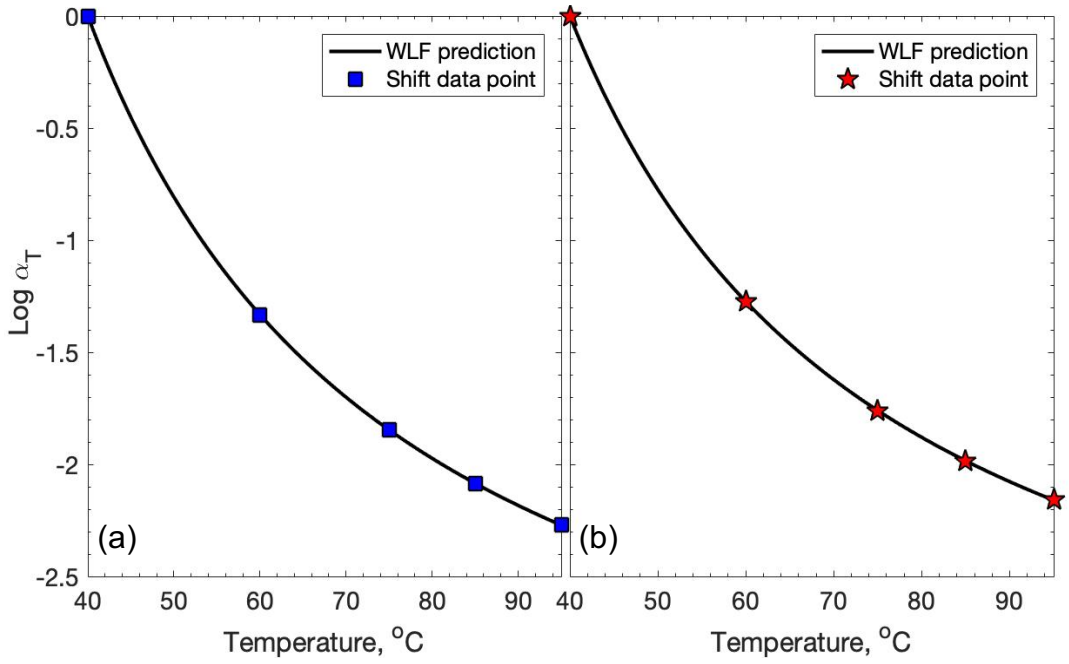


**Figure 4.49** WLF curves of shift factors of the hydrolytic degradation in which the temperature of interest was set at 40 °C: (a) PLA–Con and (b) PLA–Cex

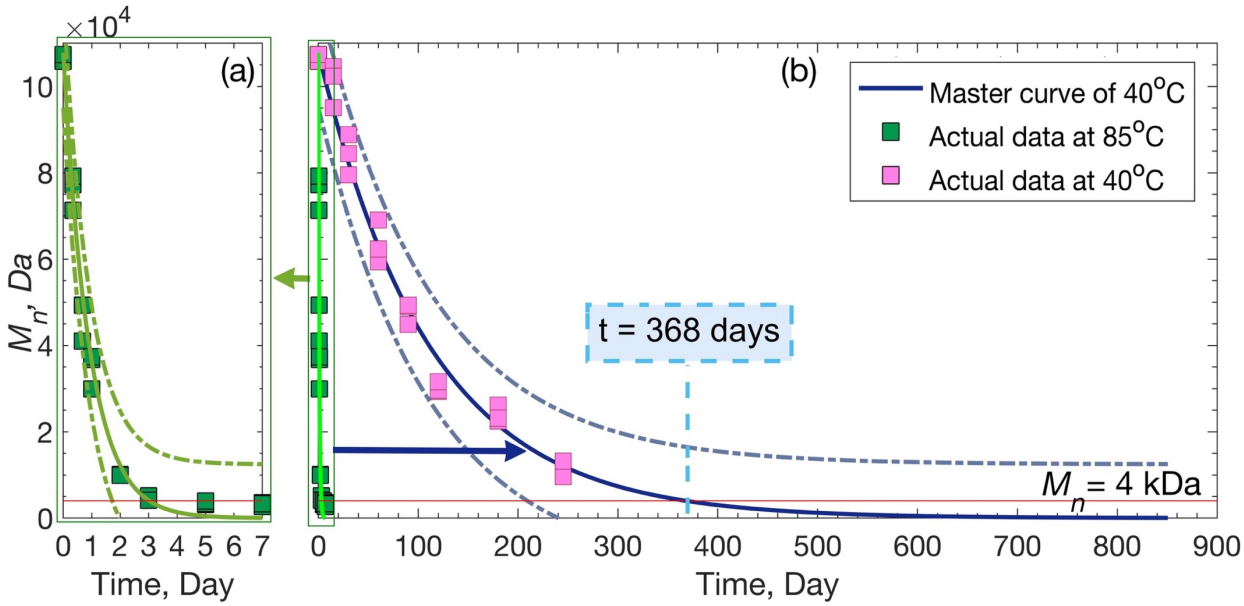


**Figure 4.50** The demonstration of the master curve generating from the hydrolytic degradation of PLA–Con at 85 °C to predict the hydrolysis at 40 °C. (a) represents the actual experimental data (■) and predicted line (—) with 95%prediction interval (- — -) and (b) represents the comparison between a master curve of 40 °C (—) with 95%prediction interval (- — -) shifted from the actual data at 85 °C and the actual experimental data at 40 °C (■). The line (—) shows the solubility limit of PLA oligomer.

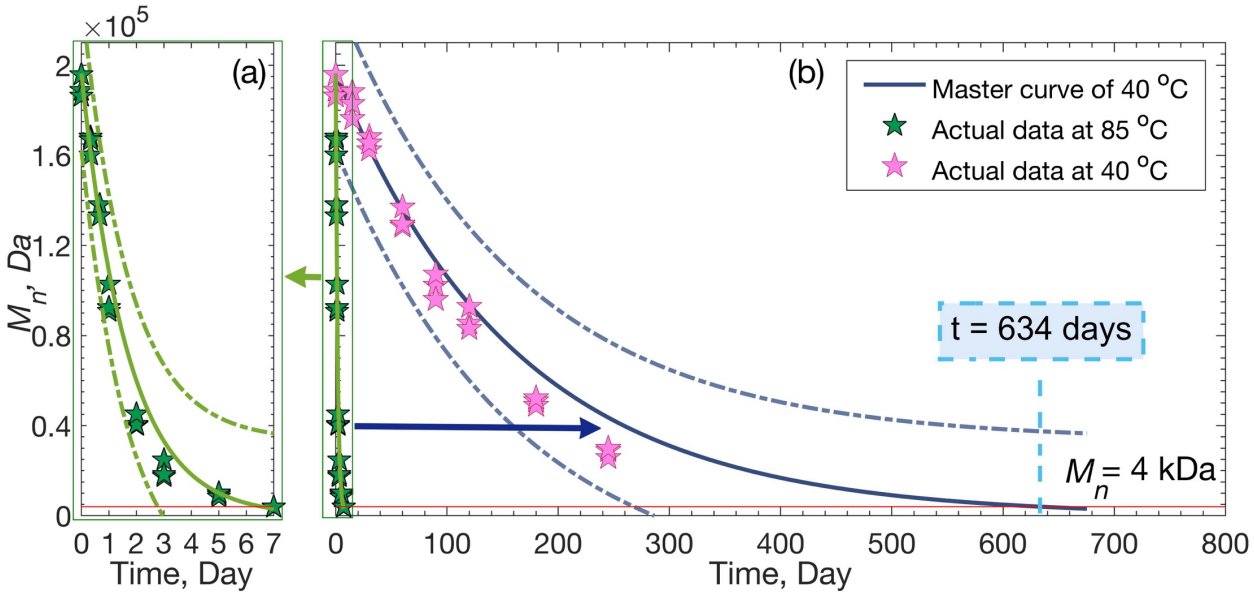


**Figure 4.51** The demonstration of the master curve generating from the hydrolytic degradation of PLA–Cex at 85 °C to predict the hydrolysis at 40 °C. (a) represents the actual experimental data (★) and predicted line (—) with 95% prediction interval (- — -) and (b) represents the comparison between a master curve of 40 °C (—) with 95%prediction interval (- — -) shifted from the actual data at 85 °C and the actual experimental data at 40 °C (★). The line (—) shows the solubility limit of PLA oligomer.

# APPENDICES

## APPENDIX A: Visual observation of structure change during degradation

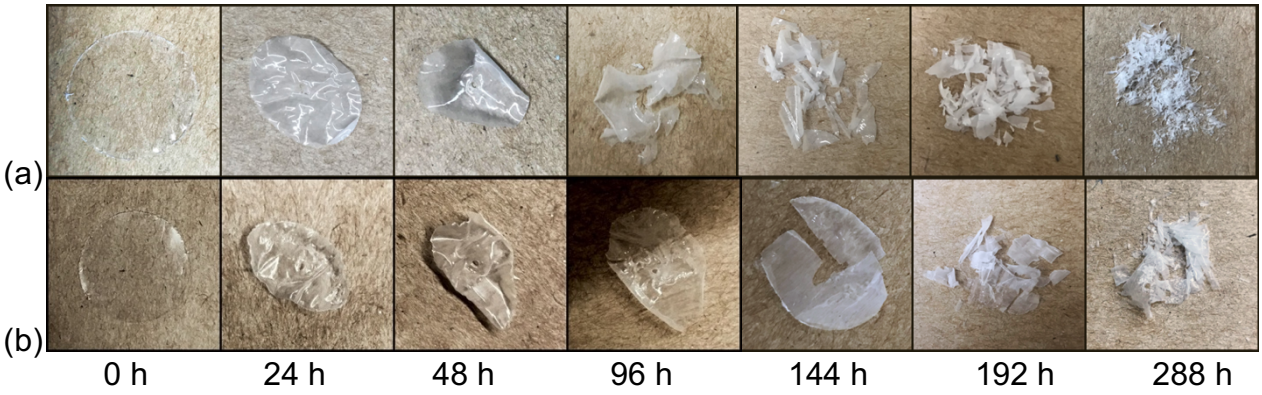


**Figure A.1** Visual observation of PLA–Con and PLA–Cex film during degradation in water at 75 °C

## APPENDIX B: Parameter estimation of the activation energy of the hydrolytic degradation in water

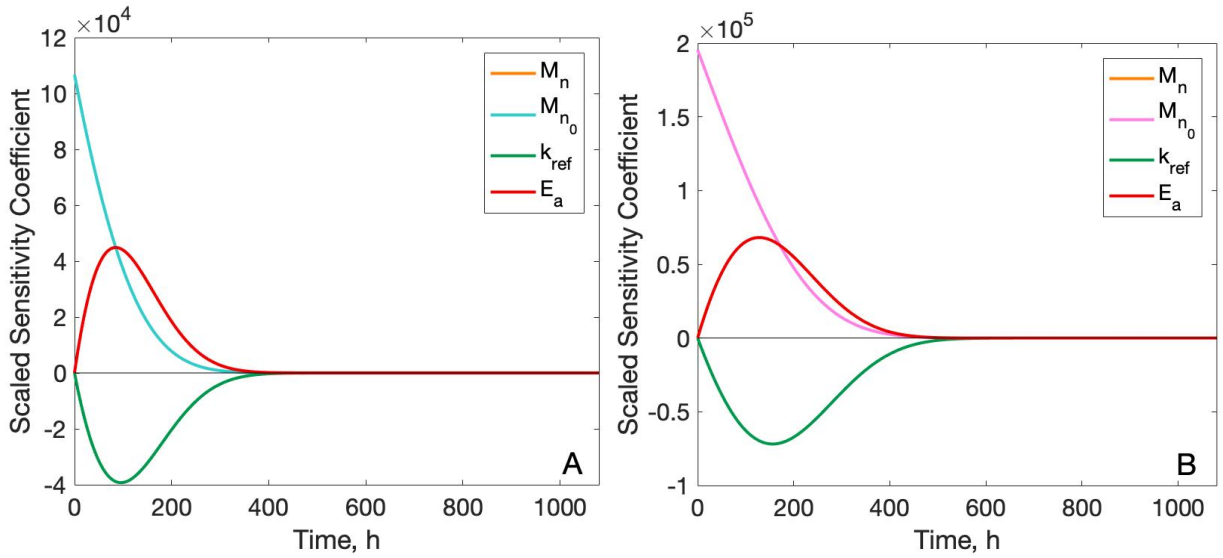


**Figure B.1** Scaled sensitivity coefficient plots of the three parameters (A) PLA–Con using initial parameter values of $M_{n_0}$= 100 kDa, $k_{ref}$ = 0.025 $h^{-1}$, and $E_a$ = *50* kJ/mol and (B) PLA–Cex using initial parameter values of $M_{n_0}$= 180 kDa, $k_{ref}$ = 0.025 $h^{-1}$, and $E_a$ = *50* kJ/mol

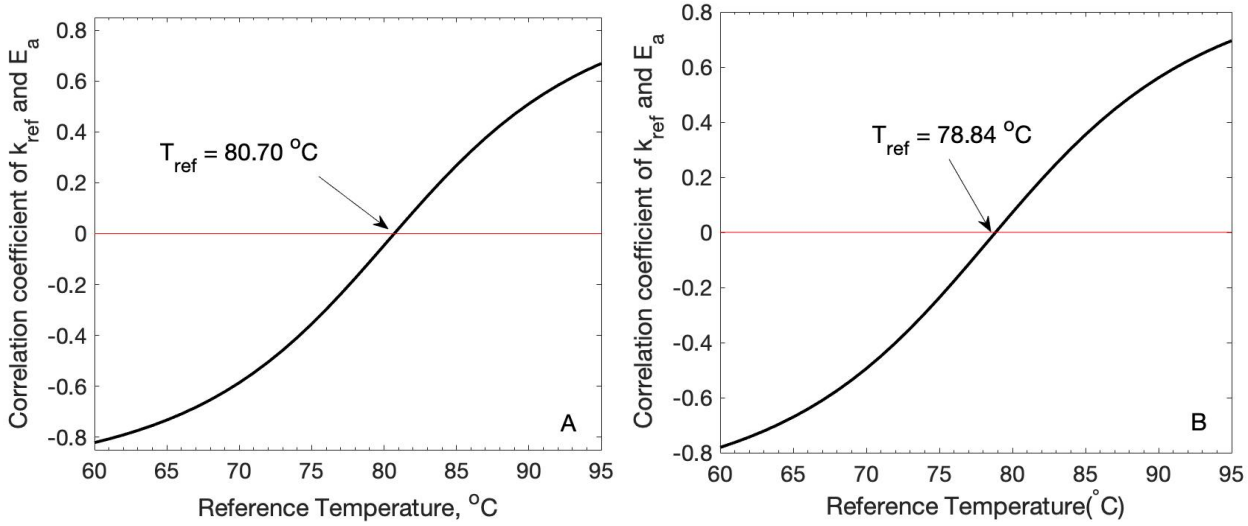


**Figure B.2** Correlation coefficient of parameter $K_{ref}$ and $E_a$ as a function of the reference temperature $T_{ref}$ for the hydrolytic degradation in water: (A) PLA–Con and (B) PLA–Cex.

**Table B.1** Correlation matrix of the kinetic parameters of PLA–Con at $T_{ref}$ = 80.70 °C

| Parameters | $M_{n0}$ | $k_{ref}$ | $E_a$ | Relative error, % |
|---|---|---|---|---|
| $M_{n0}$ | 1 | SYMMEYRIC | | 1.16 |
| $k_{ref}$ | 0.5476 | 1 | | 2.47 |
| $E_a$ | 0.0707 | $1.7964\times10^{-5}$ | 1 | 2.65 |

**Table B.2** Correlation matrix of the kinetic parameters of PLA–Cex at $T_{ref}$ = 78.84 °C

| Parameters | $M_{n0}$ | $k_{ref}$ | $E_a$ | Relative error, % |
|---|---|---|---|---|
| $M_{n0}$ | 1 | SYMMEYRIC | | 1.16 |
| $k_{ref}$ | 0.5973 | 1 | | 3.68 |
| $E_a$ | 0.0884 | $7.7559\times10^{-6}$ | 1 | 3.16 |

## APPENDIX C: Parameter estimation of the activation energy of the hydrolytic degradation in 50% ethanol

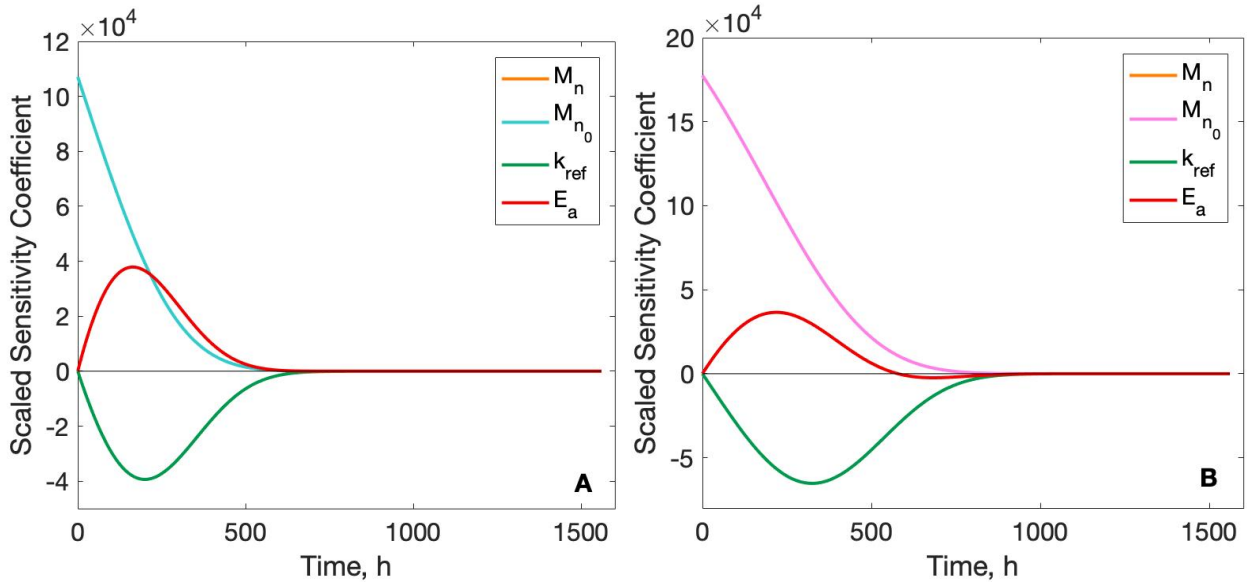


**Figure C.1** Scaled sensitivity coefficient plots of the three parameters (A) PLA–Con using initial parameter values of $M_{n0}$= 100 kDa, $k_{ref}$ = 0.01 $h^{-1}$, and $E_a$ = *70* kJ/mol and (B) PLA–Cex using initial parameter values of $M_{n0}$= 180 kDa, $k_{ref}$ = 0.005 $h^{-1}$, and $E_a$ = *70* kJ/mol

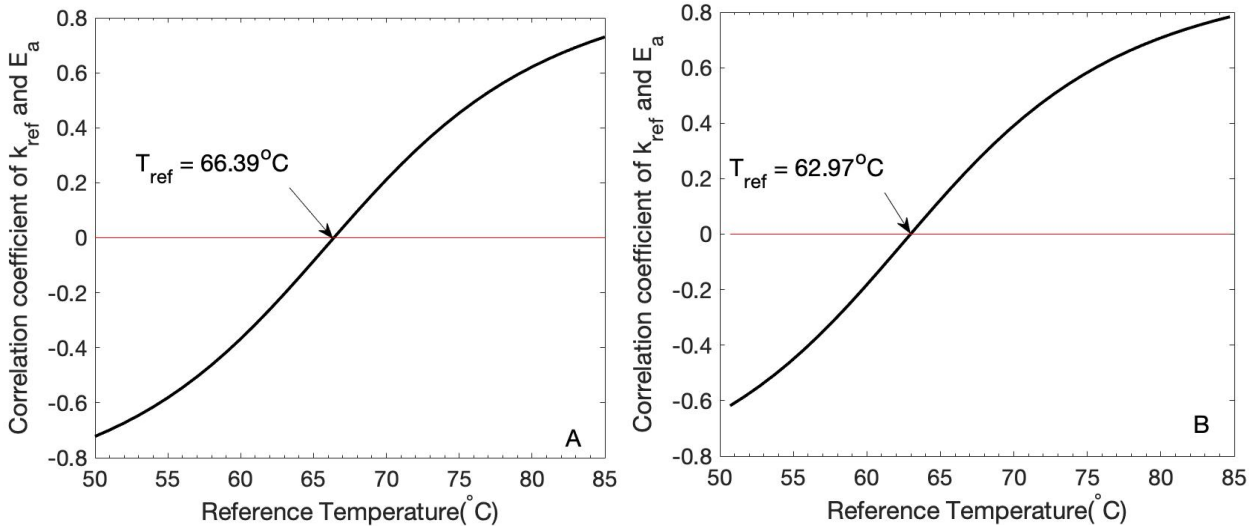


**Figure C.2** Correlation coefficient of parameter $K_{ref}$ and $E_a$ as a function of the reference temperature $T_{ref}$ for the hydrolytic degradation in 50% ethanol: (A)PLA–Con and (B)PLA–Cex

**Table C.1** Correlation matrix of the kinetic parameters of PLA–Con at $T_{ref}$ = 66.39 °C

| Parameters | $M_{n0}$ | $k_{ref}$ | $E_a$ | Relative error, % |
|---|---|---|---|---|
| $M_{n0}$ | 1 | SYMMEYRIC | | 0.98 |
| $k_{ref}$ | 0.5493 | 1 | | 2.38 |
| $E_a$ | 0.1716 | $5.5369\times10^{-6}$ | 1 | 1.92 |

**Table C.2** Correlation matrix of the kinetic parameters of PLA–Cex at $T_{ref}$ = 62.97 °C

| Parameters | $M_{n0}$ | $k_{ref}$ | $E_a$ | Relative error, % |
|---|---|---|---|---|
| $M_{n0}$ | 1 | SYMMEYRIC | | 0.89 |
| $k_{ref}$ | 0.5683 | 1 | | 2.29 |
| $E_a$ | 0.1717 | $-2.6217\times10^{-4}$ | 1 | 1.813R |

**APPENDIX D: Example calculation of VTF and WLF to construct a master curve**

**Given:** $E_{VTF}$* of PLA–Con = 2699 J/mol

*$E_{VTF}$ was measured within the temperature range 40-95 °C and estimated from the parameterization of the first order reaction and the VTF equation.

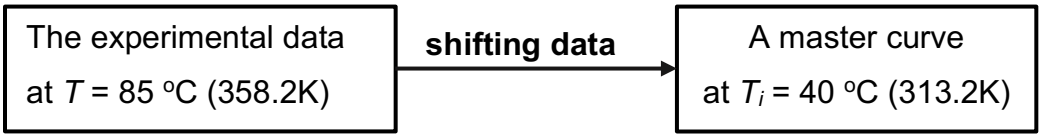


**Calculate:** Determine $C_1$ and $C_2$ using Eq. (3.17). $T_i$ = 40 °C (313.2 K),

$T_s$ = $T_g$-50 = 52.4 °C-50 (276.1 K), $R$ = 8.314 J/K*mol

$$C_1 = \frac{E/R}{2.303\,(T_i - T_s)} \text{ and } C_2 = (T_i - T_s) \qquad (3.17)$$

$C_1$ = - 3.8 and $C_2$ = 37.1 K

Determine log $\alpha_T$ using Eq. (3.16). T = 85 °C (358.2K)

$$\log\alpha_T = -\frac{C_1(T - T_i)}{C_2 + (T - T_i)} \qquad (3.16)$$

$\log\alpha_T$ = - 2.1, and 1/ $\alpha_T$ = 121.51

Determine the shifted time by multiplying the degradation time of 85 °C (shown in **Table D.1**) by 1/$\alpha_T$. A master curve of 40 °C can be constructed by plotting the prediction line of the $M_n$ at 85 °C as a function of the shifted time. Another method is to multiply the range of hydrolysis time by 1/$\alpha_T$ and plot as a function of prediction line of hydrolysis at 85 °C shown in **Figure D.1.**

**Table D.1** Experimental data of the hydrolytic degradation of PLA–Con in water at 85 °C

| Time, h | $M_n$ | Shifted time (Time * $1/\alpha_T$) |
|---|---|---|
| 0 | 106133 | 0 |
| 0 | 105785 | 0 |
| 0 | 107359 | 0 |
| 8 | 77266 | 972 |
| 8 | 79211 | 972 |
| 8 | 71324 | 972 |
| … | … | … |
| 120 | 3158 | 14582 |
| 120 | 3375 | 14582 |
| 120 | 3954 | 14582 |
| 168 | 3561 | 20415 |
| 168 | 2694 | 20415 |
| 168 | 3344 | 20415 |

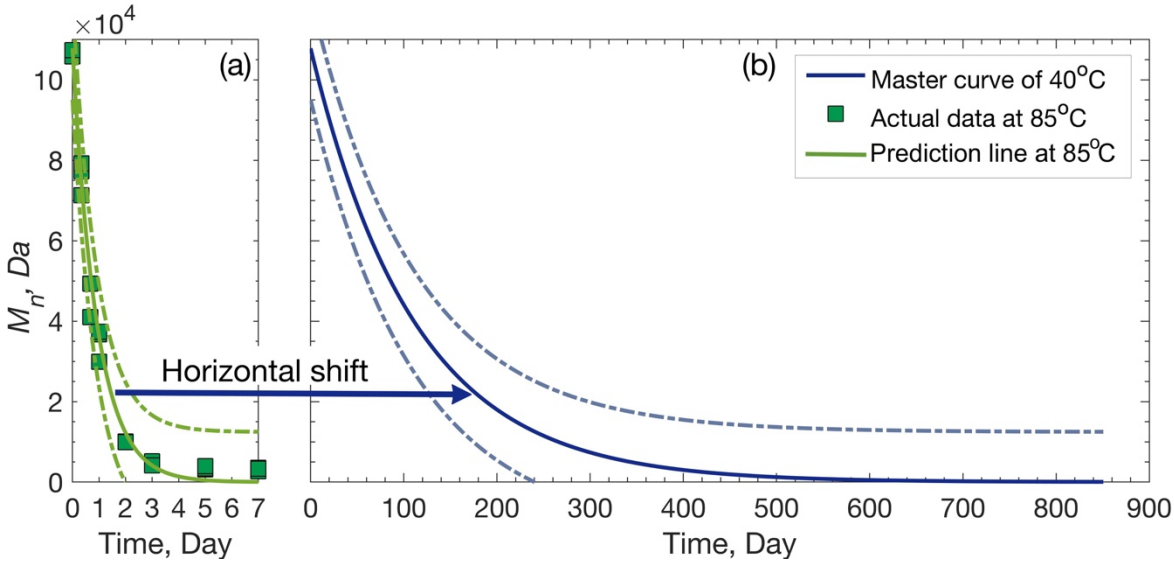


**Figure D.1** The demonstration of the master curve generating from the hydrolytic degradation in water of PLA–Con at 85 °C to predict the hydrolysis at 40 °C: (a) The actual experimental data at 85 °C (■) and predicted line (—) with 95% prediction interval (- — -) and (b) a master curve of 40 °C (—) with 95% prediction interval (- — -).

# REFERENCES

## REFERENCES


[1] Capone C, Di Landro L, Inzoli F, Penco M, Sartore L. Thermal and mechanical degradation during polymer extrusion processing. Polym Eng Sci 2007;47:1813–9.

[2] Olabisi O, Adewale K. Handbook of Thermoplastics. CRC Press; 2016.

[3] Al-itry R, Lamnawar K, Maazouz A. Reactive extrusion of PLA , PBAT with a multi-functional epoxide : Physico-chemical and rheological properties. Eur Polym J 2014;58:90–102.

[4] Frenz V, Scherzer D, Ag B, Germany L, Villalobos M, Awojulu AA, et al. Multifunctional Polymers as Chain Extenders and Compatibilizers for Polycondensates and Biopolymers . Chain Extension vs . Solid State Polymerization 2008:1682–6.

[5] Gupta MC, Deshmukh VG. Thermal oxidative degradation of poly-lactic acid. Colloid Polym Sci 1982;260:514–7.

[6] Iñiguez-Franco F, Auras R, Dolan K, Selke S, Holmes D, Rubino M, et al. Chemical recycling of poly(lactic acid) by water-ethanol solutions. Polym Degrad Stab 2018;149:28–38.

[7] Baimark Y, Cheerarot O. Effect of chain extension on thermal stability behaviors of polylactide bioplastics. Orient J Chem 2015;31:635–41.

[8] Al-Maydama H, El-Shekeil A, Khalid MA, Al-Karbouly A. Thermal degradation behaviour of some polydithiooxamide metal complexes. Eclética Química 2006;31:45–52.

[9] Iñiguez-Franco F, Auras R, Ahmed J, Selke S, Rubino M, Dolan K, et al. Control of hydrolytic degradation of Poly(lactic acid) by incorporation of chain extender: From bulk to surface erosion. Polym Test 2018;67:190–6.

[10] Xu H, Matkar R, Kyu T. Phase-field modeling on morphological landscape of isotactic polystyrene single crystals. Phys Rev E - Stat Nonlinear, Soft Matter Phys 2005;72.

[11] Jing J, Zhang Y, Tang X, Li X, Peng M, Fang Z. Combination of a bio-based polyphosphonate and modified graphene oxide toward superior flame retardant polylactic acid. RSC Adv 2018;8:4304–13.

[12] Ma P, Cai X, Zhang Y, Wang S, Dong W, Chen M, et al. In-situ compatibilization of poly(lactic acid) and poly(butylene adipate-co-terephthalate) blends by using dicumyl peroxide as a free-radical initiator. Polym Degrad Stab 2014;102:145–51.

[13] Siparsky GL, Voorhees KJ, Fudu M. Hydrolysis of Polylactic Acid (PLA) and Polycaprolactone (PCL) in Aqueous Acetonitrile Solutions: Autocatalysis. J Environ Polym Degrad 1998;6:31–41.

[14] Xu H, Yang X, Xie L, Hakkarainen M. Conformational Footprint in Hydrolysis-Induced Nanofibrillation and Crystallization of Poly(lactic acid). Biomacromolecules 2016;17:985–95.

[15] Chen HM, Shen Y, Yang JH, Huang T, Zhang N, Wang Y, et al. Molecular ordering and α′-form formation of poly(l-lactide) during the hydrolytic degradation. Polymer (Guildf) 2013;54:6644–53.

[16] Kong Y, Hay JN. Multiple melting behaviour of poly(ethylene terephthalate). Polymer (Guildf) 2002;44:623–33.

[17] Lyu SP, Schley J, Loy B, Lind D,Hobot C,Sparer R,et al. Kinetics and time-temperature equivalence of polymer degradation. Biomacromolecules 2007;8:2301–10.

[18] Gleadall A. Computer Simulation of Polymer Chain Scission in Biodegradable Polymers. J Biotechnol Biomater 2013;03:1–5.

[19] Iñiguez-Franco F, Auras R, Burgess G, Holmes D, Fang X, Rubino M, et al. Concurrent solvent induced crystallization and hydrolytic degradation of PLA by water-ethanol solutions. Polym (United Kingdom) 2016;99:315–23.

[20] Pan J, Chen X. Modelling degradation of amorphous biodegradable polyesters: Basic model. Woodhead Publishing Limited; 2014.

[21] Castro-Aguirre E, Auras R, Selke S, Rubino M, Marsh T. Impact of nanoclays on the biodegradation of poly(lactic acid) nanocomposites. Polymers (Basel) 2018;10:1–11.

[22] Vieira AC, Vieira JC, Ferra JM, Magalhães FD, Guedes RM, Marques AT. Mechanical study of PLA-PCL fibers during in vitro degradation. J Mech Behav Biomed Mater 2011;4:451–60.

[23] Pan J. Modelling Degradation of Bioresorbable Polymeric Medical Devices. Elsevier Science; 2014.

[24] Tsuji H, Ikarashi K. In vitro hydrolysis of poly ( l -lactide ) crystalline residues as extended-chain crystallites . Part I : long-term hydrolysis in phosphate-buffered solution at 37 C 2004;25:5449–55.

[25] Ahmed J, Varshney SK, Ahmed J, Varshney SK. Polylactides — Chemistry , Properties and Green Packaging Technology : A Review POLYLACTIDES — CHEMISTRY , PROPERTIES AND GREEN PACKAGING TECHNOLOGY : A REVIEW 2011;2912.

[26] Badia JD, Strömberg E, Karlsson S, Ribes-Greus A. The role of crystalline, mobile amorphous and rigid amorphous fractions in the performance of recycled poly (ethylene terephthalate) (PET). Polym Degrad Stab 2012;97:98–107.

[27] Xu H, Ince BS, Cebe P. Development of the crystallinity and rigid amorphous fraction in cold-crystallized isotactic polystyrene. J Polym Sci Part B Polym Phys 2003;41:3026–36.

[28] Di Lorenzo ML, Gazzano M, Righetti MC. The role of the rigid amorphous fraction on cold crystallization of poly(3-hydroxybutyrate). Macromolecules 2012;45:5684–91.

[29] Schick C, Wurm A, Mohammed A. Formation and disappearance of the rigid amorphous fraction in semicrystalline polymers revealed from frequency dependent heat capacity. Thermochim Acta 2003;396:119–32.

[30] Lee JH. Solubility of Physical Blowing Agents in Semi-Crystalline Polymers: Consideration of Rigid Amorphous Fraction. University of Toronto, 2014.

[31] Del Río J, Etxeberria A, López-Rodríguez N, Lizundia E, Sarasua JR. A PALS contribution to the supramolecular structure of poly(l -lactide). Macromolecules 2010;43:4698–707.

[32] Dlubek G, Sen Gupta A, Pionteck J, Häßler R, Krause-Rehberg R, Kaspar H, et al. Glass transition and free volume in the mobile (MAF) and rigid (RAF) amorphous fractions of semicrystalline PTFE: A positron lifetime and PVT study. Polymer (Guildf) 2005;46:6075–89.

# CHAPTER 5

# Conclusions

## 5.1 Overall conclusions

The primary goals of developing biodegradable polymeric materials are not only attaining biodegradability but also achieving comparable properties to substitute the use of the fossil-based polymer. PLA is one of the biodegradable materials currently used on a commercial scale. It has been extensively researched to increase its performance and expand the application fields, especially in the packaging industry; however, the critical weakness of PLA is that it undergoes hydrolytic degradation which limits its uses in many applications, especially for products used in a high temperature or product with a long shelf life [1–3].

In the first phase of this study, the effect of a multi-functional epoxy chain extender has been investigated. The increase of the average molecular weight indicated the connection between the chain ends of PLA and the reactive epoxides of the chain extender. A long-chain branching structure was expected from the reaction. The effect of the chain extender content and the residence time of the melt blending process were investigated using the FCCCD/RSM and it was found that they significantly affected the variation of molecular weight. The higher chain extender content, the more reactive epoxy groups there were to connect the molecular chains. However, the chain extension reaction requires adequate reaction times for the reaction to proceed extensively. The optimal condition was determined as the point where additional combinations of the two factors could not improve the weight average molecular weight due to the effect of the thermal degradation and the restriction on the accessibility of the chain ends in the

reactive sites [4,5]. As a result, the optimization of this process could be achieved by using the chain extender content of 1.5 wt% and residence time of 17 minutes.

For the second phase, hydrolysis experiments were conducted in water and 50% ethanol at various temperatures to explore the effect of the modified PLA with the chain extension. The result revealed that the rate constants of hydrolytic degradation were significantly lower than the ones of unmodified PLA film in both water and 50% ethanol at all temperature conditions. This indicates that incorporation of the chain extender can enhance the hydrolytic degradation stability of PLA, which not only extends the period of service time but also maintains its properties for a longer period of time.

The activation energy of hydrolysis defined as the minimum energy required to initiate the hydrolytic degradation was eventually determined using the Arrhenius equation. The results show that the activation energy values obtained from both materials, the modified and the unmodified PLA films, were not significantly different indicating that the presence of the chain extender did not alter the mechanism of the hydrolytic degradation of modified PLA.

As discussed, the effects of chain extension reaction could provide a higher molecular weight and probability of a branched structure. Among the lower molecular weight chains, the higher number of chains and also chain ends compared to the higher molecular weight chains can increase the rate of end scission, which sequentially produced more monomers to accelerate the hydrolytic degradation [6]. Moreover, the carboxylic end that is naturally more active compared to the hydroxyl group on the other end was reacted with the epoxide group of the chain extender and became inactivated [7,8]. Therefore, the chain ends of the initial sample of modified PLA film could be altered.

Deleting of the carboxylic terminal could reduce the autocatalytic reaction due to a decrease in the acid dissociation of the carboxylic ends.

There are numerous mathematical models used to describe the rate constant of the hydrolytic degradation. A first-order reaction model is the simplest and most commonly used, which assumes that the concentration of the overall ester bonds remains constant throughout the hydrolytic experiment. However, the ester units available for degradation can considerably decrease due to the formation of crystallites which resist hydrolytic degradation. Furthermore, the small oligomer chains and monomers gradually produced from chain scissions became soluble and are dissolved in the hydrolysis media. The second model used in this thesis was the degradation model proposed by Pan [9]. It provides an insight into the hydrolytic degradation process of PLA by considering the change in the total number of ester units of all chains. According to the result of the model analysis, the rate constants obtained from the latter model were higher than ones from the first order reaction model.

In the final phase of this work, the hydrolytic degradation process over a wide range of temperatures was determined. The VTF and WLF equations were used to evaluate the horizontal shift factor to construct the master curve at the temperatures of interest. The result demonstrated the feasibility of using the mathematical model to explore the relationship between time and temperature. The accelerated testing at higher temperatures allows the prediction of the hydrolytic process at low temperatures.

## 5.2 Future work

The future work should focus on achieving a better understanding of the molecular structure of the modified PLA with chain extender during hydrolytic degradation. First, the degree of branching expected from the chain extension reaction has to be verified to provide more information about the molecular structure and its behavior during the hydrolysis. Moreover, the three-phase model theory should be investigated. The existence of RAF probably changes entirely the hydrolytic mechanism due to the differences in behavior of the RAF.

In this work, the reference model for the degradation was simplified by removing the rate constant of non-catalytic degradation as discussed in **section 3.2.9** due to the high correlation between the non-catalytic and auto catalytic rates. For the future work, it would be useful to address the hydrolytic mechanism including both mechanisms. Moreover, the activation energy from the reaction rate constants of the reference model was done by the basic method explained in **section 3.2.10** resulting in a high correlation between $k_0$ and $E_a$. Therefore, the model parameterization process should be improved in future work.

# REFERENCES

## REFERENCES


[1] Laura M, Lorenzo D. Synthesis, Structure and Properties of Poly(lactic acid). vol. 279. Cham: Springer International Publishing; 2018.

[2] Iñiguez-Franco F, Auras R, Burgess G, Holmes D, Fang X, Rubino M, et al. Concurrent solvent induced crystallization and hydrolytic degradation of PLA by water-ethanol solutions. Polym (United Kingdom) 2016;99:315–23.

[3] Tsuji H. Hydrolytic Degradation. Poly(Lactic Acid), Hoboken, NJ, USA: John Wiley & Sons, Inc.; 2010, p. 343–81.

[4] Rudin A, Choi P. Step-Growth Polymerizations 7. In: Rudin A, Choi P, editors. Elem. Polym. Sci. Eng., 2013, p. 305–39.

[5] Schlüter DA, Hawker C, Sakamoto J. Synthesis of Polymers: New Structures and Methods. Wiley; 2012.

[6] Gleadall A, Pan J, Kruft M-A, Kellomäki M. Degradation mechanisms of bioresorbable polyesters. Part 2. Effects of initial molecular weight and residual monomer. Acta Biomater 2014;10:2233–40.

[7] Al-itry R, Lamnawar K, Maazouz A. Improvement of thermal stability , rheological and mechanical properties of PLA , PBAT and their blends by reactive extrusion with functionalized epoxy. Polym Degrad Stab 2012;97:1898–914.

[8] Haralabakopoulos AA, Tsiourvas D, Paleos CM. Chain Extension of Poly ( ethylene terephthalate ) by Reactive Blending Using Diepoxides 1998:2121–7.

[9] Pan J. Modelling degradation of semi-crystalline biodegradable polyesters. Model. Degrad. Bioresorbable Polym. Med. Devices, Woodhead Publishing Limited; 2014, p. 53–69.